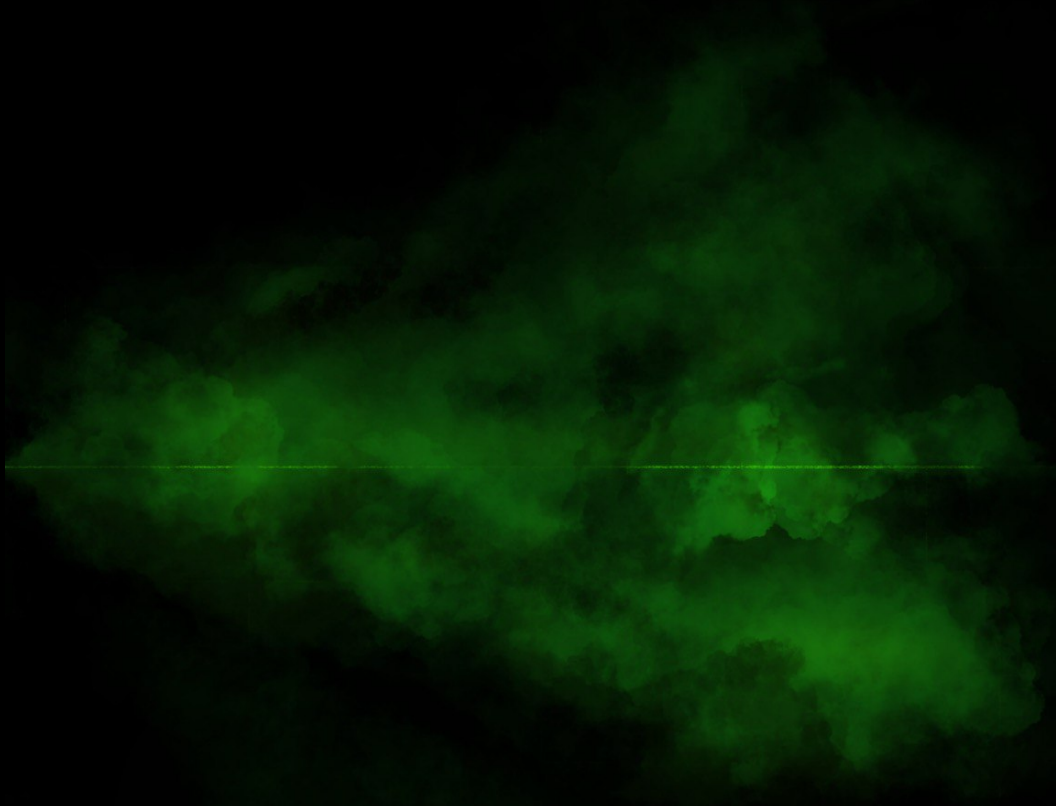

Visualisation of the airflow pattern of exhaled droplets in a classroom



Written by Yat Long Liu

Visualisation of the airflow pattern of exhaled droplets in a classroom

by

Yat Long Liu

Author:
Yat Long Liu

Student number:
4217918

Thesis committee of TU Delft:
Prof. dr. ir. P.M. Bluysen
Dr. C. (Clara) García-Sánchez
Dr. ir. M.A. Ortiz Sanchez
Dr. ir. H.R. Schipper

*On partial fulfilment of the requirements
for the degree of Master of Science in*

Civil Engineering

*at the Delft University of Technology,
to be defended publicly on Friday, 17th December, 2021 at 16:00*



DELFT UNIVERSITY OF TECHNOLOGY

Abstract

Civil Engineering and Geosciences
MSc Track: Building Engineering

Master of Science in

Visualisation of the airflow pattern of exhaled droplets in a classroom

by Yat Long Liu

The airborne transmission of SARS-CoV-2 in educational buildings has raised concerns during the current COVID-19 pandemic. In this study, a portable fog generator system was designed and assembled to visualise the airflow pattern of exhaled droplets in a classroom. The system consists of five components: medium, fog generator, buffer, pump, and manikin head. The medium was made of a combination of glycol and demineralised water, which produced a fog composed of droplets mimicking to some extent human breath. The fog was produced with the fog generator and passed through a pipe into the buffer for build-up. After accumulation, the fog is pumped through another pipe and is exhaled out of the mouth of the manikin. The experiments were conducted in a simulated classroom. The lights of the room were dimmed and six lasers were used to make the fog more visible. Four different ventilation regimes were examined: no ventilation, natural ventilation (open windows and door), mixing ventilation ($600 \text{ m}^3/\text{h}$), and a combination of natural + mixing ventilation. The experiments were recorded with a camera and analysed to determine the horizontal distance of the path taken by the fog and to measure the time it remained visible after exhalation from the mouth. During the experiments, it could be observed with the naked eye that the glycol droplets travel much further and linger in the air for longer than what is captured in the recordings. Furthermore, not all the droplets were visible with the camera, especially the smaller ones of a few micrometres in diameter. The recordings showed that the droplets travelled the furthest at natural ventilation (1.8 metres). The combination of natural + mixing ventilation regime had the highest indoor air velocity, causing the droplets to reach the shortest distance (0.5 metres). In conclusion, the type of ventilation, classroom layout, and exhalation location play an important role in determining the airflow pattern, as they affect how long and how far the glycol droplets travel. Applying any type of ventilation is critical in transmission control and reduces the possibility of aerosol accumulation in the classroom as smaller droplets can linger in the air for many hours until they settle on a surface.

Acknowledgements

This thesis was written as the final requirement of the Master of Science in Civil Engineering at the Delft University of Technology. It was an extra challenging period to write my thesis during COVID-19. I am incredibly proud of having been able to finish my research. Its completion is in large part also due to all the people who supported, challenged, and stuck with me along the way.

First of all, I would like to thank all my supervisors. They provided much needed support and assistance during the last twelve months of writing my thesis. My sincere thanks to Philomena Bluysen, the chair of the committee, who inspired my interest in researching the topic of ventilation in schools and COVID-19. Her extensive knowledge regarding building physics and valuable feedback on my thesis helped greatly me for the process. Next, I would like to thank Roel Schipper for structuring my report. He helped me to keep the information concise and to the point while also addressing the broader context of my research. I would also like to thank Clara García-Sánchez for providing me with insightful feedback during the theoretical background of my thesis. Her knowledge and enthusiasm about computational fluid dynamics have really motivated me to continue with it. My deepest gratitude goes to Marco Ortiz, as his unwavering patience aided me while figuring out my experimental complications. I am going to miss the casual conversations and good laughs we had during these experiments.

Secondly, special thanks to my tutors Dadi Zhang and Er (Erica) Ding for helping me with doing the measurements. I enjoyed the time when we the schools and the snacks we shared at the SenseLab.

Furthermore, I would like to thank my parents, Kwok Kwan and Kuk Ying, and my sister, Dionne, for their continuous love and support. I cannot begin to express my gratitude to my girlfriend, Yasmin. She has been my greatest support throughout this whole process. Sharing my thoughts and findings with her during the research helped me gain the confidence to continue my thesis.

Lastly, I would also like to thank my friends. My sincerest thanks to Alex, Rafael and Victor for their inspiration and the great times we spent together during the courses. Brendan, Lorenzo, Oliver and Wing, thank you for helping me reach the top. Also, Abdul, Ali, Brahm, Brendan, Illias, Marc, Onno, Ruben and Shaniel, my sincerest gratitude for motivation during my study years at Civil Engineering.

Hoofddorp, December 2021
Yat Long Liu

Contents

Abstract	v
Acknowledgements	vii
1 Introduction	1
1.1 The impact of COVID-19	1
1.2 Transmission routes	1
1.3 Schools in the Netherlands	2
1.4 Objective and research questions	3
1.5 Scope	3
1.6 Outline	3
2 Literature review	4
2.1 Indoor environmental factors affecting SARS-CoV-2	5
2.1.1 Mechanism of action	5
2.1.2 Droplet size	5
2.1.3 Impact of temperature and relative humidity	7
2.1.4 Ventilation in buildings	8
Air filters	9
2.1.5 Distance	10
2.1.6 Duration	12
2.2 Airflow pattern visualisation	14
2.2.1 Human subjects	14
High-speed imaging	15
Schlieren imaging	15
2.2.2 Manikins	17
Bubble	17
Fog	18
Fluorescent	19
Tracer gas	20
2.3 Conclusion	21
3 Methodology	22
3.1 Experimental site	23
3.1.1 The test chambers	23
3.1.2 The experience room	24
3.2 Baseline measurements	26
3.2.1 Ventilation regimes	26
No ventilation	26
Natural ventilation (only windows open)	26
Mixing ventilation (ceiling inflow, bottom exhaust)	27
Natural + mixing ventilation	27
3.2.2 Setup	27

3.2.3	Baseline conditions	28
3.3	Materials	30
3.3.1	Instrument research	30
	Medium	31
	Fog generator	31
	Pipe	32
	Buffer	33
	Pump	34
	Manikin	35
3.3.2	Visualisation equipment	36
3.3.3	Assembling guide	38
3.3.4	Final setup	40
3.4	Experiment: Airflow pattern visualisation	41
3.4.1	Setup	41
3.4.2	Data collection	42
3.4.3	Data analysis	42
3.5	Theoretical comparison	46
4	Results	47
4.1	Baseline measurements	48
4.1.1	Air velocity	48
4.1.2	Temperature	52
4.1.3	Relative humidity	52
4.2	Experiment: Airflow pattern visualisation	53
4.2.1	Duration	53
4.2.2	Distance	53
4.2.3	Percentage of fog plume per ventilation regime	54
4.2.4	Basic indoor parameters	55
4.3	Theoretical results	55
4.3.1	Duration	55
4.3.2	Distance	58
4.3.3	Basic indoor parameters	61
4.4	Comparison between the results of the portable fog generator system and the theory	62
4.5	Conclusion	64
5	Discussion	66
5.1	Interpretation	66
5.1.1	Air velocity	66
5.1.2	Temperature	66
5.1.3	Relative humidity	67
5.1.4	portable fog generator system	67
5.1.5	Airborne transmission through breathing in schools	67
5.2	Implications	68
5.3	Limitations	68
5.3.1	Layout	68
5.3.2	Manually operated	68
5.3.3	The presence of the operators	68
5.3.4	Low budget	68
5.3.5	Errors during the measurements	68
5.3.6	Unable to identify the droplet size	68

5.3.7	Time	69
5.3.8	No control on the other variables	69
5.4	Recommendations for further research	69
6	Conclusion	70
6.1	Instruments	70
6.2	Visualisation technique	70
6.3	Ventilation regimes	71
6.4	The optimal method to reduce the aerosol spread	71
6.5	The value of the portable fog generator system	71
A	Invoice of the materials for the portable fog generator	73
B	Logbook	75
C	Baseline measurement data	96
D	Video frame of the maximum travel distance per ventilation regime	101
E	Settling velocity and duration	103
F	MATLAB script	108
G	Comparison of the basic indoor parameters with MATLAB	113
	Bibliography	119

List of Figures

1.1	Transmission routes (Otter et al., 2016)	2
2.1	Schematic diagram of SARS-CoV-2	5
2.2	Droplet sizes affected by relative humidity	6
2.3	Respiratory droplets size distribution during talking	7
2.4	The effect of ventilation on the number of respiratory droplets (Somsen et al., 2020).	9
2.5	Wells curve (Wells, 1934)	10
2.6	Horizontal travel distances in metres at different velocities (Xie et al., 2007)	11
2.7	The settling velocity of particles in calm air	13
2.8	The settling velocity of particles as a result of stirred settling	13
2.9	Types of airflow pattern visualisation	14
2.10	Experimental setup of high-speed imaging (Scharfman et al., 2016)	15
2.11	Schlieren imaging (Tang et al., 2011a)	16
2.12	Setup of schlieren imaging (Tang et al., 2011a)	16
2.13	3D-printed head producing air-filled soap bubbles (Bluyssen, Ortiz, and Zhang, 2021)	17
2.14	Visualizing the effectiveness of face masks when the fog is exhaled through a manikin (Verma, Dhanak, and Frankenfield, 2020)	18
2.15	Setup mechanically breathing simulator with a fog machine (Arumuru et al., 2021)	19
2.16	Setup with using fluorescent ink (Ortiz, Ghasemieshkaftaki, and Bluyssen, 2021)	19
2.17	The fluorescent dye on the manikin's face and operator's clothes during the dental procedure (Teichert-Filho et al., 2020)	20
2.18	Visuals of a thermal manikin during exhaling tracer gas (Nielsen, 2009)	21
3.1	Overview of the SenseLab (Bluyssen et al., 2017)	23
3.2	Experiments conducted in the test chamber	24
3.3	Classroom setup in the experience room (TUDelft, 2017)	25
3.4	Heating, ventilation and air conditioning system	25
3.5	Ventilation system at the SenseLab (Bluyssen et al., 2017)	26
3.6	The four ventilation regimes	27
3.7	Layout of the SenseLab during the baseline measurements	28
3.8	Setup of the baseline measurements with the manikin	28
3.9	Measurements at three height levels	29
3.10	Measurements at the windows, ceiling inlets and plinths	29
3.11	Instruments needed for the portable fog generator system	30
3.12	Medium	31
3.13	Fog machine	32
3.14	Pipes	33
3.15	Buffer	33
3.16	The holes on the lid of the buffer	34

3.17 Pump	34
3.18 Manikin	35
3.19 Laser placements	36
3.20 Effect of using multiple lasers	37
3.21 Step 1: installing the buffer	38
3.22 Step 2: installing the pipe	38
3.23 Step 3: connecting the buffer and the pipe	38
3.24 Step 4: connecting the pipe with the pump	39
3.25 Step 5: placing the fog machine on the buffer	39
3.26 Step 6: connecting the pump with the manikin	39
3.27 Final setup of the portable fog generator system	40
3.28 Overview of the setup to capture the airflow pattern	41
3.29 The setup of the airflow pattern visualisation experiment by placing the camera behind the manikin	42
3.30 The distances between the manikin's mouth and the lasers are indicated with vertical lines	43
3.31 Image subtracting technique by the program Fiji	43
3.32 Subtraction technique on two different ventilation regimes	44
3.33 The greyscale ranging black to white	45
3.34 The mean intensity of two images	45
4.1 Air velocity of the four ventilation regimes	48
4.2 The average air velocities of the four ventilation regimes	49
4.3 The average air velocities at six locations	50
4.4 The average air velocity at different ventilation regimes at different heights	51
4.5 The average air velocity at different heights	51
4.6 The temperature of the four ventilation regimes	52
4.7 The duration until the droplets are not visible anymore	53
4.8 The travel distance of the droplets produced by the portable fog generator system	54
4.9 Results of the mean grey intensity in different ventilation regimes	55
4.10 The settling velocity with a particle diameter from 0.1—10 μm at 297.45 K	57
4.11 The duration in hours with a particle diameter between 0.1—10 μm at 297.45 K	58
4.12 The trajectory of particle sizes from 1—500 μm based on the basic indoor parameters of the experience room during the experiment	60
4.13 The trajectory of particle sizes from 10—100 μm based on the basic indoor parameters of the experience room during the experiment	61
4.14 The trajectory of particle sizes from 1—500 in combination with the airflow pattern experiment	63
4.15 The trajectory of particle sizes from 10—100 in combination with the airflow pattern experiment	64
A.1 Invoice of the materials for the portable fog generator	74
C.1 Baseline measurements: <i>no ventilation</i> and <i>natural ventilation</i> part 1.	97
C.2 Baseline measurements: <i>no ventilation</i> and <i>natural ventilation</i> part 2.	98
C.3 Baseline measurements: <i>mixing ventilation</i> and <i>natural + mixing ventilation</i> part 1.	99
C.4 Baseline measurements: <i>mixing ventilation</i> and <i>natural + mixing ventilation</i> part 2.	100
D.1 No ventilation. Distance = 1.3 metres.	101
D.2 Natural ventilation. Distance = 1.8 metres.	102
D.3 Mixing ventilation. Distance = 0.9 metres.	102

D.4	Natural + mixing ventilation. Distance = 0.5 metres.	102
E.1	The settling velocity with a particle diameter from 0.1—100 μm at 297.45 K. . .	104
E.2	The duration in hours with a particle diameter from 0.1—100 μm at 297.45 K. . .	104
E.3	The settling velocity with a particle diameter from 0.1—1 μm at 297.45 K.	105
E.4	The duration in hours with a particle diameter from 0.1—1 μm at 297.45 K.	105
E.5	The settling velocity with a particle diameter from 10—50 μm at 297.45 K.	106
E.6	The duration in seconds with a particle diameter from 10—50 μm at 297.45 K.	106
E.7	The settling velocity with a particle diameter from 50—100 μm at 297.45 K.	107
E.8	The duration in seconds with a particle diameter from 50—100 μm at 297.45 K.	107
G.1	The effect of the air velocity on the distance	114
G.2	The effect of the temperatures on the distance	116
G.3	The effect of relative humidity on the distance	118

List of Tables

2.1	Different classes of particles with the most important concern of particles $<7 \mu\text{m}$ (Probs, 2020).	12
4.1	The temperature and relative humidity during the airflow pattern visualisation experiment.	55
4.2	Settling velocity for particle diameters from 0.1 to 100 μm based on the temperature of the experience room.	57
G.1	The increase in horizontal distance when coughing (10.6 m/s).	113
G.2	The increase in horizontal distance when sneezing (46 m/s).	113
G.3	Height difference between $T = 19.3\text{—}24.3 \text{ }^\circ\text{C}$	115
G.4	Height difference between $T = 24.3\text{—}29.3 \text{ }^\circ\text{C}$	115
G.5	Height difference between $T = 24.3\text{—}34.3 \text{ }^\circ\text{C}$	115
G.6	Height difference between $\text{RH} = 10.7\text{—}50.7\%$	117
G.7	Height difference between $\text{RH} = 30.7\text{—}50.7\%$	117
G.8	Height difference between $\text{RH} = 50.7\text{—}70.7\%$	117
G.9	Height difference between $\text{RH} = 50.7\text{—}90.7\%$	117

Chapter 1

Introduction

1.1 The impact of COVID-19

On December 31st of 2019, the first report identifying the coronavirus disease 2019 (COVID-19) was published in Wuhan, China. During the following three months COVID-19 spread throughout most parts of the world. On February 11th of 2020, the World Health Organization (WHO) officially declared the spread of COVID-19 a global pandemic (Huang et al., 2020). The coronavirus disease is caused by infection with the severe acute respiratory syndrome coronavirus 2 (SARS-CoV-2). The period between exposure to an infection and the appearance of the first symptoms (the incubation period) ranges from 2–14 days. (Gorbalenya et al., 2020). Hence, it can take at least 5–6 days before the first symptoms are experienced (WHO, 2021). However, some infected people are asymptomatic and are unknown carriers of the virus. Common symptoms include fever, cough, dyspnea, cold complaints, myalgia and sudden loss of smell or taste. The disease can cause serious illness and in the worst case can lead to death if not treated properly (Wang et al., 2020). The origin of the coronavirus has yet to be identified, although it is likely from a zoonotic source such as pangolins or bats as both animals were associated with SARS outbreaks in the past (Zhu et al., 2020). SARS-CoV-2 has a spherical form with an average diameter of 0.065–0.125 μm . However, the virus is always bonded to water droplets increasing the total size to larger than 1.0 μm . The virus can be filtered with face masks to prevent further distribution of the virus. The virus can linger in the air for many hours. Environmental conditions (e.g. air velocity, temperature and relative humidity) affect the lifespan of the virus. To slow down or halt the spread of COVID-19, preventive measures are necessary. These measures include wearing face masks, applying adequate hygienic measures, social distancing, vaccination and applying adequate ventilation (Oran and Topol, 2021).

1.2 Transmission routes

During the beginning of the global pandemic, the WHO stated that the coronaviruses can only be transmitted through droplets (coughing, talking or sneezing), indirect contact (via fomites) or direct contact (shaking hands). Transport by droplets is considered to be airborne transmission. Initially, it was thought that only large respiratory droplets played a role in the transmission of COVID-19 as smaller droplets (aerosols) would evaporate faster, thus less likely to infect other users (Ram et al., 2021). At first, it was not thought that aerosols can linger in the air for many hours and travel long distances. However, as more evidence regarding SARS-CoV-2 was published, more evidence hinted towards airborne transmission of COVID-19 through aerosols (Morawska et al., 2021, Miller et al., 2020). In Figure 1.1 the four different transmission routes are shown.

The focus of this thesis lies in airborne transmission of COVID-19. The aerosols play an important role in respect to indoor air filtration and building ventilation. Indoor environments with poor ventilation are prime hotspots, as aerosols can accumulate in the room. Aerosols require a longer time to fall to the floor in a poorly ventilated room. This increases the chance of a person becoming infected when he or she passes through another person's breathing space.

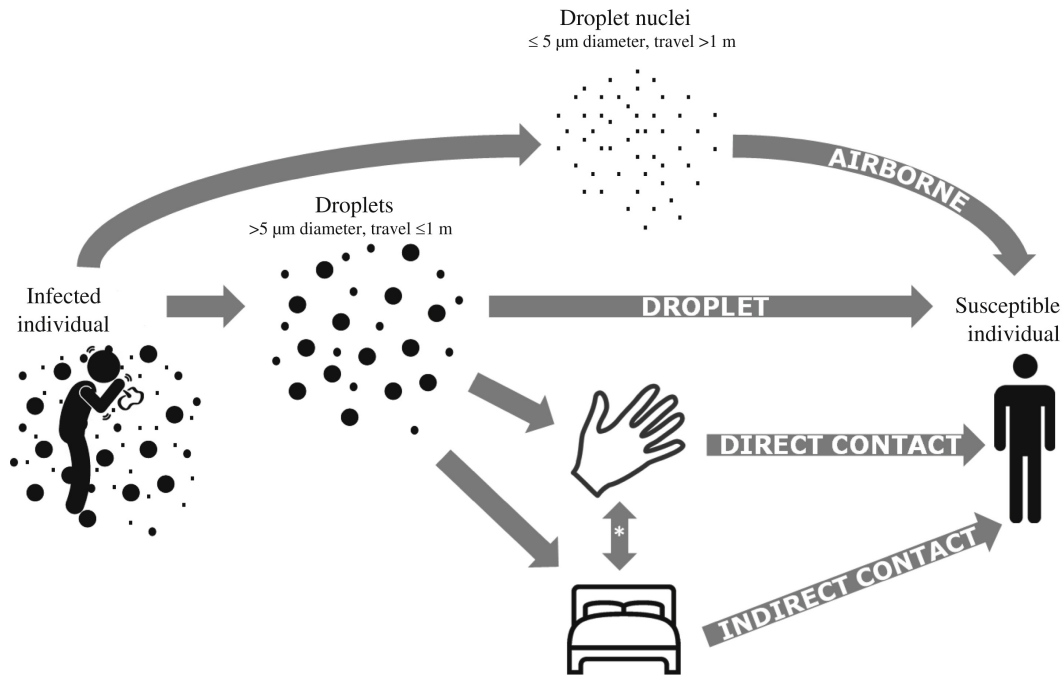


FIGURE 1.1: The infected individual on the left is the source and the susceptible individual on the right is the receiver. Four transmission routes are displayed here: airborne, droplets, direct contact and indirect contact (Otter et al., 2016). Used with permission from the author.

1.3 Schools in the Netherlands

Classrooms are perfect settings for outbreaks as a large number of people stay there for a long period while sharing the same indoor air. The Dutch government established the National Ventilation Coordination Team (LCVS) to research the relationship between ventilation, air quality and virus distribution through the air at educational buildings by placing CO_2 monitors. Only 38% of all 7340 elementary and secondary schools in the Netherlands meet the ventilation requirements from the Building Decree of 2012 (LCVS, 2020). A third of the schools only have natural ventilation, which is often inadequate to supply enough fresh air in the classroom. Mechanical ventilation is an option to increase the fresh air supply if needed. An emphasis on the importance of adequate ventilation in educational buildings is needed urgently to reduce the risk of airborne transmission.

1.4 Objective and research questions

Many educational buildings are not properly ventilated (LCVS, 2020). This poses a problem, as proper ventilation is necessary in order to reduce the amount of coronavirus in the air in a classroom. The objective of this thesis was to design and assemble a portable fog generator system to visualise the airflow pattern of aerosols produced by pupils in a classroom. This system mimics human breath and can be brought to schools to determine where the aerosol accumulation is located. This indicates if additional ventilation measurements are needed. To achieve the objective of this thesis, the following main question is formulated:

'How is the airflow pattern of 'exhaled' droplets affected in a classroom under different ventilation regimes?'

The sub-questions are defined as follows:

1. Which instruments are needed to assemble a portable system mimicking the human breath?
2. How can one record and analyse the visualisation of the exhaled droplets?
3. How do different ventilation regimes affect the airflow pattern?
4. What is the most efficient method to reduce the spread of aerosols in classrooms through ventilation?
5. What is the added value of this portable system in airborne transmission control at educational buildings?

1.5 Scope

The scope of this thesis is limited by the following aspects:

- The setup of the portable fog generator system is a simplified representation of the complex human respiratory system.
- The experiments were conducted in a simulated classroom in the SenseLab instead of a real classroom.
- The experiments were based on a single imaginary pupil sitting on a chair behind the desk in the classroom. Aside from this pupil, there were no other occupants in the room except for the operators during the experiments.

1.6 Outline

Chapter 1 begins with an introduction on the topic, presents the research question, scope and structure of the thesis. In Chapter 2 an overview of the literature regarding the different parameters affecting the spread of SARS-CoV-2 and state of the art experimental studies visualising the airflow pattern are presented. The research methods and information regarding which data were needed and how to analyse this is discussed in Chapter 3. Additionally, the process of designing and assembling the portable fog generator system is described here as well. In Chapter 4 the results are presented. Chapter 5 discusses the most important findings of the results and recommendations are given for further research. Chapter 6 concludes this report by answering the research questions and presenting the conclusions.

Chapter 2

Literature review

This chapter begins with a literature review of how the entry mechanism of the virus operates. Different parameters affect the lifespan of droplets and aerosols. These parameters determine how the particles behave in such conditions. All this information is used to calculate the distance particles can travel and the duration they linger in the air. Different case studies will be discussed. The second part of this chapter describes different techniques used in visualising the movements of the droplets and aerosols. Each technique has its benefits and disadvantages, therefore it is important to determine the technical gap of each one of these techniques. The information is used to learn which technique(s) is the most applicable to design and assemble a portable fog generator system to visualise the human breath.

2.1 Indoor environmental factors affecting SARS-CoV-2

The conditions of the indoor environment can increase the infectious rate of the virus. Low relative humidity increases the number of aerosols that can be formed, due to the increased possibility of evaporation. The temperature influences the inactivation of the virus. It seems that high temperatures reduce the lifespan of the virus in the droplet. The indoor air velocity regulates the distribution of the droplets. Research can determine whether strong air currents cause exposure to larger droplets further than 1.5 metres, increasing the chance of direct transmission (Dbouk and Drikakis, 2020).

2.1.1 Mechanism of action

The entry mechanism of SARS-CoV-2 and its structural characteristics provide insights into understanding how it is responsible for airborne transmissions. The virus is composed of mainly four structural proteins: spike (S), envelope (E), membrane (M), and nucleocapsid (N) proteins as can be seen in Figure 2.1.

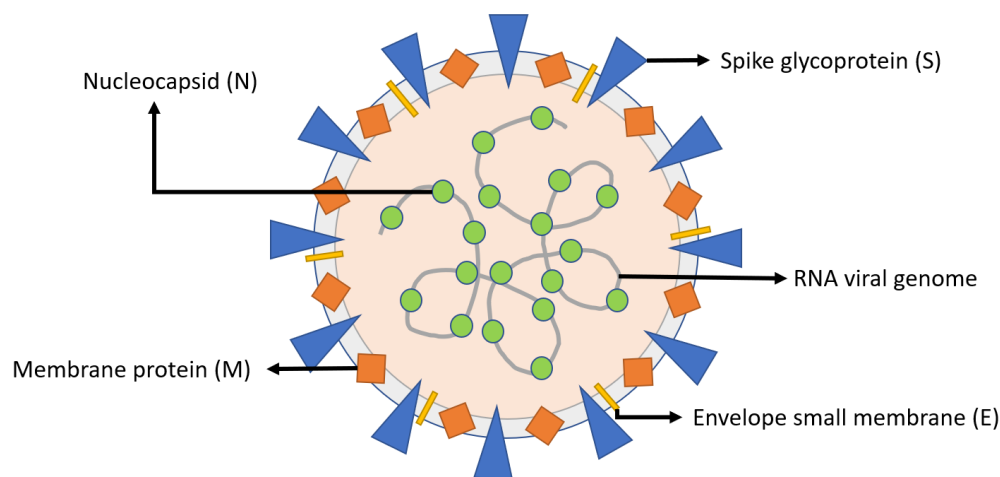


FIGURE 2.1: Schematic diagram of the SARS-CoV-2 coronavirus particle with the four structural proteins. Adapted from Min and Sun, 2021.

The S-protein is used to enter the human cell. This protein has a shape similar to a crown, from which the Latin name Corona is derived. The proteins act like grappling hooks that allow the virus to latch onto the membrane of the host cells and crack them open for infection (Wrapp et al., 2020). The E-protein is the smallest structural protein. It aids the assembly of new virus particles once it has infected a cell. The M-protein is the most abundant protein on the viral surface and it is believed to be the central organizer for the coronavirus assembly (Masters, 2006). The N-protein gives the virus its structure and enables it to replicate. The virus' envelope is made from a layer of lipids, a waxy barrier containing fat molecules as well as protecting the genetic code. It will break down in contact with soap. This is the reason why hand-washing with soap is important to prevent the spread of the virus (Wong and Saier, 2021).

2.1.2 Droplet size

Droplets and aerosols are released through talking, breathing, coughing and sneezing. These particles leave the human airways at almost 100% relative humidity (RH) into the indoor

environment where the RH of the air is much lower. The RH induces the droplet size transformation and affects the inactivation rates of the virus (Yang and Marr, 2011).

The Köhler theory is applied to determine the final size of the droplet. The hygroscopic growth of particles is composed of proteins and inorganic salts and is based on equilibrium thermodynamics. This equilibrium describes that there is no tendency for the state of a system to change spontaneously. The evaporation rate of water droplets of different diameters in the air is defined as Equation (2.1) (Holterman, 2003):

$$\frac{dD}{dt} = \frac{4M_L D_\infty P_a (1 + 0.276 Re^{1/2} Sc^{1/3})}{RT_\infty} \ln \left[\frac{1 - p_{sat}(T_w)/P_t}{1 - RH \cdot p_{sat}(T_\infty)/P_t} \right] \quad (2.1)$$

where:

$\frac{dD}{dt}$ = evaporation rate of the droplet's diameter [m/s]

M_L = molecular mass [kg/mol]

D_∞ = diffusion coefficient of vapor

P_a = atmospheric pressure of air [Pa]

RH = relative humidity of the indoor air [%]

p_{sat} = saturated vapour pressure [Pa]

R = gas constant of 8.3144 [J · mol⁻¹K⁻¹]

T_∞ = indoor air temperature [K]

T_w = wet-bulb temperature [K]

Sc = Schmidt number, calculated with $\mu_a/\rho_a D_\infty$ (Seinfeld, 2016).

The water particles around the virus start to evaporate until they reach equilibrium and shrink up to half their original diameter as seen in Figure 2.2. The rate the water evaporate depends on the chemical composition of the virus and RH of the indoor environment. At 50% RH, the salt concentrations rise sharply due to the water loss and can deactivate most of the virus. Below 30% RH, the 'dry' aerosol releases even more water to the indoor environment. As a result, the dissolved salts start to crystallise and the salts are not harmful to the virus anymore. The viruses are more active and can be infectious for longer as they remain much longer in the air (Gómez et al., 2014).

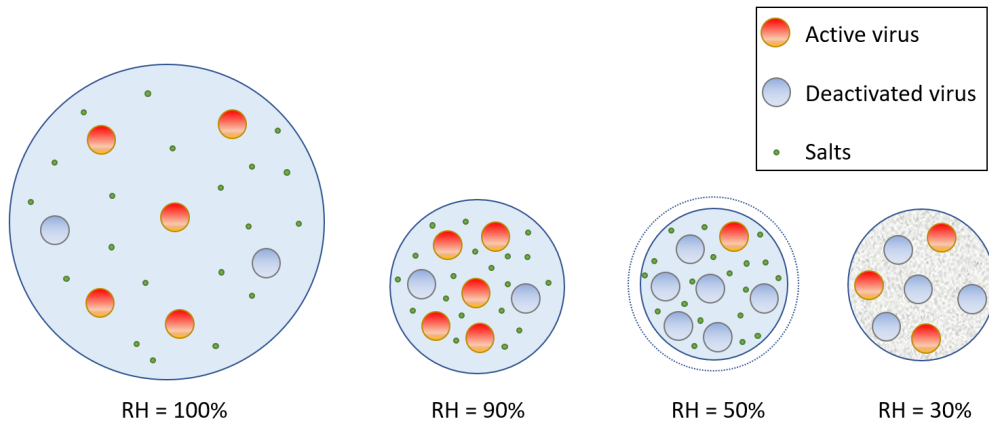


FIGURE 2.2: The aerosols consist of active, deactivated viruses and salts. At 90% RH, the exhaled droplets shrink to almost half of their original diameter. At 50%, the aerosols shrink even more and cause the viruses to be deactivated due to the rise of the salt concentration. At 30%, the dry aerosol preserved the viruses through crystallisation of the dissolved salts.

The study of Xie measured the size distribution of respiratory droplets during talking (Xie et al., 2009). Figure 2.3 shows the distribution of various diameters of droplets. A total of 5138 droplets were measured ranging from 0—1500 μm . About 37% of the measured respiratory droplets are smaller than 50 μm , which are more prone to linger in the air for a longer period and evaporate before falling on the ground. The droplets with a diameter of >75 μm are more likely to fall on the ground before evaporation.

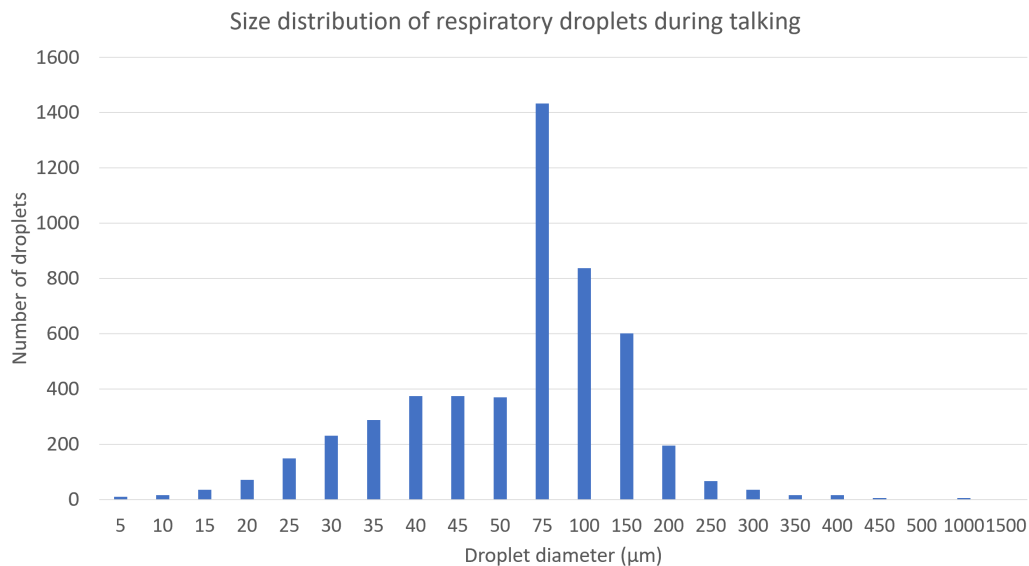


FIGURE 2.3: Respiratory droplets size distribution during talking. The majority of the droplets are larger than 75 μm and will fall on the ground before evaporation. Adapted from Xie et al., 2009.

2.1.3 Impact of temperature and relative humidity

The survival of SARS-CoV-2 depends on environmental factors such as temperature and relative humidity. In 1965, the first human coronaviruses were discovered, namely 229E and OC43. Casanova et al. (2010) investigated these two virus species to have a better understanding of how these viruses survive while influencing the temperature and RH. The specimen was placed on the stainless steel surface and various environmental parameters were altered. The result showed there is a linear relationship between the survivability of the virus and the temperature. The inactivation progress was faster at 40°C than at 20°C. The virus survived the longest when the RH is below 20% and above 80%, with 50% being the best value to rapidly increase the inactivation.

Biryukov et al. (2020) investigated the lifespan of the virus by placing it on nonporous surfaces and increasing the relative humidity and temperature. The results show that the lifespan ranged from 6.3—18.6 hours, depending on the RH between 20—80% with an indoor temperature of 24°C. By increasing the temperature to 35°C, the half-life of the virus was reduced to 1.0 to 8.9 hours.

Wu et al. (2020) studied the relation between daily cases and deaths due to COVID-19 by analyzing meteorological conditions of 166 countries (excluding China). By using a log-linear generalised additive model (GAM) to analyze the effects of different variables such as temperature, relative humidity, wind speed, median age of the population, human development index and population density. The findings provide preliminary evidence that the spread and viability of COVID-19 seem to be lower in warm and hot climates. Wu noticed that an

increase in both relative humidity and temperature decreased the daily infected cases. It seems that countries near the equator were not greatly affected by the spread of COVID-19, especially in the tropics where high RH and temperature characterize the weather. The high temperature caused the breakdown of the M-protein of the virus (Raamsman et al., 2000). In a colder environment, the virus is more stable and can sustain much longer in the 'dry' air. It makes the human host much more susceptible to viruses as the mucous membranes and nasal systems are more amenable below a RH of 20% (Kudo et al., 2019).

To reduce the transmission of SARS-CoV-2 in buildings, an optimal configuration of indoor temperature and relative humidity needs to be achieved. Lowering the RH to between 40—65% would likely have little impact on reducing the lifespan of the virus (Lynch and Goring, 2020). The virus is highly susceptible above a temperature of 30°C and relative humidity of at least 78% (Raines, Doniach, and Bhanot, 2021). However, these values are not attainable due to the thermal comfort of the users within the building. A better solution is to reduce the transmission of the virus in the air as much as possible, for example by applying adequate ventilation.

2.1.4 Ventilation in buildings

Many buildings are not properly facilitated with ventilation and filtration systems. These are necessary to reduce the spread of SARS-CoV-2 as ventilation plays a significant role in the current pandemic. Natural ventilation, such as an open window, seldom provides sufficient ventilation if the room on the opposite wall has no air pressure difference.

Without proper ventilation, every indoor environment can be dangerous as the aerosols and large droplets are accumulating in the air, thus increasing the risk of being infected through airborne transmission. An effective method is to increase the amount of fresh air so that the infected particles are removed through ventilation and the larger droplets settle down due to gravity on surfaces (Yang and Marr, 2011). This is defined as the air exchange rate and describes how much fresh outdoor air is brought into the room to remove the 'old' air in *litre per second per person (l/s/p)*. The air exchange must not adversely affect people's health. With ventilation, the removal of 'old' air and a direct supply of fresh outside air are required. In educational buildings, it is recommended to use a minimum air exchange rate of 11 l/s/p and preferably 14 for slightly physically strenuous work (RIVM, 2021).

Somsen et al. (2020) measured the amount and duration of respiratory droplets during speech and coughing. The number of particles passing through a stationary laser sheet was counted and measured by using an algorithm that detects reflections caused by the particles. Although the experiment was done with healthy volunteers, the droplet size distribution was comparable with someone who had the virus. The results in Figure 2.4 show that the amount of the droplets, in a room without ventilation had halved in about 5 minutes. By using any form of ventilation resulted in a much lower amount. This shows the importance of ventilation in an enclosed environment to decrease the spread of the coronavirus.

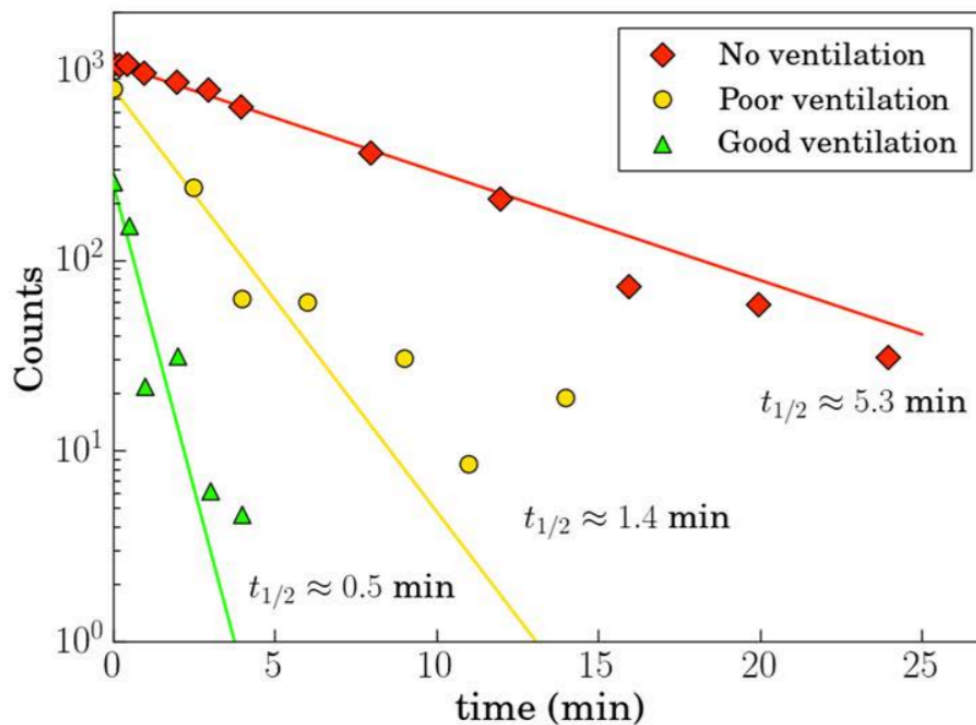


FIGURE 2.4: Three different ventilation regimes were tested: no ventilation, mechanical ventilation and mechanical + natural ventilation. (Somsen et al., 2020). Used with permission from the author.

The combination of large indoor gatherings and a low air exchange rate can lead to a superspreading event. This happened during a choir rehearsal at the Skagit Valley Chorale in Washington. After a choir practice of 2.5 hours, 87% of the group developed confirmed symptoms of SARS-CoV-2 (Hamner et al., 2020). The facility was badly ventilated, while everyone was singing next to each other. It was a recipe for disaster, as this led to a significant accumulation of aerosols (Miller et al., 2020).

Another case was a COVID-19 outbreak at a restaurant. Researchers noticed a relation between the airflow from an air conditioner and the spread of the coronavirus. They established this based on numerical simulation and analysis of nine people who ended up in a restaurant. The cause for the outbreak is the lack of fresh air supply. The indoor air was contaminated with the virus and could not be diluted or replaced with fresh air (Lu et al., 2020).

Schijven researched the effectiveness of different mechanical ventilation rates by reviewing articles on speaking, coughing, sneezing, singing and breathing by infected persons. By increasing the ventilation rate from 100 to 600 m^3/h , the number of aerosol droplets decreased by a factor of 8 to 13 for sneezing and coughing. In other scenarios, this factor is reduced to a factor of 4 to 9 (Schijven et al., 2021).

Air filters

High-Efficiency Particulate Air (HEPA) are used to filter pollution from the indoor air. This special type of filter is commonly used in aeroplanes and hospitals. It captures microscopic particles such as dust, pollen, bacteria and particulate matter. The 'true' HEPA must remove at least 99.97% of all particles between 0.15–0.20 μm and are graded for the particle size they

perform worst at. While the SARS-CoV-2 virion ranges from $0.06\text{--}0.14\ \mu\text{m}$, the coronavirus tends to travel in droplets that are larger than $0.30\ \mu\text{m}$ which fit within the range of the HEPA filters (Fehr and Perlman, 2015). The particles travel through the filter and are trapped with different fibreglass diameters, ranging from $0.002\text{--}0.5\ \mu\text{m}$. Minimum Efficiency Reporting Value (MERV) filters can also be used. This filter can remove up to 75% of the coronaviruses in the air, which can reduce the flow of particles to $>0.3\ \mu\text{m}$. MERV filters can be installed at most standard ventilation systems while having low operation energy cost in comparison with the regular HEPA filter.

The virus particles that have not perished yet by the HEPA filter can be inactivated by using ultraviolet (UV) lighting. It purifies and sterilizes the particles by tearing down the DNA to remove the membrane wall of the viruses, thus preventing them from spreading in the air (Sabino et al., 2020). This method of killing bacteria and viruses is primarily used at hospitals and airports. It is also used in environments where there is no access to ventilation or filtering of the air supply. Some air purifiers use a built-in corona UV-C lamp to neutralise the virus, bacteria and fungi even before these micro-organisms enter the filter. By using a lower wavelength ($207\text{--}221\ \text{nm}$) the damage on human tissues is prevented (Buonanno, Stabile, and Morawska, 2020).

2.1.5 Distance

William F. Wells was one first researchers who studied the evaporation of respiratory droplets of different sizes and is known for the Wells curve in Figure 2.5. It gives information about how far and how long the respiratory droplet will sustain in the air after exhalation. Wells assumed that droplets would either completely evaporate before hitting the ground, while droplets larger than $170\ \mu\text{m}$ in diameter fall on the floor within the 6-foot rule (1.8 metres) from the source.

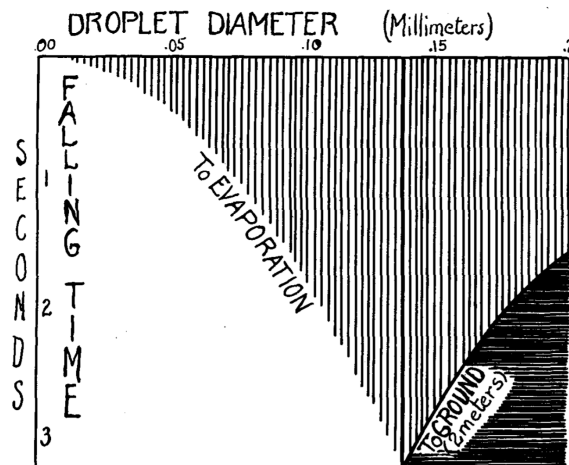


FIGURE 2.5: Falling and evaporation times of droplets of varying diameter at 18°C . On the horizontal axis are the diameters of the droplets. The vertical axis describes the duration in seconds before the droplets fall on the ground. According to the chart, droplets up to $170\ \mu\text{m}$ in diameter fall would completely evaporate before falling to the ground of a 2-meter height (Wells, 1934). Used with permission from the author.

During the beginning of the pandemic, several countries started to adopt a required 1.5 or 2-meter distance rule, assuming that it would prevent the spread of the virus (GOV, 2021).

At the time of writing, the WHO recommended a 1-meter social distancing policy on the assumption that only large droplets transmit SARS-CoV-2 (WHO, 2021). However, different authors have doubted if Well's 6-foot rule was sufficient to protect against the spread of the coronavirus. The study of Well lacked empirical data, many assumptions were made and a simplified calculation was used.

Dbouk and Drikakis (2020) made a numerical model to research how far droplets could travel at different air velocities. The respiratory droplets settled within 2 metres when the air velocity was nearly zero. In the case of 4–15 km/h, droplets can travel up to 6 metres and decrease in both concentration and size.

A study by Bourouiba has shown that respiratory droplets, produced from sneezing, coughing and breathing, can travel up to 7–8 metres (under perfect favourable environmental conditions) at a horizontal distance from the source and sustain in the air for a few minutes (Bourouiba, 2020).

Xie et al. (2007) made a numerical model to study how far respiratory travel by using droplet size ranging from 0.3–200 μm . According to the results, some droplets can travel more than 6 metres in the horizontal direction. This depends on the RH of the environment and initial jet velocities between 1–50 m/s. Simulations were conducted with different initial jet velocities at how far the droplet travels in the horizontal distance in Figure 2.6. The particles with a smaller diameter have a shorter lifespan as they evaporate quickly, while the large droplets settle due to gravity. The sweet spot of the droplet lies between 30–50 μm . At a velocity of 1 m/s most of the droplets start to evaporate. While sneezing (50 m/s) results in droplets travelling much further than 6 metres.

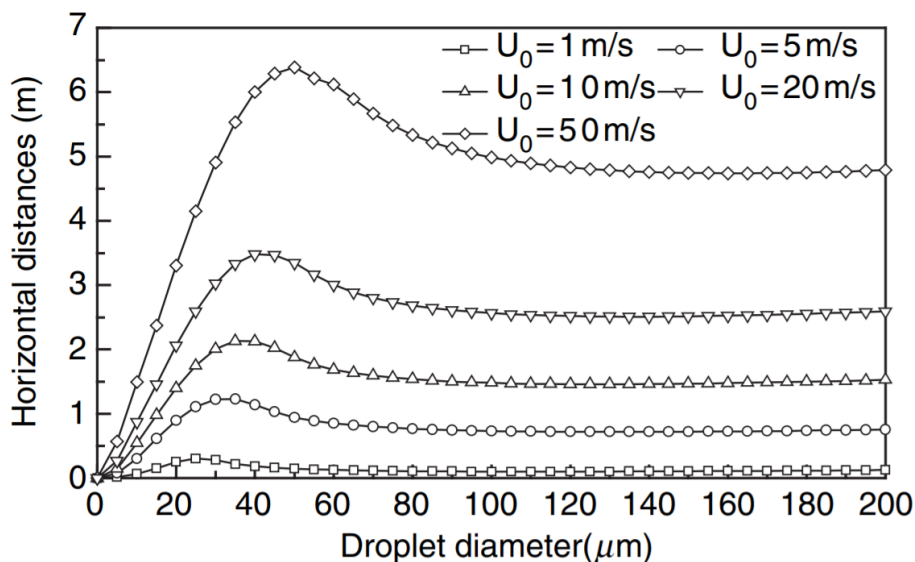


FIGURE 2.6: Horizontal travel distances at different velocities. The higher the initial jet velocities, the further the droplets reach. Droplet diameters above 50 μm will fall on the floor due to gravity (Xie et al., 2007). Used with permission from the author.

It is difficult to determine how far the virus can travel, as respiratory droplets come in different sizes and various environmental factor influences the path it takes. Current evidence suggests that long-range transmission of a few metres of the coronavirus occurs inconsistently, though it is certain that transmission via aerosols is evident. Although most exhaled

particles fall within short range, most rooms have a low indoor air velocity of around 0.1 m/s . The airflow of the room will be more govern than gravity to settle this small particle within 2 metres of the source (Bourouiba, 2020).

2.1.6 Duration

The size of a particle is one of the main characteristics to determine how long it will sustain in the air. The size of respiratory droplets is immediately reduced after exhalation due to differences in the RH of the mouth and environment. While larger particles of $>1350 \mu m$ are dominated by Newton's law, smaller particles are governed by Stokes' law. The velocity of a falling droplet, in still air, can be calculated by using Stokes' law when the Reynolds number is <1 (eq. 2.2):

$$v = \frac{gd^2\rho_p C}{18\mu} \quad (2.2)$$

where:

v = settling velocity [m/s]

g = gravitational field strength [m/s^2]

d = particle diameter [m]

ρ = density of the particle [kg/m^3]

C = Cunningham correction factor

μ = dynamic viscosity [$Pa \cdot s$]

The average distance between a particle before hitting other particles is called the mean free path. When d approaches the same size as the mean free path of air particles, it will cause the drag force to be smaller than what has been predicted by Stokes' law. Therefore, C is used to correct the formula as d becomes smaller. An overview of different classes of particles is given in Table 2.1

Particle diameter [μm]	Physics law	Description
>1350	Newton	Very large droplets
100-1350	Stokes	Small droplets
7-100	Stokes	Aerosol particles
<7	Stokes	Aerosol particles + slip correction factor

TABLE 2.1: Different classes of particles with the most important concern of particles $<7 \mu m$ (Probs, 2020).

The result of Stokes' law can be seen in Figure 2.7. Aerosols are considered to have a diameter $<5 \mu m$ and should fall within the 6-foot range. According to the graph, it takes at least 30 minutes for a particle to fall on the ground from a height of 1.5 metres. Within that given time there is enough room for the particle to travel beyond 6-foot as it can be carried through local turbulent airflows. The same principle can be applied for larger particles ($>100 \mu m$).

In most scenarios, the indoor air velocity is not stationary. The air particles in classrooms are constantly being disturbed, causing a stirred settling. By reducing the aerosol concentration by a factor of 10, an estimation is given how long it will take for the aerosols to fall from a height of one meter in Figure 2.8.

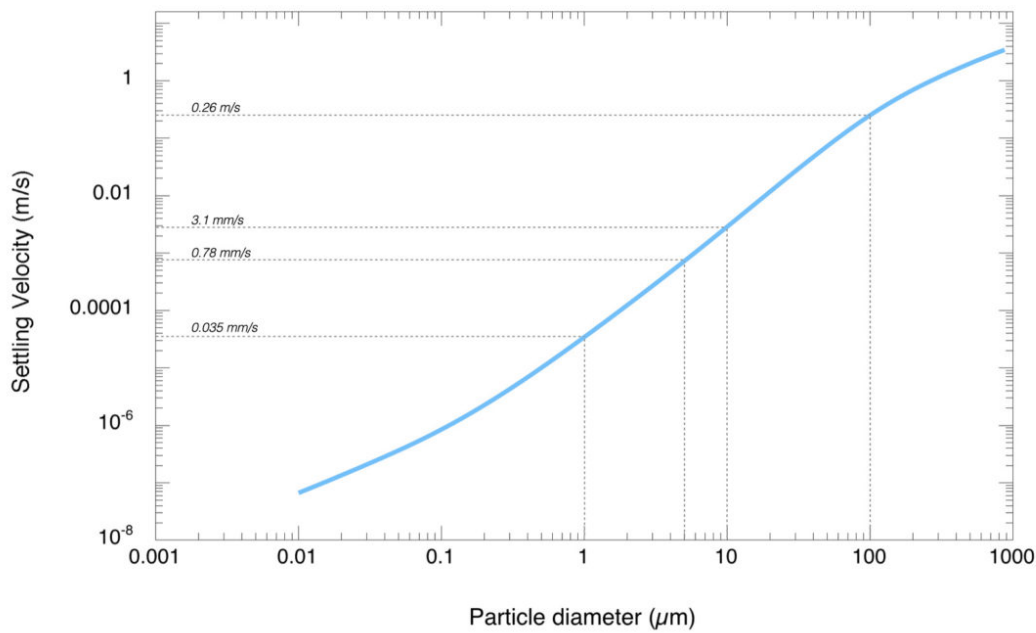


FIGURE 2.7: The velocity of different sized particles in calm air, with the following indoor values: density of 1000 kg/m^3 , air temperature of 293.15 K and air pressure of 101.3 kPa (Kulkarni, 2011, edited by Andrew Maynard). *Used with permission from the author.*

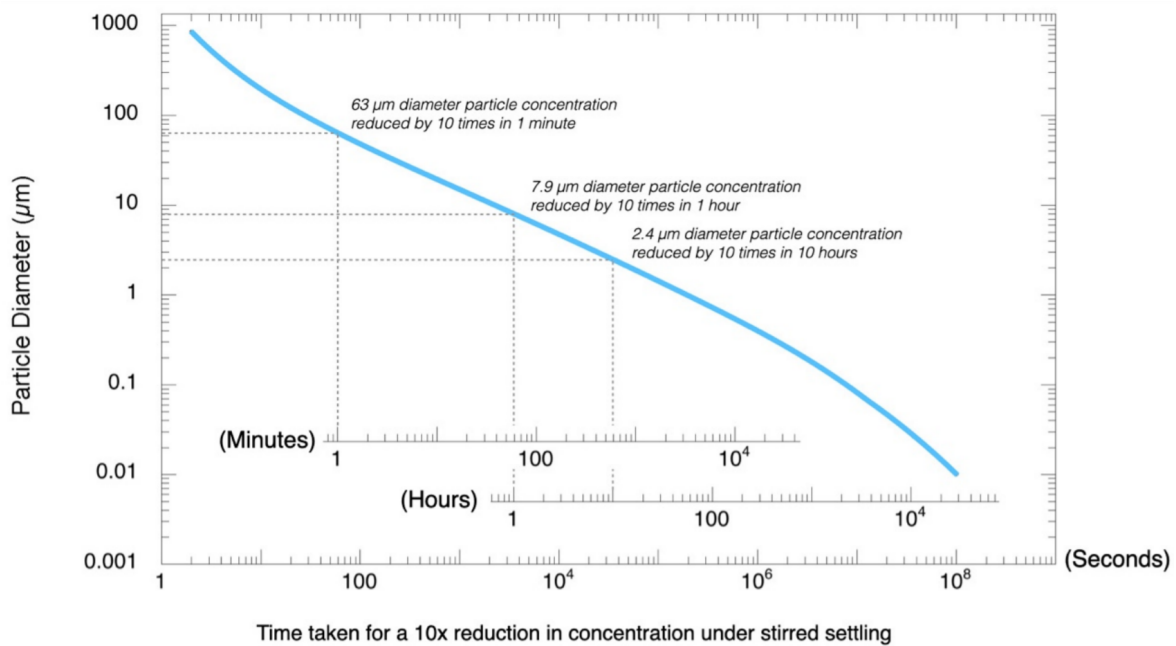


FIGURE 2.8: The velocity of different sized particles, under stirred settling falling, from one meter. The following values were used: density of 1000 kg/m^3 , air temperature of 293.15 K and air pressure of 101.3 kPa (Kulkarni, 2011, edited by Andrew Maynard). *Used with permission from the author.*

2.2 Airflow pattern visualisation

The primary objective of the visualisations is to create evident visuals that can be understood by everyone. It gives the audience direct information without reading any text. The visuals can help to create awareness of how ventilation affects the airflow pattern of aerosols. The emphasis is to demonstrate how aerosols spread after exhalations. An overview of the different visualisation techniques is shown in Figure 2.9. The first step is to decide whether to use the characteristics of the human respiratory system or (thermal) manikins to simulate a pragmatic scenario. The next step is the type of medium to produce the droplets. This can be either saliva, glycol, fluorescent ink, air-filled soap bubbles or gas.

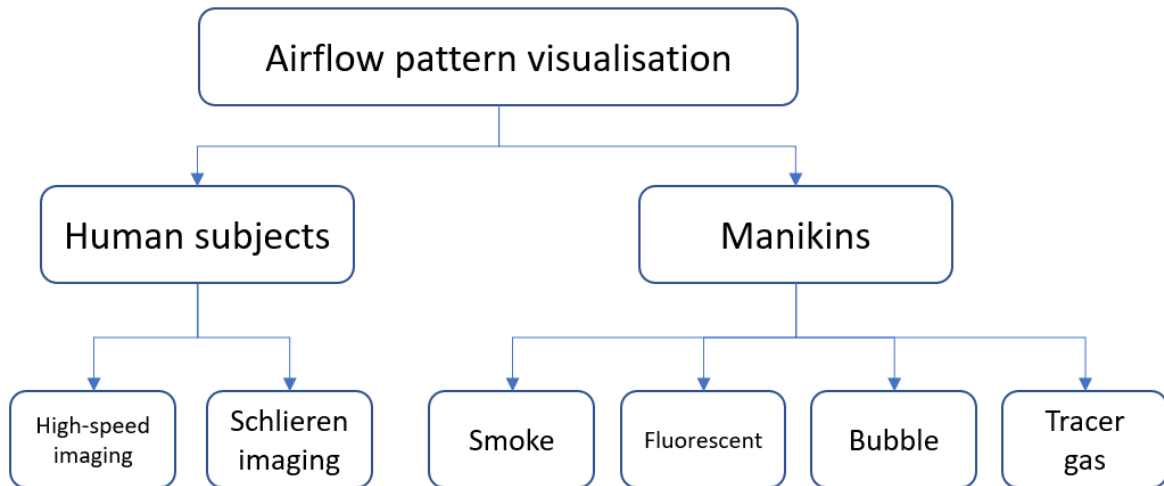


FIGURE 2.9: The airflow pattern visualisation is done with either human subjects or manikins. Different techniques can be used, depending on the type of simulation.

2.2.1 Human subjects

The experiments with human subjects are preferred as it creates a realistic scenario. The medium of saliva and complex respiratory system are difficult to replicate. An important factor is the physical difference between every human subject. The respiratory behaviour differs greatly depending on various factors of the person such as age, sex, height, respiratory diseases and health issues. The best method is to have a large number of participants to get an accurate result. Using human subjects is only applicable if there is no risk of mental or physical damage involved. The use of gas or fluid should be limited as much as possible as high doses might affect the health.

High-speed imaging

A straightforward setup to capture the airflow pattern of droplets is to use a high-speed camera to capture the respiratory droplets, while the human subject stands behind a black background (Figure 2.10). This special type of camera can capture up to 8000 frames per second. A bright light source needs to illuminate the area where the droplets are located. This increases the contrast as the droplets scatter the light into the camera. A white diffuser can be used to capture the droplets at close range to create better visuals (Scharfman et al., 2016).

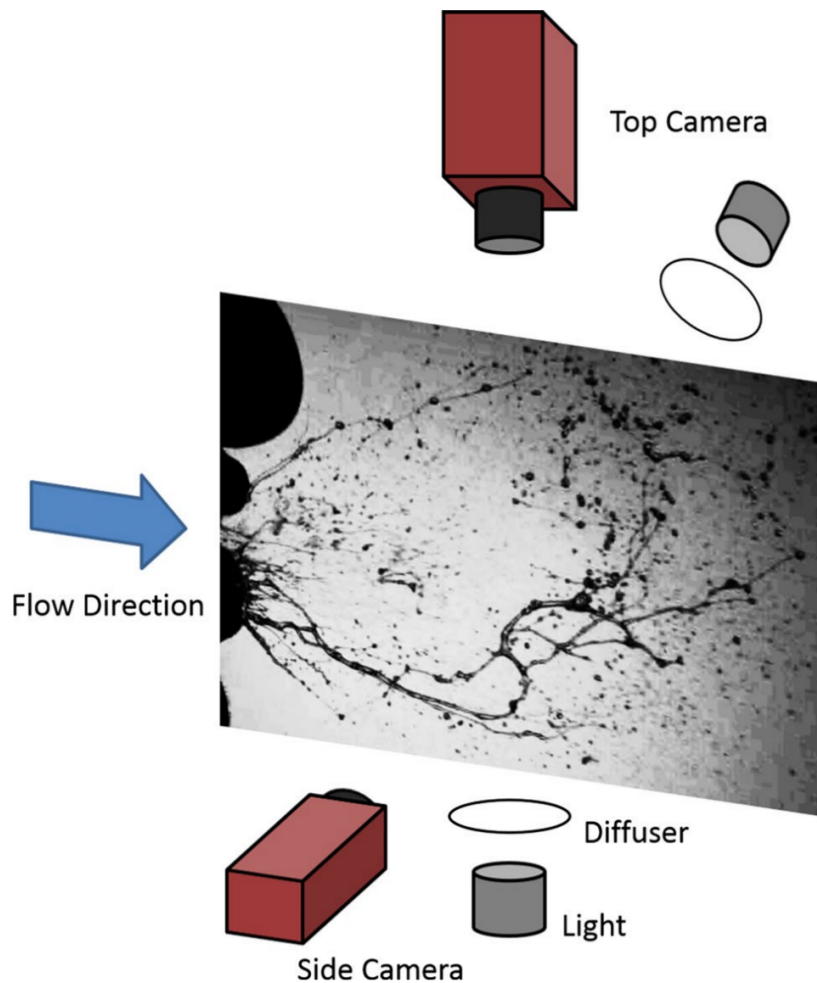


FIGURE 2.10: The experimental setup of high-speed imaging (Scharfman et al., 2016). *Used with permission from the author.*

Schlieren imaging

The schlieren imaging technique is used to visualise differences in air currents, temperature gradient, pressure and composition of air (Figure 2.11). The light rays are deflected due to differences in temperature and densities of the air current between the human breath and the indoor environment. The exhaled human breath varies between 29–32°C and the indoor room temperature ranges from 18–25°C (Pifferi et al., 2009). This technique does not show the droplets or how the virus particles are transported.



FIGURE 2.11: The subject stands one meter in front of the spherical mirror and exhales. The visual of the breath can be seen due to the difference in temperature of the breath and room (Tang et al., 2011a). *Used with permission from the author.*

The setup consists of four main components as seen in Figure 2.12. A (high-speed) camera with a telephoto lens. It must have a good optical zoom-in feature. The second component is a telescope mirror with a long focal length (around $f/5$). A point light source is needed, such as an LED. The light source diverges in the spherical mirror and converges back to something that 'cuts' the light. An item with a sharp edge, such as a knife-edge or razor blade is sufficient.

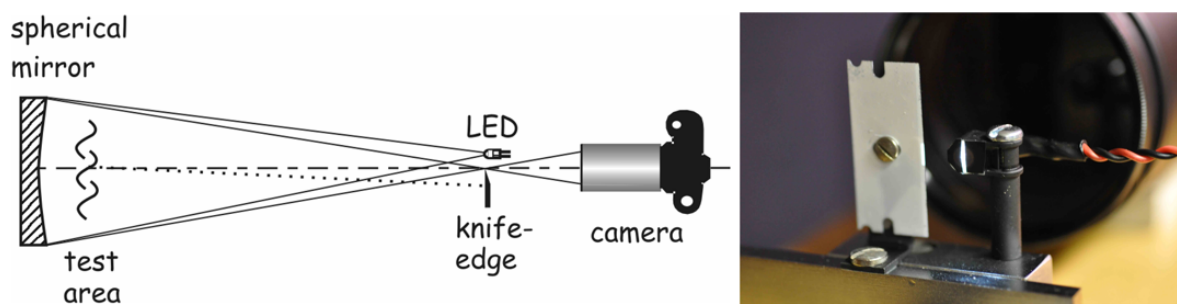


FIGURE 2.12: The schematic setup of schlieren imaging (left). The positioning of the point light source and the razorblade is important to able to create the schlieren imaging effect (Tang et al., 2011a). *Used with permission from the author.*

The main advantage of the schlieren imaging technique is that there are no possible hazardous fluids is needed to visualise the airflow. The option of using human volunteers allows a realistic airflow pattern, rather than using a manikin. It also allows the option

of performing different respiratory actions much easier. The light source is also much less intense than using lasers, which could damage the eyes. It is possible to collect footage without darkening the room. However, the test area is limited as the size of the spherical mirror determines how much of the airflow pattern can be seen. The human volunteer must stand perpendicular to the camera to be able to record the airflow pattern well enough.

2.2.2 Manikins

Manikins are human-shaped heads used to simulate different real-life scenarios for experimental usage. The most common type is the thermal manikin. Its surface can be heated to simulate the heat transfer between a human and its environment. A typical application is to analyse the thermal comfort of indoor environments with different temperatures, relative humidity and ventilation regimes. Some tests are also done to evaluate the clothing insulation value. The more advanced manikins also have a built-in respiratory system to simulate human breathing through the nose or mouth. Manikins can be used in situations when the use of a human subject is not applicable. This makes the manikin a great alternative in its use.

Bubble

Soap bubbles filled with air were used to visualise aerosols (Figure 2.13). An experimental study was performed to determine how effective a mobile HEPA filter can remove these aerosols. The bubbles were produced with a bubble generator and accumulated in a buffer. A mechanical pump transported the bubble to the mouth of the manikin.

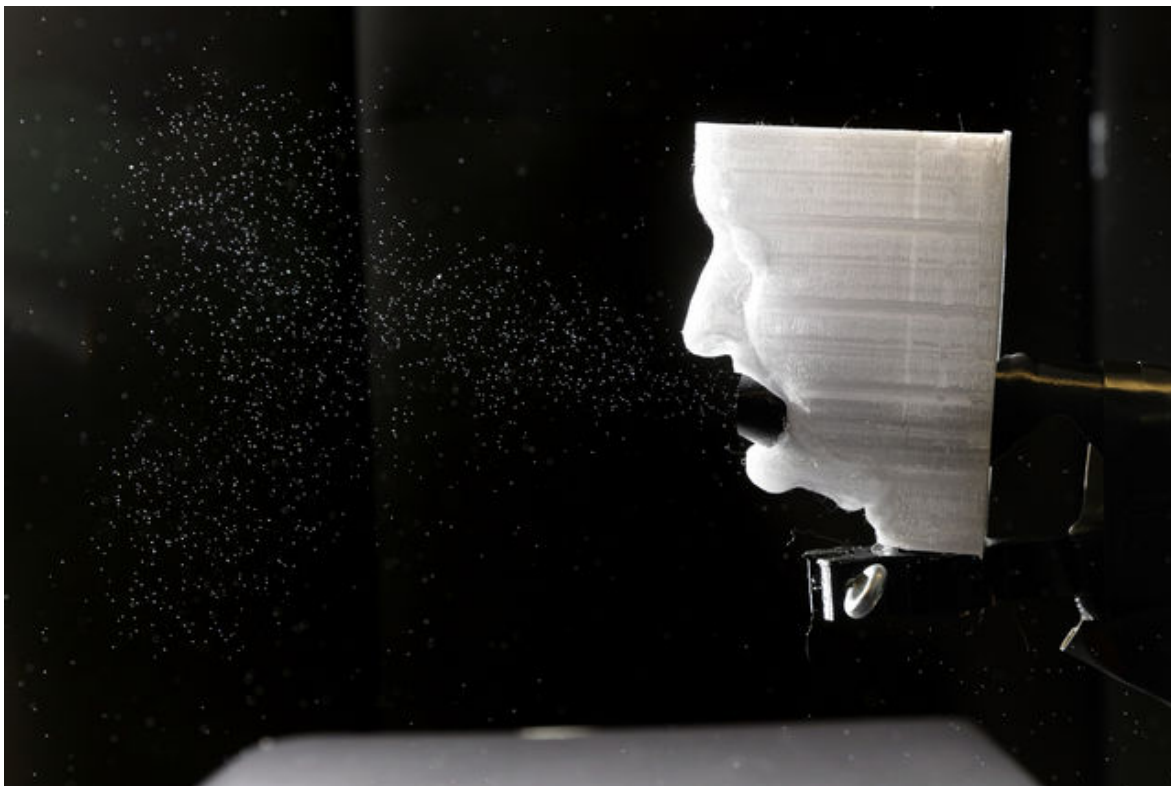


FIGURE 2.13: 3D-printed head producing air-filled soap bubbles (Bluyssen, Ortiz, and Zhang, 2021). *Used with permission from the author.*

The turbulence and air velocity in the indoor environment plays an important role in the lifespan of the air-filled soap bubbles. The lifespan of the soap bubbles can be up to two minutes in a low-turbulence setting (Bluyssen, Ortiz, and Zhang, 2021).

Fog

The fog is generated with a machine that is used for theatrical atmospheric effects, often seen at concerts or movie scenes. The two main fog effects are haze or fog and both use different types of liquids. Haze machines cost around €650 and create thin, translucent liquid particles. It lingers much longer in the air than fog. However, these droplets are not thick enough to create an opaque cloud effect. Causing it difficult to see the airflow pattern. Haze fluids are oil-based and leave an oily residue on surfaces, making them difficult to clean. The price of fog machines starts from €80. It uses glycol and demineralised water to produce a condensed form of droplets, resulting in a thick opaque cloud. This makes it easier than using haze machines to generate the visuals of the exhaled breath. A visual representation of using fog and lasers is seen in Figure 2.14

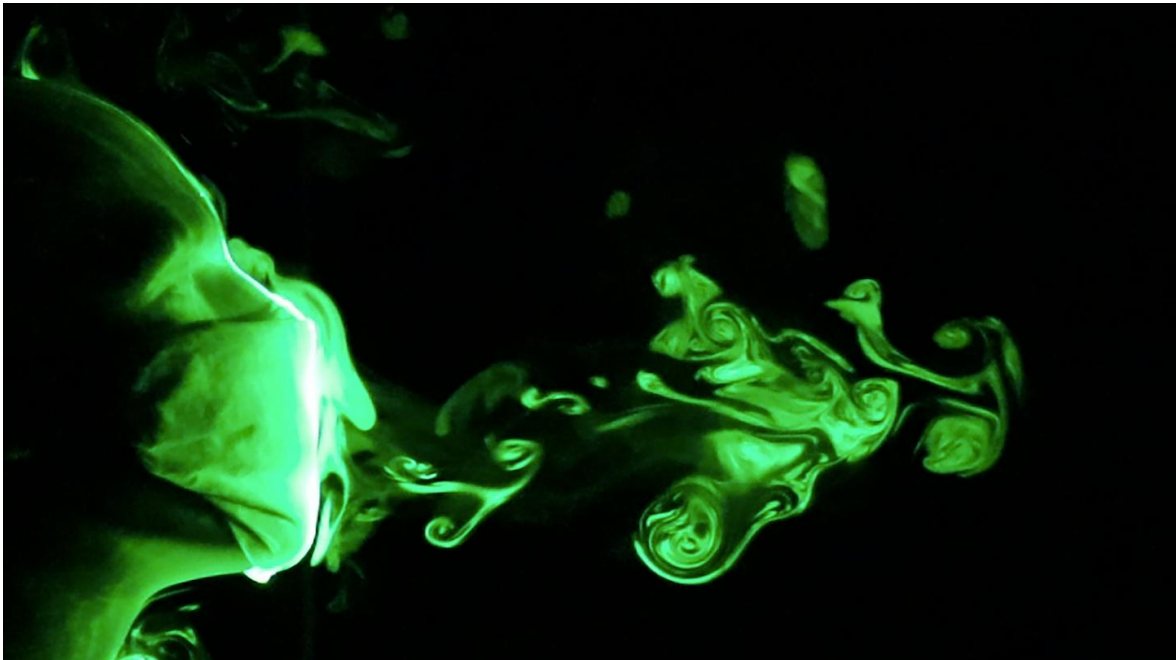


FIGURE 2.14: Visualizing the effectiveness of face masks when the fog is exhaled through a manikin (Verma, Dhanak, and Frankenfield, 2020). *Used with permission from the author.*

The setup is made out of a pump to simulate breathing, which can be mechanical as in Figure 2.15. The produced fog from the machine is transported into a box or chamber to accumulate. Finally, the fog goes through the orifice exit of the manikin. A laser source makes the fog visible and is captured with a camera. The fog liquid is easily self-made by using glycerin or glycol in combination with demineralised water. The camera captures the airflow pattern until the condensed form of droplets scatters. The particles are too small for the camera to record. A laser is required to emphasise the fog as the bundles of droplets reflects the light into the camera. The laser must be placed precisely at the manikin's orifice exit to create a vertical sheet of the airflow pattern. The room must be kept dark for optimal visualisation.

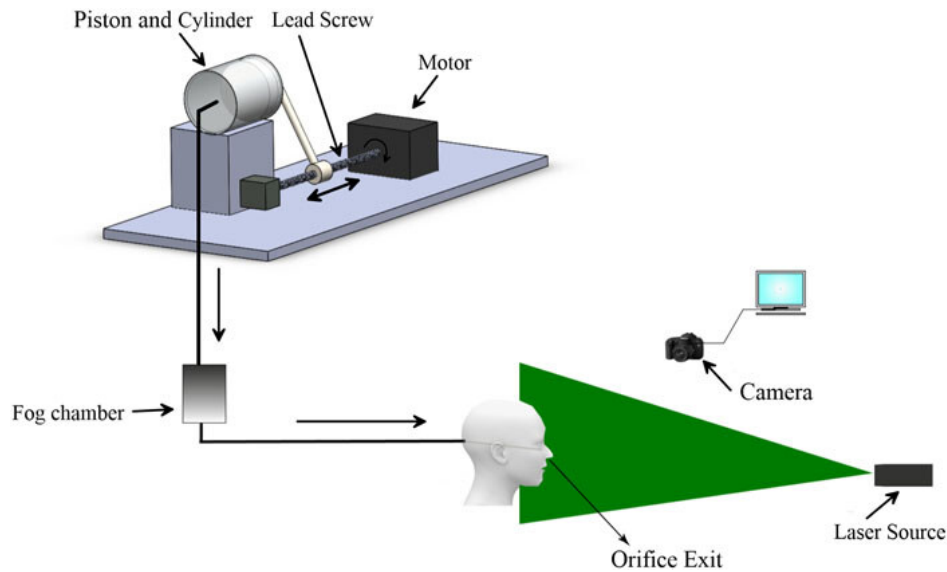


FIGURE 2.15: Setup of the mechanically breathing simulator with a fog machine (Arumuru et al., 2021). *Used with permission from the author.*

Fluorescent

The fluorescent mist was used to visualise the leakage that escaped with different types of face masks. The medium was made with nine parts of distilled water and one part of fluorescent tracking liquid. Any other ratios would either result in not enough mist or less fluorescent effect.

The setup in Figure 2.16 uses a mechanical pump that mimics the human breath. A PVC tube is connected between the machine and the box. Inside the box is an ultrasonic nebulizer to build up the mist. The mist exits from the manikin's mouth. Six UV lights are placed around the setup to emphasise the mist. The drawback of using fluorescent mist is thoroughly cleaning was necessary. Lots of different equipment was needed as well.



FIGURE 2.16: Setup of the manikin with a face mask. A long PVC tube is connected from outside the experiment site with the box. The manikin is resting on top of the box (Ortiz, Ghasemieshkaftaki, and Bluysen, 2021). *Used with permission from the author.*

The use of the fluorescent medium was also tested in various studies in dental clinics. Aerosols are transmitted during dental drilling as the patients keep their mouths open during the process. Risk is present of direct contact with infected instruments or surfaces that have not been cleaned properly (e.g. residues of blood or saliva). In addition, fluid droplets originating from airways can become airborne during dental procedures, thus enabling a potential threat of spreading the infection to both dental staff and patients. A simulated dental procedure resulted in the images of Figure 2.17.



FIGURE 2.17: The fluorescent dye on the manikin's face and operator's clothes during the dental procedure (Teichert-Filho et al., 2020). *Used with permission from the author.*

The fluorescent dye was found on the apron, gloves, face mask, dental chair and on the floor. The use of this medium provides a clear representation of how the aerosols may disperse during operation.

Tracer gas

Visuals of the exhaled airflow can be simulated with tracer gas. The setup is easy and inexpensive. This gas is made from N_2O and CO_2 to simulate aerosol droplets. The results were measured with a gas analyser with different response times. Most gas molecules are smaller than $5 \mu m$ in diameter and stay suspended in the air, acting similar to aerosols of the same diameter (Tang et al., 2011b). An important distinction between the movement behaviour of tracer gas and human respiratory droplets is the difference in molecular weight. The gas particles are lighter than respiratory droplets, thus it flows differently when reaching a surface. The respiratory droplets of a few microns tend to 'stick' to the surface due to an adhesive force, while gas molecules reflect from the surface (Andersson et al., 1983). Tracer gas can be dangerous if used at high concentrations, thus a manikin is advised to use. A setup using tracer gas and a thermal manikin is used in Figure 2.18.

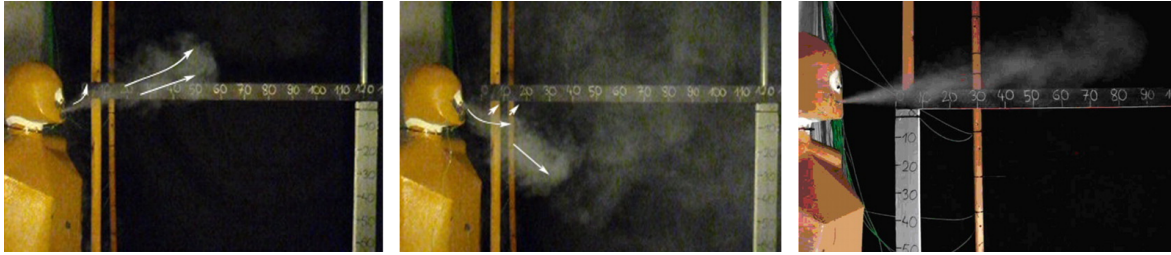


FIGURE 2.18: Visuals of a thermal manikin during exhaling. Tracer gas is used to simulate the airflow pattern of the mouth (left), nose (middle) and coughing (right) (Nielsen, 2009). *Used with permission from the author.*

2.3 Conclusion

A brief explanation of the mechanism of SARS-CoV-2 was given. The survival rate of the virus is strongly dependent on indoor environmental conditions. Relative humidity of $<20\%$ and $>80\%$ increases the serviceability of the virus. A low percentage of RH makes the virus more active, while simultaneously making the environment feel 'dry'. This condition makes humans more susceptible to getting infected. Temperature $>24^{\circ}\text{C}$ noticeably decreases the lifespan of the virus, with a preference for $>34^{\circ}\text{C}$. Unfortunately, these temperatures do not make it pleasant for any occupants. The indoor air velocity regulates the distribution of the droplets.

It is important to have some form of ventilation to decrease the spread of the virus, especially in enclosed environments with many occupants. The diameter of the respiratory droplets is mostly dependent on these environmental factors. These droplets evaporate and thus shrink immediately after exhalation due to the difference in RH. The smaller the diameter of the droplet, the longer it can sustain in the air for many hours before falling on the ground. This accounts for 37% of the exhaled droplets during speech. Some droplets can travel up to more than 6 metres in the horizontal direction, which is much higher than the assumed '1.5-meter distance' rule in the Netherlands.

The main purpose of the visualisation techniques is to directly observe how the respiratory droplets (either as saliva or other types of fluid/gas) behave in the indoor environment with different ventilation regimes. Multiple techniques were described in this chapter by using either human subjects or manikins. Both have their properties with pros and cons.

The use of human subjects results in realistic results. A large number of subjects are needed to have a valid result since every person's physique and health is different. The high-speed imaging technique is easy to assemble as it requires few instruments. The schlieren imaging is a bit more complicated but provides a nice visual effect. However, the test area is often less than 100 centimetres as it depends on the size of the spherical mirror.

When it becomes potentially dangerous to use human subjects, manikins can be used. Advanced manikins, such as thermal manikins, can mimick well to the human body to a certain degree. Different mediums can be applied, such as soap bubbles, tracer gas, fluorescent ink. For this thesis, the mobility of the design is important. Therefore, the use of a fog machine is chosen. As this is a low-cost and easy option to assemble (Verma, Dhanak, and Frankenfield, 2020, Arumuru et al., 2021). The knowledge and practice gap of these different techniques will be used to determine which technique best fits the final design in the next chapter.

Chapter 3

Methodology

A quantitative approach was applied to determine how different ventilation regimes affect the airflow pattern of the droplets. The methodology chapter starts by describing the experimental site, where the tests and measurements were performed. The basic indoor parameters are temperature, air velocity and relative humidity. Due to limited time and in-completion of the final setup, it was necessary to execute the baseline measurements before the airflow pattern visualisation experiment. The goal of these baseline measurements is to research how the different ventilation regimes and the breathing of the manikin influence the conditions of the basic indoor parameters of the indoor environment. The next part is describing materials that are necessary for the development of the portable fog generator system. An assembling guide is added with a photo of the final product, followed by the setup and how the data collection was performed for the airflow pattern visualisation experiment. The objective of this experiment is to visualise how the exhaling droplets are influenced by the various ventilation regimes. The visualisation helps to understand how it affects droplets' travel distance, the duration it lingers in the air and the percentage of fog plume per ventilation regime. Lastly, a theoretical comparison will be made to determine how accurate the portable fog generator system is in comparison with the theory.

3.1 Experimental site

The experiments were conducted in the SenseLab, which is a playground for the senses, located in the Science Center in Delft and is built around the four indoor environmental air quality (IEQ) factors (Bluyssen et al., 2017). Each factor has its test chamber, while the experience room integrated all IEQ: air, thermal, lighting and acoustical quality. This can be seen in Figure 3.5.

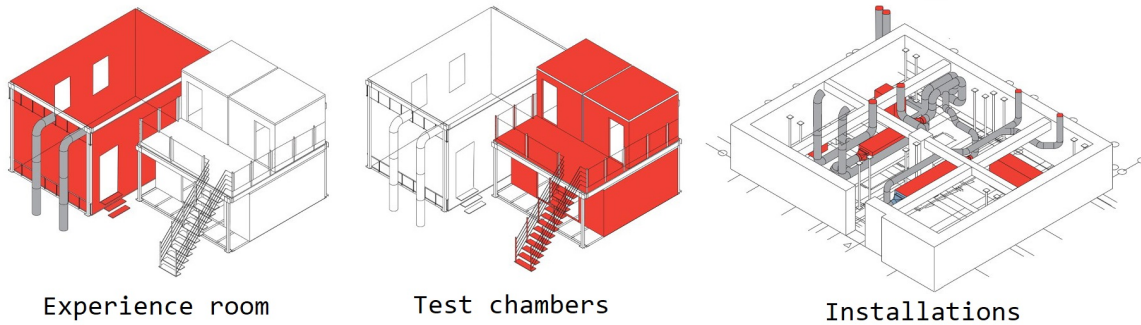


FIGURE 3.1: The SenseLab consists of the experience room, four test chambers and installations in the basement. Each of the four IEQ has its test chamber, while the experience room incorporated all four of them (Bluyssen et al., 2017).
Used with permission from the author.

3.1.1 The test chambers

One of the four test chambers was used as a workstation to assemble and test the setup. Earlier experiments and measurements were conducted in the test chamber until the setup was finalised and other experiments were. The walls, ceiling and floor were taped with black garbage bags to improve the visibility of the fog. A few of these tests can be seen in Figure 3.2. After finalising the setup, the next step was to perform experiments in the experience room.

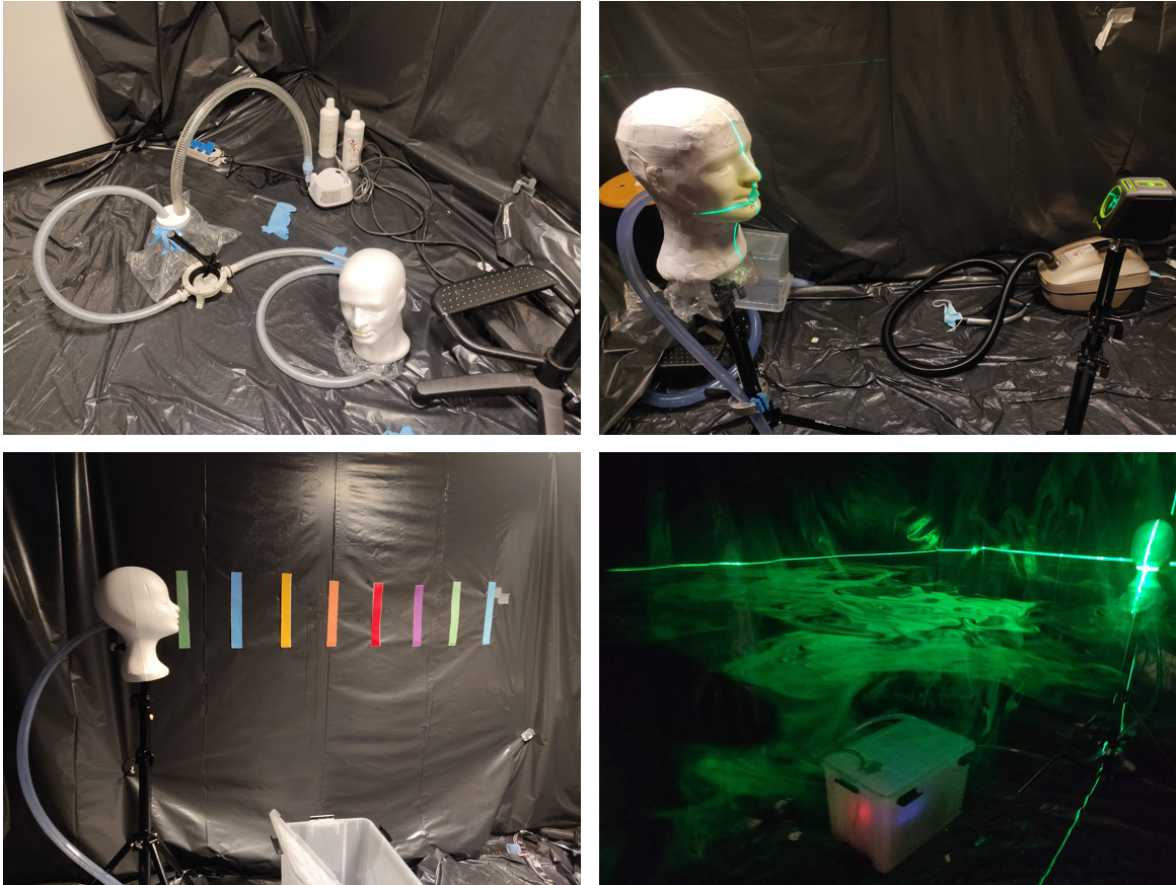


FIGURE 3.2: One of the first setups was by using a nebulizer, small plastic jar and plastic bags/gloves to prevent leaks (top left). Testing the application of the laser on manikin from previous experiments (top right). Preliminary setup to measure the distance of the fog plume with a distance of 10 centimetres between each strip (bottom left). Improving the visibility of the fog by turning off the light of the test chamber. The chamber was quickly filled with fog as the buffer was completely airtight (bottom right).

3.1.2 The experience room

The layout of the experience room is similar to a classroom of secondary schools in the Netherlands as seen in Figure 3.3. For the baseline measurements and airflow pattern visualisation experiment, the placement of the tables and chairs were different.

The dimension of the experience room was $6.5 \times 4.2 \times 3.0 \text{ m}$. The frame was made out of steel and the walls are from laminated glass. The room has a raised floor with two windows and a door (both also made entirely of laminated glass). The ceiling has LED lamps that can be adjusted to different light configurations. Furthermore, there is a computer outside the experience room that can regulate the air temperature and ventilation rate (Figure 3.4). There are two air handling units (AHUs) in the basement, one for the test chambers and one for the experience room. The chiller is installed outside, next to the SenseLab. The indoor temperatures can be controlled between 15–25°C.



FIGURE 3.3: Classroom setup in the experience room. The four ceiling grilles and the plinth on the floor provide the air supply or intake (TUDelft, 2017).
Used with permission from the author.

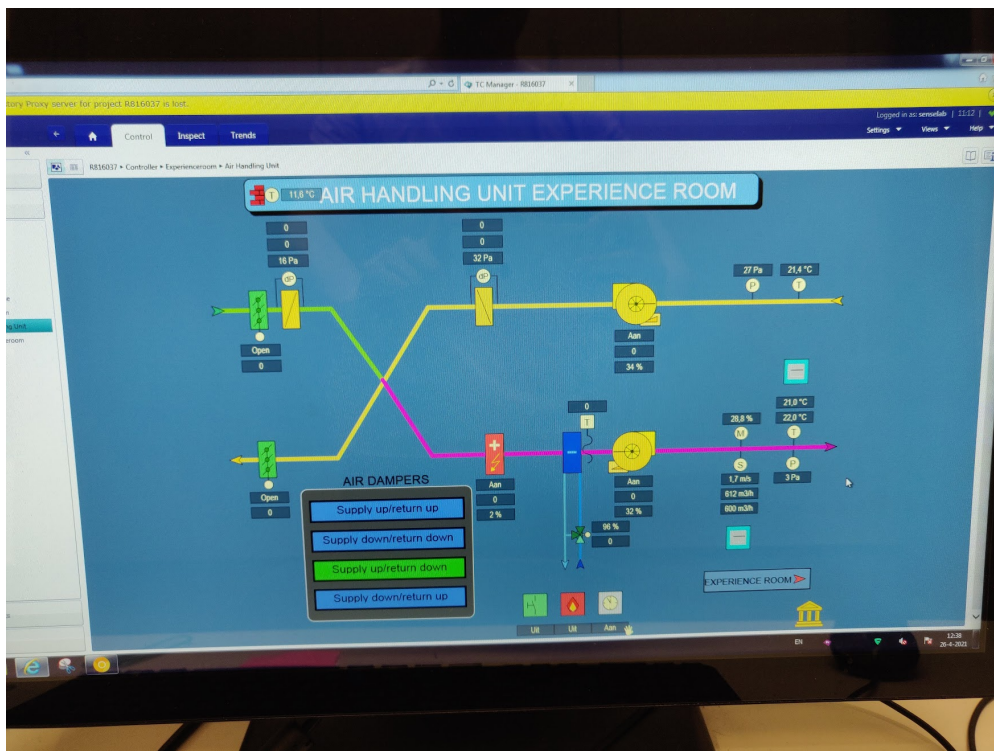


FIGURE 3.4: The heating, ventilation and air conditioning system is run by the program TC Manager.

The ventilation can be regulated through natural ventilation, displacement ventilation (DV) and mixing ventilation (MV) as seen in Figure 3.5. Natural ventilation is achieved by opening the windows. The DV starts at the bottom of the room and goes upwards towards the ceiling. The air supply is at the perforated plinth on the long side of the room and exhaust in the ceiling on the short side. The MV goes from the ceiling to the floor. The air supply is in the plenum of the ceiling grilles. Each grill has a dimension of $600 \times 600 \text{ mm}$. The exhaust is

located on the short side of the room. The holes of the plinth have a maximum air velocity of 0.3 m/s and a diameter of 3 mm with a plinth height of 160 mm .



FIGURE 3.5: Natural ventilation (left), displacement ventilation: plinth for air supply at the long sides of the room (middle) and exhaust through the ceiling (right) (Bluyssen et al., 2017). Used with permission from the author.

3.2 Baseline measurements

The baseline measurement, the before measurement, is data that has been taken before any adjustments have been made. In this case, it is the comparison with the *no ventilation regime* before applying any other ventilation regimes. The baseline measurements were performed on two separate days as it was a time-consuming process. The *no ventilation* and *natural ventilation* were measured in the afternoon, while the *mixing ventilation* and *natural + mixing ventilation* the day after in the morning. The objective was to determine if the air velocity of the manikin's breath had any influence on the basic indoor parameter under different ventilation regimes.

3.2.1 Ventilation regimes

The four ventilation regimes are illustrated in Figure 3.6. It is a combination of windows open or closed and whether mechanical ventilation is applied. Changing the configuration affects the three basic indoor parameters, which are the variables.

No ventilation

In this regime, both windows are closed. The indoor air velocity will be very little, causing the droplets to linger much longer in the air before it falls on the floor or surface. The results of the no ventilation regime will be used as a baseline to examine if there are any discrepancies between the other ventilation regimes.

Natural ventilation (only windows open)

Natural ventilation is an uncontrolled form of ventilation, which uses the outdoor wind and buoyancy to supply the building with fresh air. Fresh air enters primarily through both windows. However, it can also be infiltrated through seams and cracks of the building. A disadvantage of natural ventilation is that unfiltered air enters, which can be harmful to health. Noise pollution, especially if the room is located near a road or school. Warm air is removed from the room, without any method of heat recovery. The presence of drafts in turn affects the thermal comfort of the user, this is the most common during cold periods. This type of ventilation accounts for 29% of the schools (LCVS, 2020).

Mixing ventilation (ceiling inflow, bottom exhaust)

Mixing ventilation is mechanically controlled where the air supply and exhaust can be regulated. The temperature can also be adjusted. The air supply is provided at the ceiling and exhaust from the bottom at the short side of the room. The filtration system can be installed to remove (harmful) odours, particulates and microorganisms. The performance of the mechanical ventilation can be compromised if not installed and maintained correctly. The ventilation rate was set to $600 \text{ m}^3/\text{h}$.

Natural + mixing ventilation

The final ventilation regime is the combination of natural + mixing ventilation. People who are unaware of the presence of mechanical ventilation are likely to open the windows. This is because they notice that the window is open, thus that fresh air is coming into the room. However, this interrupts the balance what mechanical ventilation is trying to achieve. More infiltrated air is brought into the room and increases energy use.

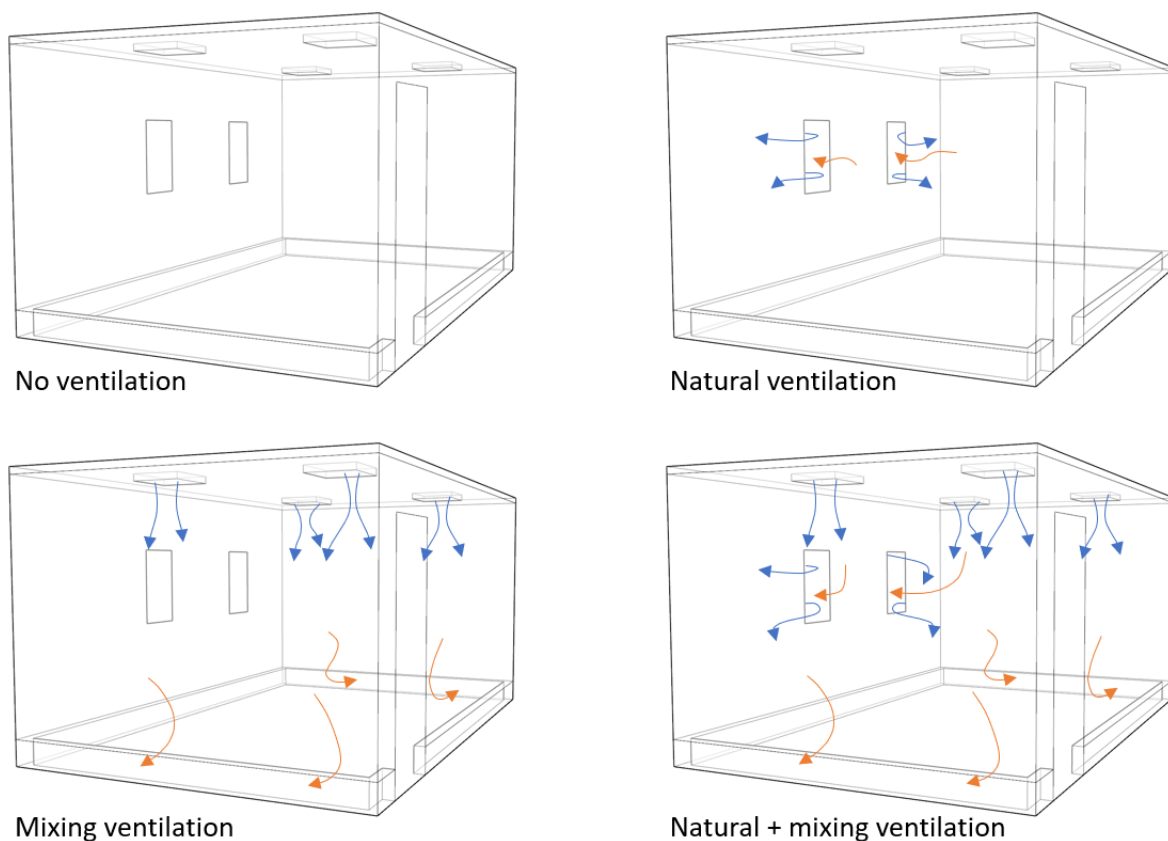


FIGURE 3.6: There is neither air supply nor exhaust in the no ventilation regime (top left). Fresh air comes in through the windows and circulates in the room. (top right). The air supply comes down through the four ceiling grilles and is exhausted through the short side of the room (bottom left). At the last ventilation regime, there is a combination of both natural and mechanical ventilation. More of the air is being pushed downwards (bottom right).

3.2.2 Setup

The manikin's mouth is situated 120 centimetres above the floor to simulate a pupil sitting behind the desk. According to the RIVM, someone who coughs or sneezes spreads the

majority of the respiratory droplets within a radius of 150 centimetres around themselves (*RIVM (2020) n.d.*). Six locations (A, B, C, D, E and F) were chosen with a distance of 150 centimetres between each table at the long side of the room. Each location has three different heights. Figure 3.7 shows the layout of the setup in the experience room.

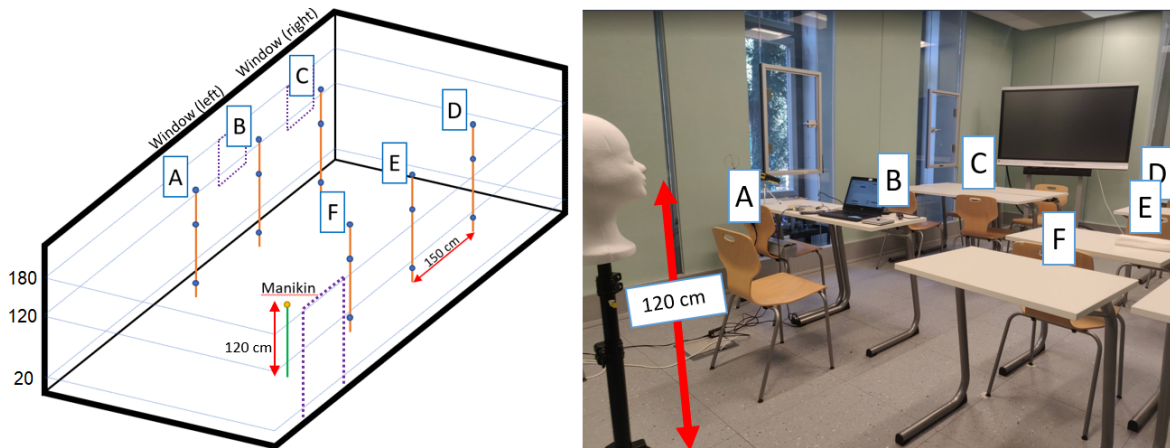


FIGURE 3.7: Schematic layout of the experience room and its locations (left). The setup before the start of the first measurement (right).

Important to note is that the portable fog generator system was not finished during that time. The original idea was to use glycol as the medium while the manikin was breathing. Instead, the indoor air of the room was used as the medium as seen in Figure 3.8. It would not matter much for the results, as the goal was not to visualise it yet. The baseline measurement is focused on how the breathing of the manikin is influenced by the different ventilation regimes.



FIGURE 3.8: Unfinished setup with only the manikin on the tripod. The pump was connected with the tube during the baseline measurements. The indoor air of the room was used as the medium, instead of glycol.

3.2.3 Baseline conditions

The variables are temperature, relative humidity and air velocity. These basic indoor parameters are affected by changing the ventilation regime. The air velocity was measured with

the Dantec ComfortSense monitor. The relative humidity and the temperature with the Onset HOBO MX1102 data loggers and Trotec PC220. In the experience room, three different heights were selected for measurement: feet (20 centimetres), sitting (120 centimetres) and standing (180 centimetres) as seen in Figure 3.9.

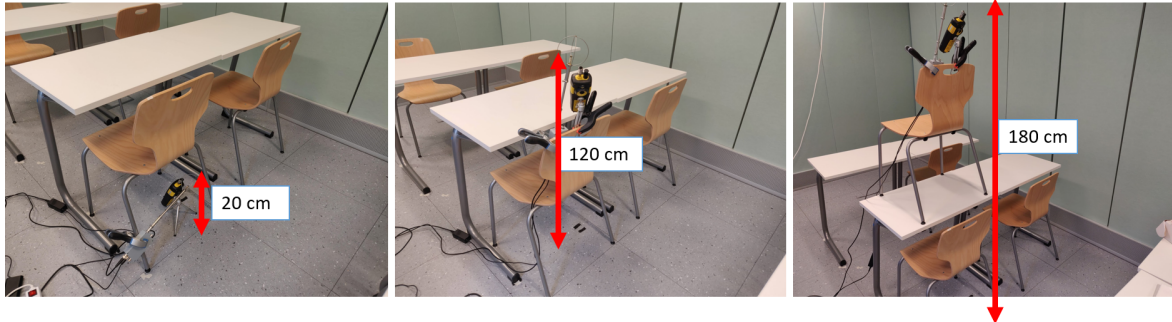


FIGURE 3.9: The setup for measuring the basic indoor parameters. It was measured at three different heights: ankle (left), head (middle) and standing (right).

The basic indoor parameters of the windows, ceiling inlets and plinths at the short side of the room were measured in Figure 3.10.

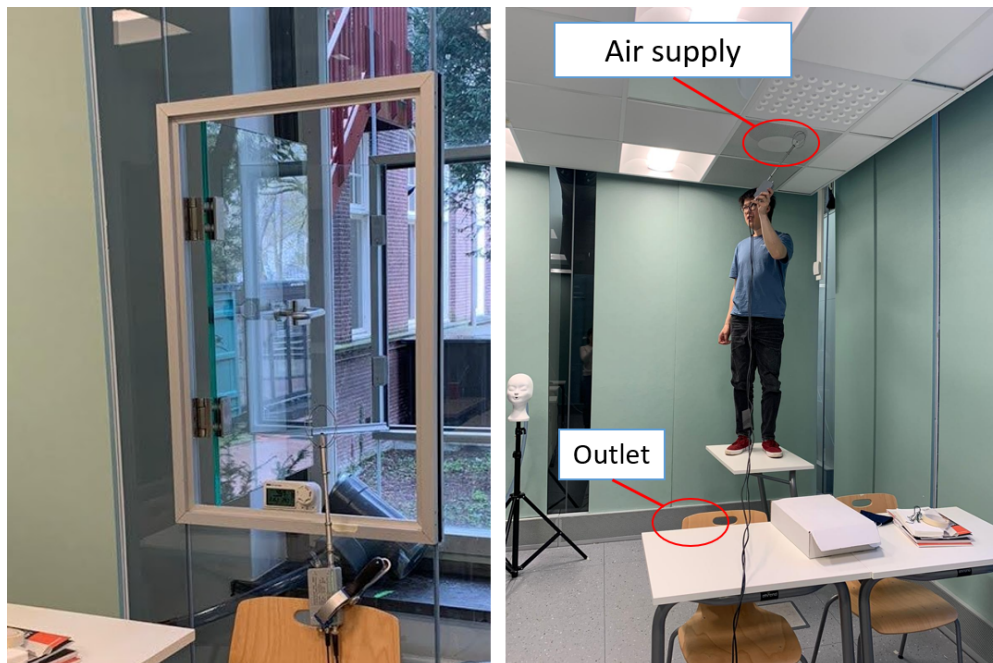


FIGURE 3.10: The Onset HOBO MX1102 data loggers and Dantec ComfortSense monitor were placed near the window (left). Measuring the basic indoor parameters at the ceiling and on the floor (right).

While the manikin was 'breathing' in the back of the room, the basic indoor parameters were recorded for one minute per location. A total of 18 measurements were performed. A clamp was attached to the chair with the measuring tools to assure that it did not move. First, the height of 120 centimetres was measured. Then the tools were attached to one of the legs of the chair. Lastly, the tools were clamped on the top of the chair and placed on the table to measure at a height of 180 centimetres.

The measuring tools had to be moved after each run to a different location or height. To prevent the movements of the operators from affecting the measurements, there was a pause of thirty seconds between each measurement. This was enough for the air velocity to settle down before performing the next measurements. The operators were wearing face masks to not affect the indoor air velocity.

The *no ventilation* and *natural ventilation* regime were measured in the morning. The *mixing ventilation* and *natural + mixing ventilation* were recorded on the next day in the morning. This may influence the consistency of the results.

3.3 Materials

Based on the literature review in Chapter 2, the most important aspects for the design and development of the portable fog generator system had been decided. Furthermore, the materials needed for the design should be easy to assemble and accessible to obtain. The invoice of materials used for the setup can be found in Appendix A.

3.3.1 Instrument research

Six instruments are needed for the portable fog generator system and are listed below:

1. Medium, to be considered as the 'saliva' of the setup.
2. Fog generator, to generate fog with the medium.
3. Pipe, to connect the different instruments.
4. Buffer, to accumulate the fog that was generated.
5. Pump, to transport the fog from the buffer to the manikin.
6. Manikin, where the fog exits.

Furthermore, the lasers and camera are used for the visualisation of the airflow pattern. Thus, both pieces of equipment are not considered as part of the design and development of the portable fog generator system. The instruments needed for the system is shown in Figure 3.11.



FIGURE 3.11: The medium is poured into a small container of the fog machine. The fog machine is turned on and fog comes out of the nozzle. A pipe is placed in front of the nozzle, which is connected to the buffer. The fog is collected in it. When enough fog is accumulated, it is transported to the manikin through the pumping mechanism. The manikin exhales the fog.

Medium

Understanding the safety and risk protocols in performing experiments is important. The medium should not be harmful to the users during the experiment. The type of machine that produces the 'respiratory droplets' determines the kind of medium. Therefore, two options were considered: glycol or oil. Budget wise, glycol was chosen as the medium. The visibility of the fog is based on the ratio of demineralised water and glycol, which can be easily adjusted by the user (Figure 3.12).



FIGURE 3.12: Different types of glycol concentrations were used. The viscosity of glycol is high and can be diluted by the demineralised water, making it easier for the machine to convert the liquid into the fog.

Different ratios of demineralised water-to-glycol were tested. The high-density value of glycol makes the fog more visible, while the demineralised water decreases the viscosity. Making the fog machine easier to produce the fog from the nozzle. After lots of attempts, using an amount between 85% and 95% glycol ensures the best visual result.

Fog generator

The purpose of the fog generator is to create a cloud of droplets to visualise the airflow pattern. Another requirement is that it needs to be portable and not too expensive. Multiple options were evaluated or have been tested and described below:

Nebulizers were very compact and cost-effective. However, the container for the liquid was only 5 ml and the outflow rate was not powerful enough to produce sufficient fog to fill the buffer.

The option of using a *cleanroom fogger* was also considered. This special type of fogger is used in medical and sterile rooms and can be held with one hand. Unfortunately, the tank bottle is quite small (around 250 ml) and the price was too high (starting from €2200).

Haze machines (hazers) works only on an oil-based medium and produces much finer and more translucent particles than a fog machine. However, these particles are not visible to the naked eye as it is not able to create an opaque fog effect. This is necessary for the camera otherwise it cannot capture it. The medium leaves an oily residue on all surfaces with prolonged use. Utmost care is required to prevent this medium from being sucked into the ventilation as it is difficult to remove. Hazer costs at least €600 and the best quality of oil-based medium must be purchased from specialist retailers.

Ultimately, a *fog machine* (Ayra WSM Black 01, Figure 3.13) was chosen that meets both criteria of portability and cost-efficiency. The large tank capacity makes it suitable for long-term use. The cloud of droplets is opaque, which makes it very visible. The machine has to heat up for a few minutes before use and can be operated remotely. Periodic maintenance is necessary, especially at the nozzle to prevent clogging.



FIGURE 3.13: The Ayra WSM Black 01 comes with a remote controller.

Pipe

Pipes are needed to connect the instruments. Different types of pipes were tested, such as stretchable, very stiff or reinforced PVC. However, the stiffness of the pipe makes it difficult to position the equipment. This limits the flexibility of the setup as it depends on how far the pipes can be bent. Therefore, it was opted to use a transparent flexible pipe. It was convenient to perceive the fog flowing through the pipe. Two different diameters were required, due to the size difference of the radius of the pump and nozzle of the fog generator. The sizes 25 mm and 49 mm were chosen, respectively. To prevent the tube from becoming too long and to make corners, it is cut into smaller pieces and fitted together with 45 and 90° PVC elbow tubes as seen in Figure 3.14.

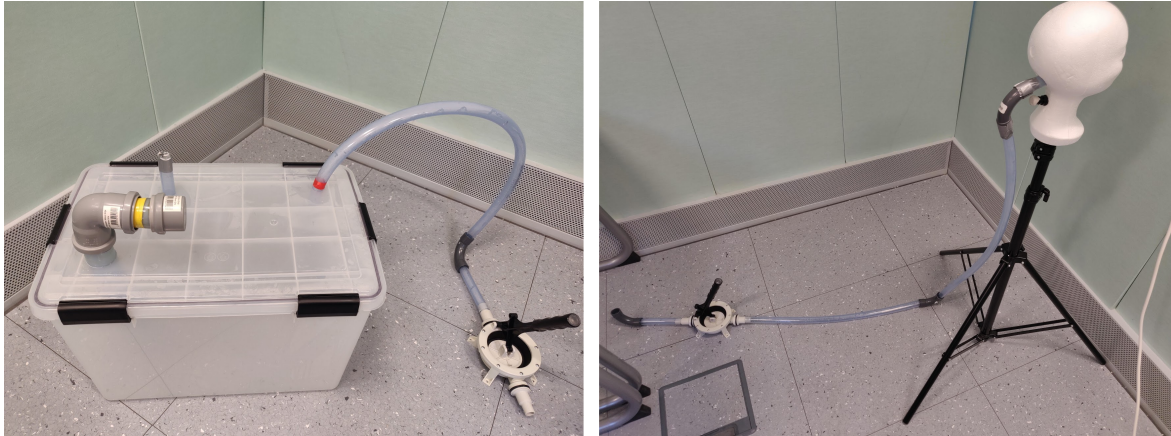


FIGURE 3.14: The big pipe with the PCV elbow tube to collect the fog from the fog machine. The narrower pipe connects the inside of the buffer with the pump. The colour indications (yellow and red) determine how far the pipe should be inserted in the buffer of the PCV elbow tube (left). The pipe connects the pump with the back of the manikin. The transparent flexible pipe is sawn in parts and connected with grey PVC elbow tubes (right).

Buffer

The function of the buffer is to accumulate the fog produced from the fog machine. During the first attempt, a volume of 20 litres was used. This was too little and the lid was not airtight. The holes where the pipes are inserted were not perfectly cut, causing even more leaks (Figure 3.15). A large buffer is recommended as it can fill up more fog, thus reducing the amount of time to refill it during the experiment. Ultimately a transparent airtight buffer of 70 litres was chosen. It takes about 20 seconds to fill the buffer.



FIGURE 3.15: With the small buffer of 20 litres an attempt was made to stop the leakage by applying duct tape around the lid and where the pipe goes through the lid (left). Fortunately, there was the option to use a laser cutter. The holes were laser drilled in the diameter of the pipes (right).

Three holes were cut with a laser to precisely fit the three pipes in Figure 3.16. The red hole is for the fog to enter the buffer. The pipe with the larger diameter was used as seen in the left picture of 3.14. The blue hole has the function of transferring the fog out of the buffer by using the pump. The yellow hole is used as a plug to create pressure difference while filling the buffer with fog. The hole needs to be open during that process. During pumping,

all three holes must be closed to create a closed environment inside the buffer. With the intention that the fog goes through the small pipe to the manikin.

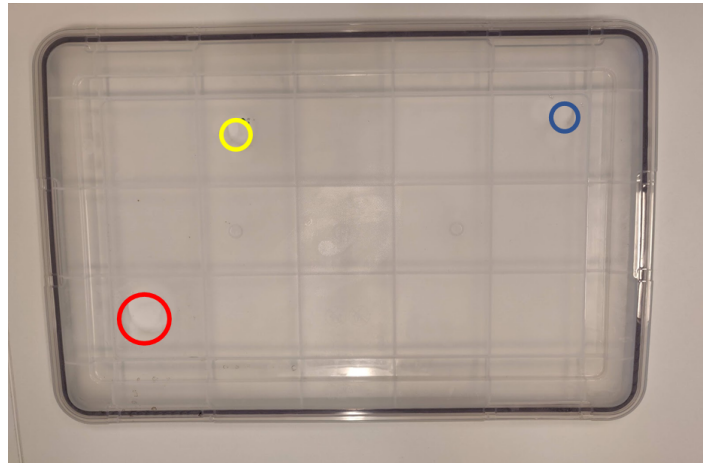


FIGURE 3.16: The red hole is to receive the fog from the fog machine. The blue hole is where the fog is transferred out of the buffer. The yellow hole needs to be open during the accumulation process and closed during pumping.

Pump

The pumping process simulates the respiratory system of a human. It simplifies the characterization of an actual breath. The pump transfers the fog from the buffer through to the mouth of the manikin. The resting tidal volume is the amount of air inhaled or exhaled in one normal breath, which is approximately between 400—500 *ml*. The pump can be either a manual or mechanical pump. A mechanical pump is preferred as the output remains constant. Unfortunately, it was not possible to find a mechanical pump that meets those criteria. Subsequently, a manual pump has been chosen as seen in Figure 3.17.



FIGURE 3.17: The Nuova Rade Handlenspomp (left). The pumping mechanism is displayed with the three figures. In this example, the inhaling process is demonstrated as the handle is pulled back. Simultaneously, the other hand must press the pump to the ground. Otherwise, it will shift during the process (right).

The Nuova Rade Handlenspomp has a pump capacity of 400 *ml*. It is commonly used for small boats to pump out the water. The drawback of this pump is that it allows a different range of velocities and volumes. It is entirely up to the skill of the operator to achieve the desired displacement.

Manikin

The most important feature of the manikin is to recreate the characteristics of a human mouth opening as shown in Figure 3.18. Akin to the pump, the manikin simplifies the characterisation of an actual breath. This could result in an overestimated exhaled velocity (Xu et al., 2014). Multiple options were considered such as a 3D-printed, wooden, plastic or silicone head model with internal airways. However, these options were disregarded due to either being too expensive, difficult to fabricate or not being able to receive it on time. Ultimately, a styrofoam head was chosen as this was the most economical option and can be easily modified. A screwdriver was used to carve out the internal parts of the head.

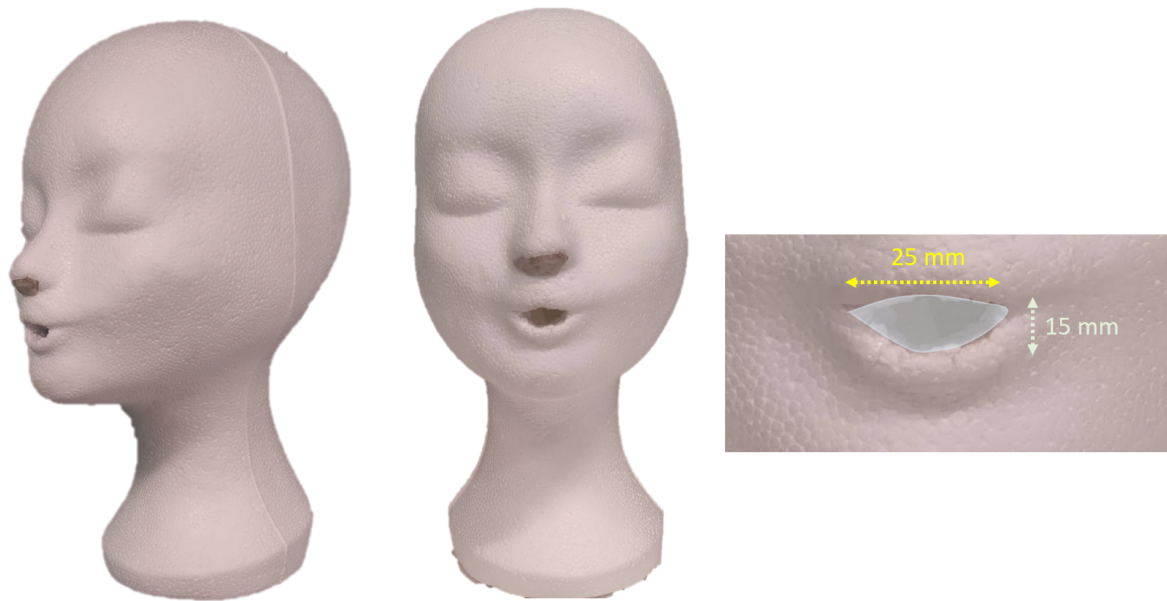


FIGURE 3.18: The styrofoam manikin was used for the experiments. The nostrils are filled with gum. The dimensions of the mouth are given.

The fog will exit through this manikin's mouth. The geometry and breathing of the mouth of a human were analysed. The recommended shape is a semi-ellipsoid with an area of 120 mm^2 as this is a representative area for a human mouth (Grymer et al., 1991).

3.3.2 Visualisation equipment

The visualisation of the fog was recorded with a mirrorless camera (E-M10 Mark II) with a wide-angle lens (Lumix G Vario 7-14mm f/4.0 ASPH). For the airflow pattern visualisation experiment, that was the best camera available at that time. If the budget was not an issue, a high-speed camera would be a better option as it captures much more frames per second and works well in low-light conditions.

Lasers were used to increase the visualisation of the airflow pattern. As a result of many trials and errors, there is a small margin for error to place the lasers as the position is essential for the rate of visibility. This does not indicate that more lasers provide for better visualization, but rather speed up the placement process of the lasers. A total of six lasers (Huepar BOX-1G) with a wavelength of 532 nm were used as seen in Figure 3.19.

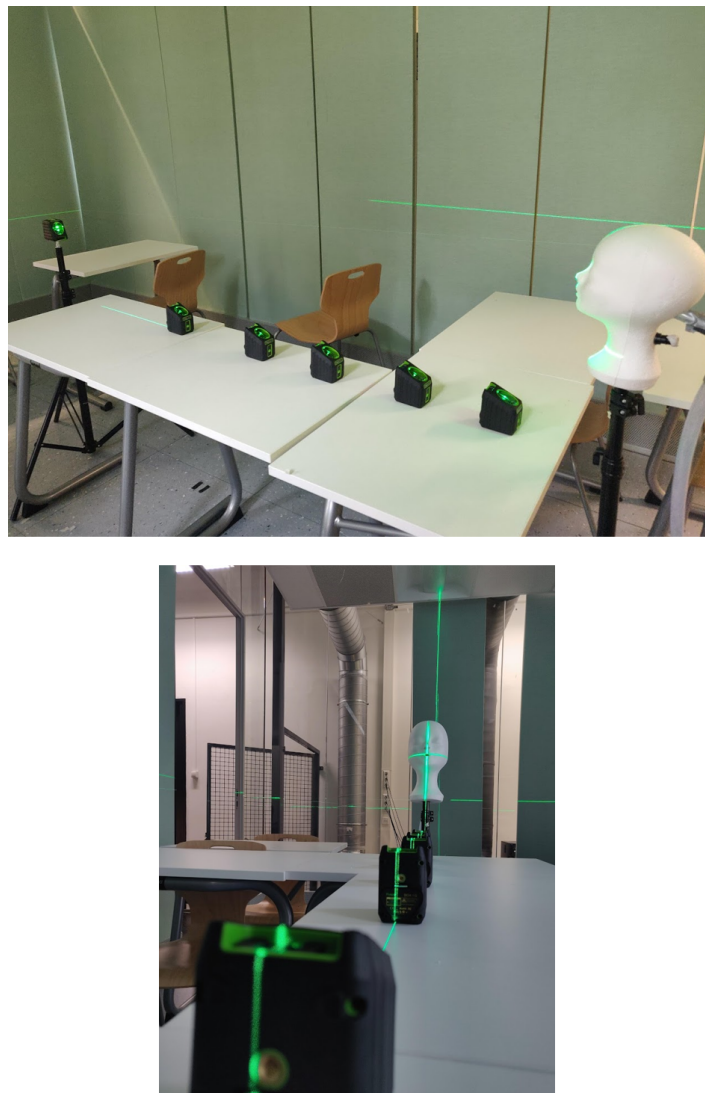


FIGURE 3.19: The six lasers are placed in a straight line pointing at the manikin (top). The horizontal and vertical planes are visible at the manikin (bottom).

To create a vertical plane, lasers were placed in a straight line from beneath the breathing area pointing at the ceiling. Another laser was placed at the back of the room, pointing to the manikin's mouth, to create a horizontal plane as seen in Figure 3.20. Furthermore, the room was dimmed to increase the visibility of the fog.

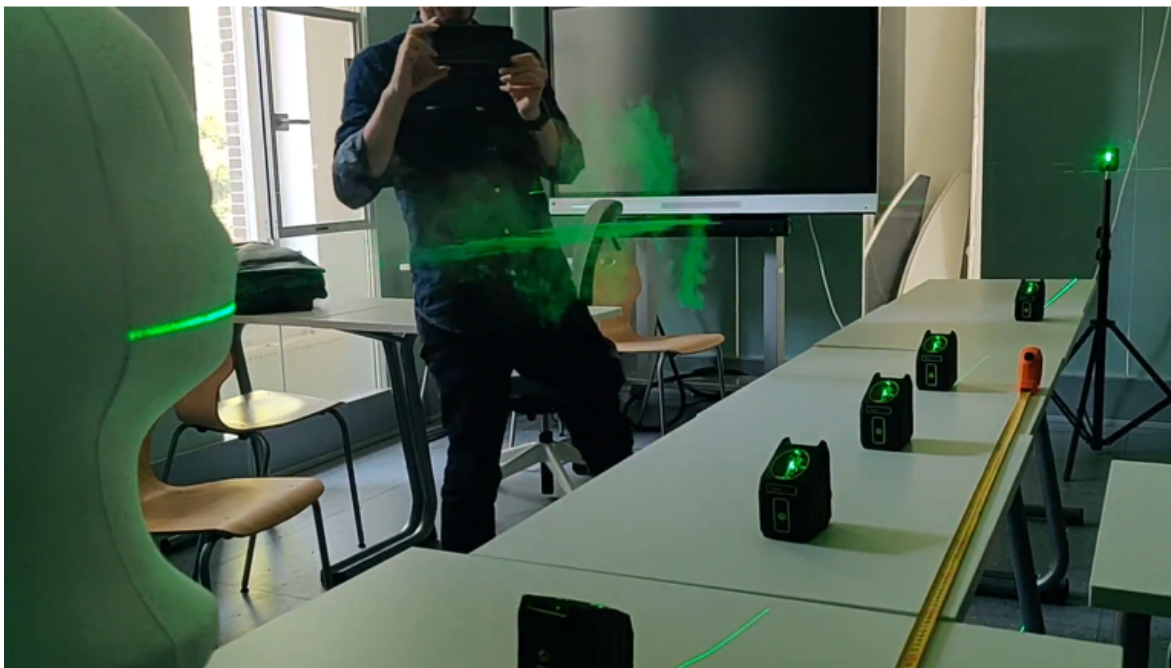


FIGURE 3.20: The difference between using one and multiple lasers in a somewhat dimmed setting of the experience room. This experiment took place in May and only the horizontal plane was visible (top). The extra set of lasers arrived in June. The placement of the tables needed to be altered to place more lasers. Both the planes are visible (bottom).

3.3.3 Assembling guide

This section describes how the mobile fog generator was assembled. A video guide is available at <https://repository.tudelft.nl> by typing the title of this thesis in the search bar.



FIGURE 3.21: A 70-litre buffer with an airtight lid. There are three holes in the lid. The pipes can be inserted through these holes.

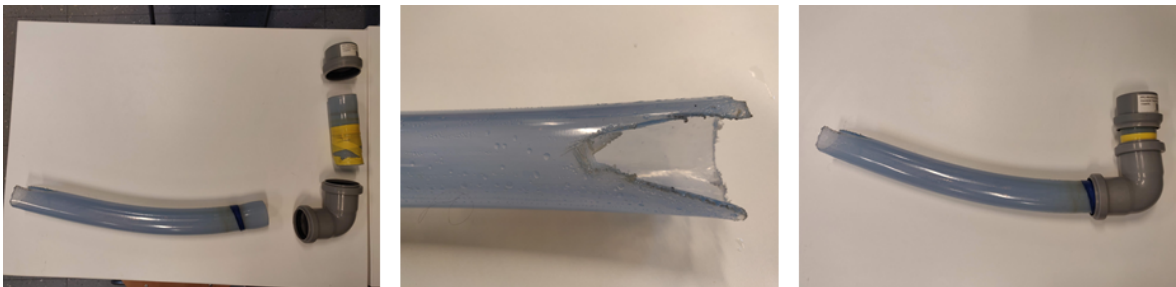


FIGURE 3.22: A pipe with a diameter of 49 mm is made for the inlet of the fog. One end of the pipe is slightly cut out so that the fog can fill the buffer.

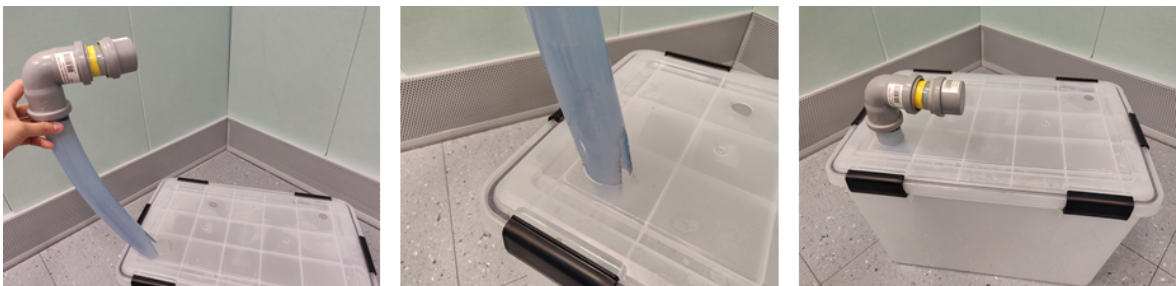


FIGURE 3.23: The pipe is inserted through the lid of the buffer. When the fog machine fills the buffer with the fog, the lid is removed and put back on when it is done.



FIGURE 3.24: A pipe with a diameter of 25 mm is inserted at the other corner of the lid. This is to transfer the fog from the buffer through the pump. Another pipe is inserted and the other side is covered with duct tape.



FIGURE 3.25: The container of the fog machine is filled with glycol and demineralised water. A ratio of 9:1 was used. The fog machine was placed on top of the lid and the legs fit exactly in the cavity. A small open distance between the pipe inlet and the nozzle is necessary. Otherwise, no fog will enter the buffer.



FIGURE 3.26: The final step is to assemble the manikin on the tripod. The cavity within the manikin was carved out with a screwdriver. The pipe was connected with PVC elbow tubes and inserted in the back of the manikin. The pump is connected to the other end of the pipe.

3.3.4 Final setup

An extensive logbook is documented in **Appendix B** on how the final version of the portable fog generator system was created. Originally, the idea was to also implement CFD to the results of the research. Due to time constraints, it was unanimously decided not to add it to the research anymore. The logbook consists of the purpose of the experiment, a summary of what has been done, the failure points and what can be improved next time. The template of the logbook is shown below:

The date of the experiment	
Goal	The objective of the experiment.
Summary	A summary of the procedures of the experiment and anything interesting happened during that day.
Failure points	Features of the experiments that did not work.
Improvements for next time	<ul style="list-style-type: none"> • Item #1 that can be improved for the next experiment. • Item #2 that can be improved for the next experiment. • Et cetera.
Setup	A picture of the setup, if available.

The final setup of the portable fog generator system can be seen in Figure 3.27.

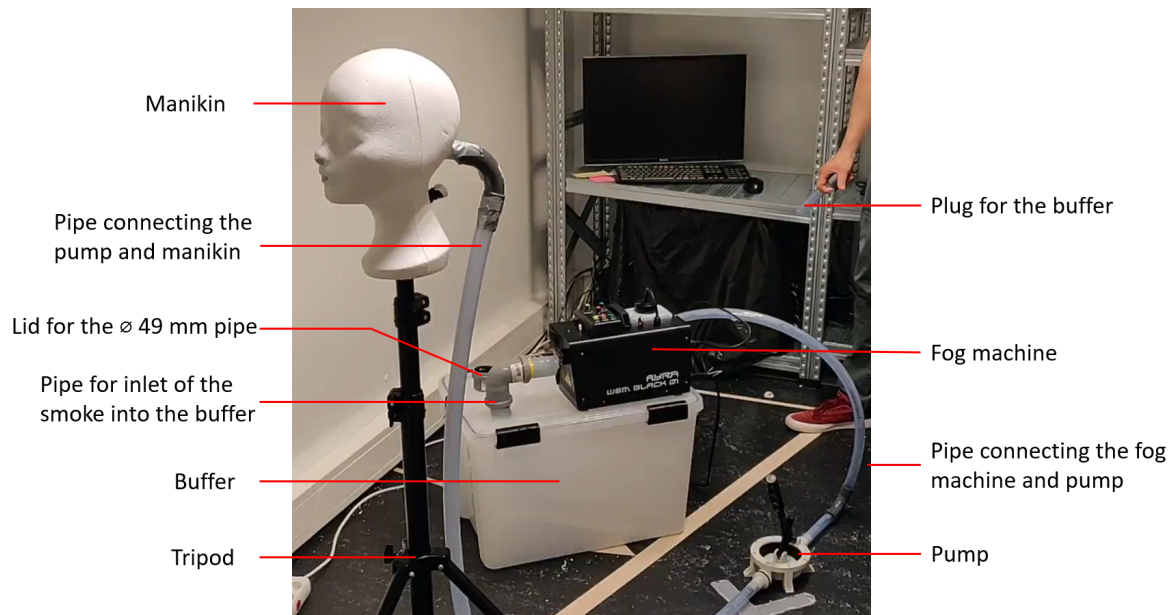


FIGURE 3.27: Final setup of the portable fog generator system.

3.4 Experiment: Airflow pattern visualisation

After designing and assembling the portable fog generator system, it was able to visualise the airflow pattern with glycol. The effect of the four different ventilation regimes on the dispersion of the droplets exhaled by the manikin are recorded and analysed. The results indicate the distance the droplets travel and the duration it lingers in the air before it is not visible anymore. Furthermore, an attempt has been made to quantify the number of droplets per ventilation regime.

3.4.1 Setup

The manikin is placed at the back of the experience room. Five lasers were put on the table, facing towards the ceiling. Another laser was placed at the end of the table. The distances between the manikin's mouth to lasers were written on the table. The lights of the room were turned off during the experiment to increase the effect of the lasers. Unfortunately, it was not possible to capture the fog pattern at the side view as seen in Figure 3.28.



FIGURE 3.28: Overview of the setup to capture the airflow pattern by placing the camera next to it to create a side view (top). During the experiment, the fog was not visible enough (bottom).

This is probably related to the positioning of the lasers and how the particles are being deflected to the camera. Previous tests have shown that placing the smartphone diagonally behind the manikin resulted in the best visual results. Therefore, the best option was to position the camera in the same place as seen in Figure 3.29.

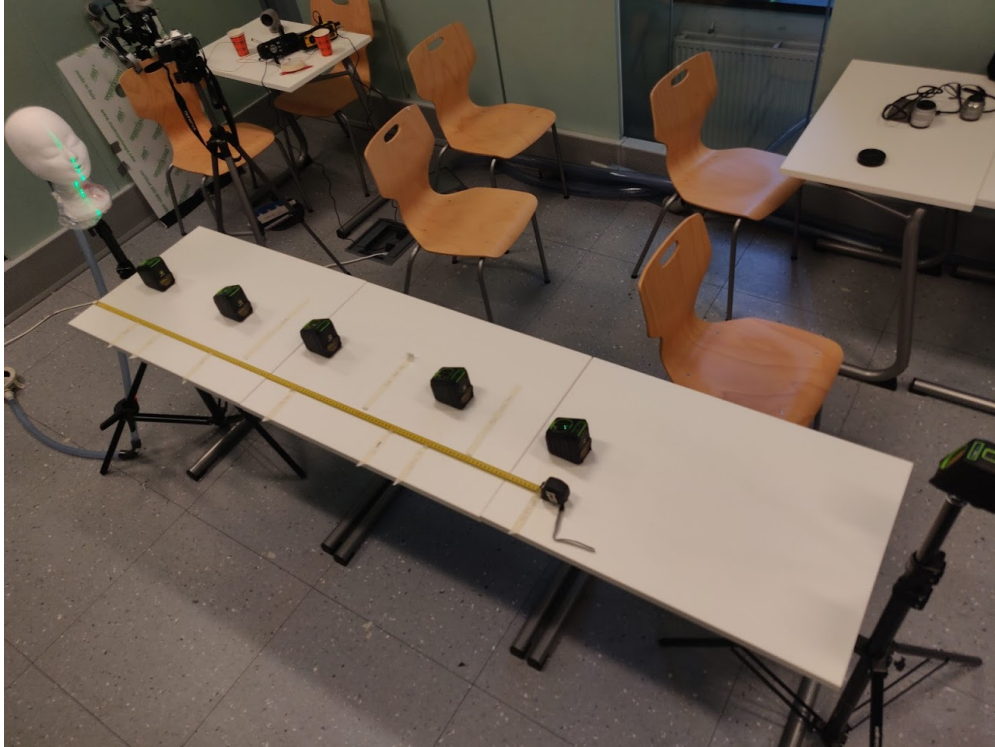


FIGURE 3.29: The setup of the airflow pattern visualisation experiment by placing the camera behind the manikin.

Both the manikin and tables are placed at the centre of the experience room so that it is equally influenced by the ceiling grills. The rest of the portable fog generator system is placed at the back of the room.

3.4.2 Data collection

The visualisation of the fog was recorded with a mirrorless camera with a wide-angle lens. Two attempts were taken for each ventilation regime. Each attempt was one minute long. To mimic the respiratory system as realistic possible, the operator based the pumping movement on its breathing. This resulted in 15 breaths per minute.

Two data loggers were placed in the room to examine if the basic indoor parameters deviated too much between each attempt and ventilation regimes. The limitation was that not all of the droplets were visible with the camera, especially the smaller ones of a few micrometres in diameter. In earlier experiments, it was observed that the droplets are a few seconds longer visible in person than in the video. To also measure the difference between video recording and what the operator saw during the experiment, a stopwatch on the smartphone was used to time how long it took before the droplets were not visible anymore.

3.4.3 Data analysis

Adjusting the ventilation regime will affect the airflow pattern as the basic indoor parameters are changed as well. The attempts were recorded and reviewed to determine how far

the droplets move in the air and how long it takes before they are no longer visible. The program **VLC** was used to review the recordings. Vertical lines were drawn to indicate the distance between the mouth and the lasers as seen in Figure 3.30. When the droplets do not progress more than a certain distance after a single exhalation, it is noted as the furthest distance. The duration was measured by how long it took before the droplet is no longer visible in the recording.

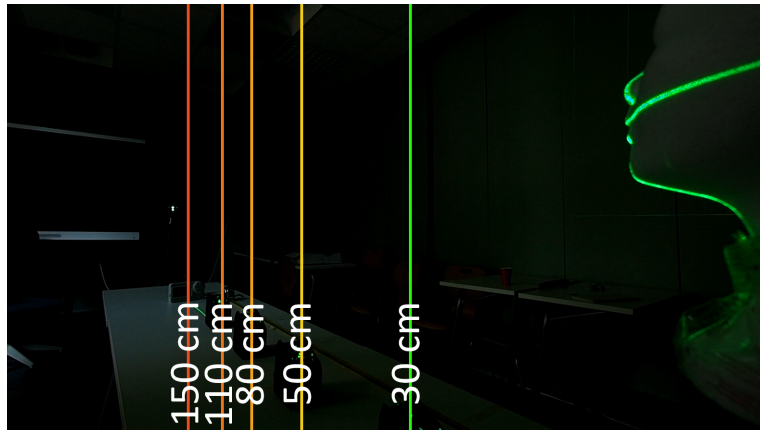


FIGURE 3.30: The distances between the manikin's mouth and the lasers are indicated with vertical lines.

With **Free Video to JPG Converter** the frames were extracted from the video with one frame each second. The next step was to use **Fiji**, an image processing program, to determine the percentages of the droplets detected by the laser per respiratory cycle.

Quantifying the number of droplets is often performed by using a high-resolution camera and Particle Image Velocimetry (PIV) software. This is not possible with the current setup, therefore an attempt is made by comparing the mean grey intensity value of the images. The most convenient method is to compare two images with each other. The comparison is made by subtracting the image at a certain time with the image before exhalation ($t = 0$) as shown in 3.31.

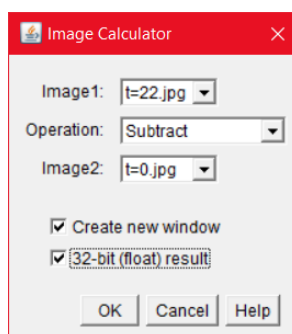


FIGURE 3.31: Subtracting two images with each other. The program used in this figure is Fiji.

The subtraction results in a frame of the droplets. However, the lasers flicker occasionally to calibrate and that can sometimes be seen in the resulting frame. An example can be seen in Figure 3.32. This method allows estimating the percentage of droplets seen in the image. 60 frames were analysed per ventilation regime (one frame per second).

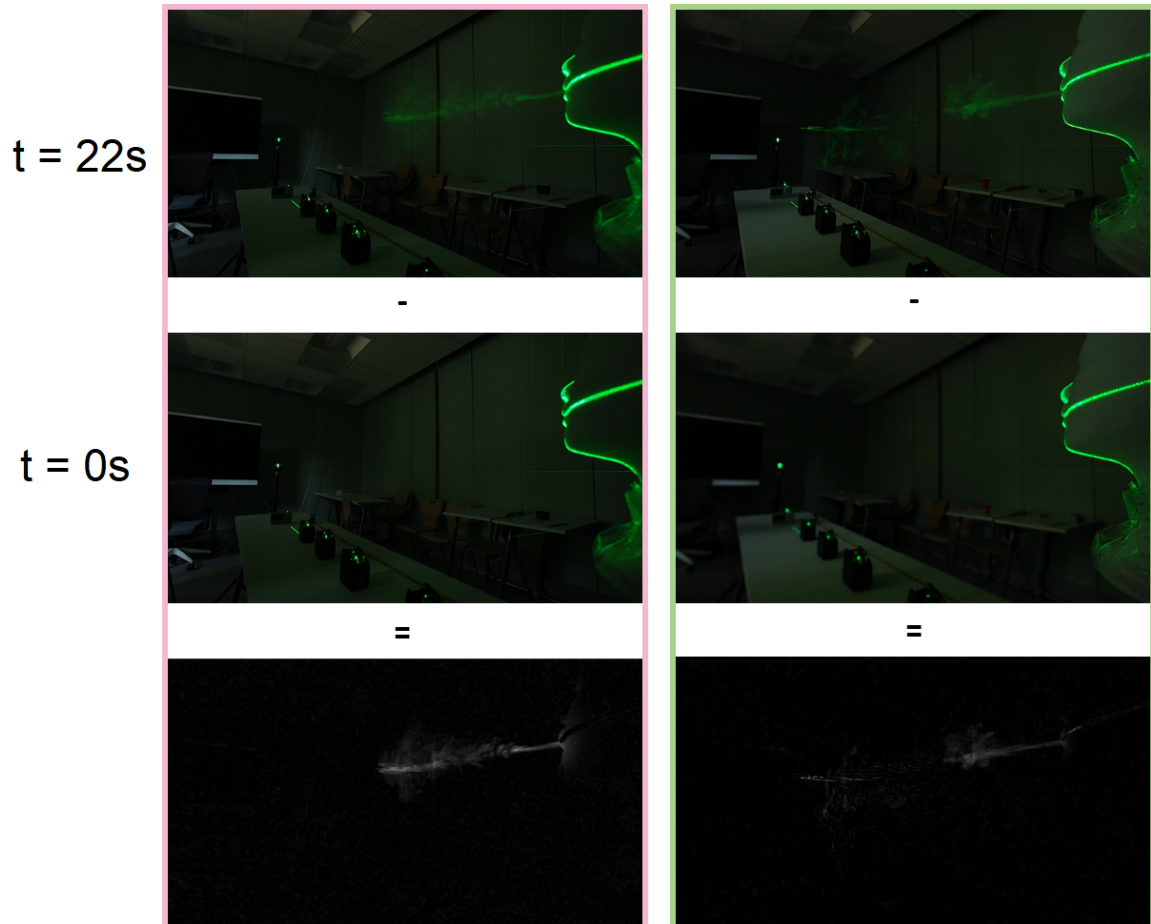


FIGURE 3.32: Two different ventilation regimes are shown here and are indicated with different coloured borders. The top images are from 22 seconds after exhalation ($t = 22$). The middle two images display the frames before exhalation ($t = 0$). The bottom row shows the subtraction of the images in greyscale.

Each pixel is represented in the greyscale colour spectrum. Figure 3.33 shows some values of the scale. The highest value is 255 (white) and the lowest is zero (black). Anything in between is a shade of grey.

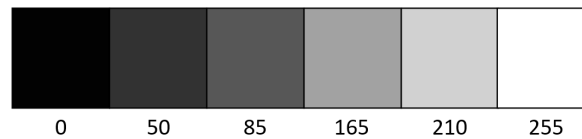


FIGURE 3.33: Different shades of grey are displayed here. White has the highest value and black has the lowest.

An example is shown in Figure 3.34. The area is calculated by multiplying the length with the width ($1920 \times 1080 = 2073600$). Each pixel is assigned a value depending on the greyscale. The mean intensity is calculated by summing the grey values and dividing by the area within the selection. The mean intensity values vary from 0 (the image is completely black) to 100 (the image is completely white). The minimum and maximum are the grey values within the selection. In general, the more droplets are visible after the subtraction method, the higher the mean intensity.

1920x1080 pixels; 8-bit; 2MB



1920x1080 pixels; 8-bit; 2MB



Results				
File	Edit	Font	Results	
	Area	Mean	Min	Max
1	2073600	1.065	0	242
2	2073600	0.697	0	244

FIGURE 3.34: The top picture shows more droplets and these pixels are non-black. The mean value (1.065) is higher than in the image at the bottom (0.697), where fewer droplets are visible.

3.5 Theoretical comparison

The final part of the methodology is the theoretical comparison. The equations in subsection 2.1.2 and 2.1.6 were used to determine how far (eq. 2.1) and how long the droplets linger in the air (eq. 2.2). These will be calculated by using excel and MATLAB. The data of the basic indoor parameter data from the airflow pattern experiment will be used. The goal is to analyse how accurate the output of the portable fog generator system is in comparison with the theory and equations.

Chapter 4

Results

The goal of this chapter is to report the main findings of the research. The first part introduces the results of the baseline measurements. Which is the effect of how the different ventilation regimes and the breathing of the manikin influence the conditions of the basic indoor parameters of the experience room. The next part is the outcomes of the airflow pattern visualisation experiment. The results present the furthest distance the droplets travel, the duration the droplets linger in the air before falling on the ground or is not visible anymore, and the percentage of detectable fog for each ventilation regime. The theoretical part describes how long should linger in the air and how far it travels by using equations and an analytical model. Lastly, results between the portable fog generator system and theory will be shown.

4.1 Baseline measurements

The baseline measurements data are shown in **Appendix C**.

4.1.1 Air velocity

The deviation in air velocity is the lowest with *no ventilation* (0.02—0.03 m/s) and greatest with *natural + mixing ventilation* (0.02—0.21 m/s). With *natural ventilation*, the air velocity is highest at 20 centimetres at location F (0.06 m/s). In the *natural + mixing ventilation* regime, location C at 120 centimetres has the highest value (0.21 m/s). An overview of how the ventilation regimes affect the air velocity is shown in Figure 4.1.

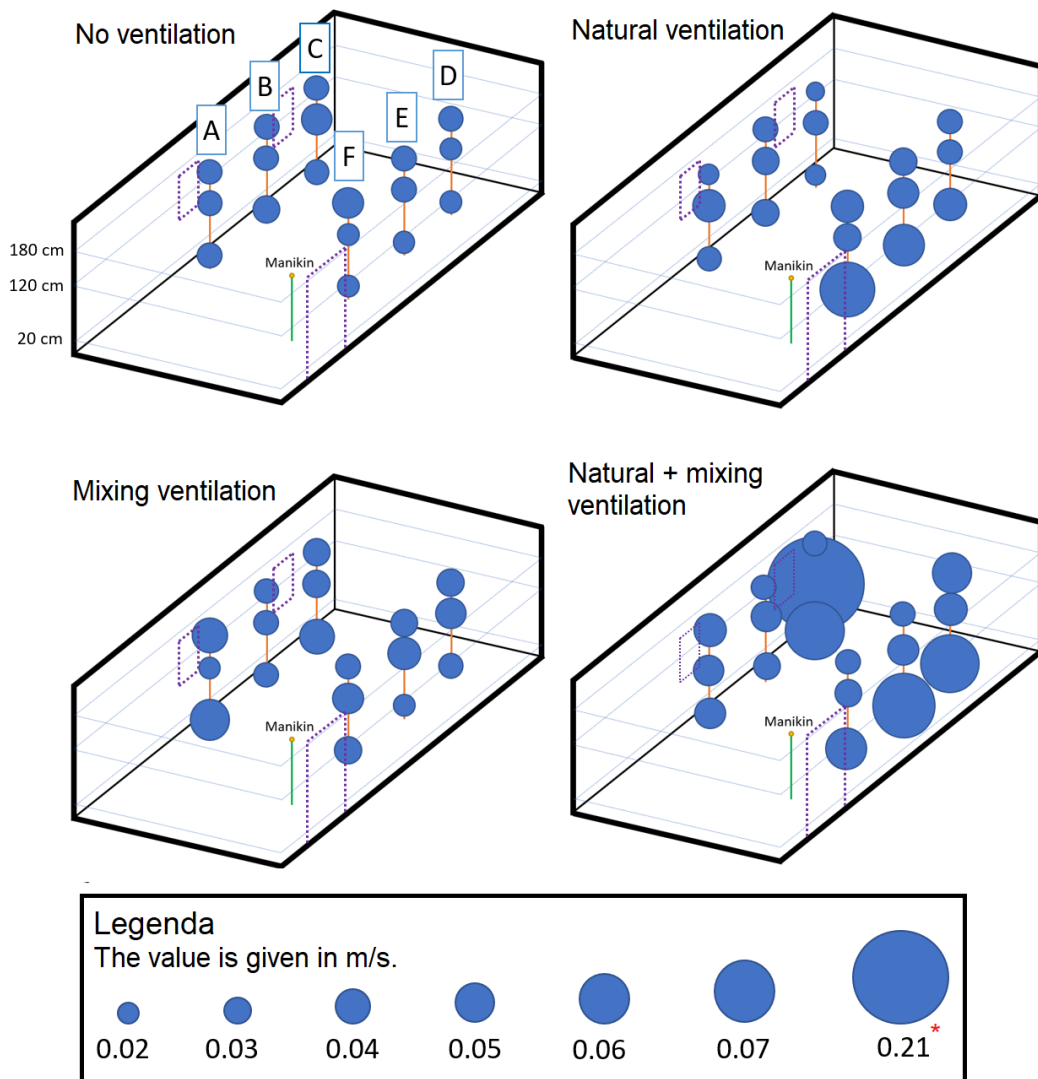


FIGURE 4.1: air velocity of the four ventilation regimes. The six locations are noted with the letter A to F and are shown at the *no ventilation* regime. The larger the bubble the higher the air velocity value. The door and windows are indicated with dotted lines. The manikin is placed at the corner of the experience room, behind location F. The different heights are displayed here in the vertical axis.

*The value of 0.21 m/s is not drawn in proportion otherwise it would be much too large.

The average air velocity per ventilation regime was analysed. The *no ventilation* regime had an average air velocity of 0.027 m/s . By opening the windows, the air velocity of the outdoor air coming inside the experience room was 0.25 m/s . The air velocity *natural ventilation* regime increased the average air velocity of the experience room to 0.031 m/s . The ceiling grilles supplied an air velocity of 0.45 m/s and the exhaust at the short sides of the experience room was 0.17 m/s . The average air velocity of the *mixing ventilation* regime was 0.032 m/s . The combination of *natural + mixing ventilation* regime resulted in an average air velocity of 0.058 m/s , which is almost twice as high in comparison with the other ventilation regimes. The combination of opening the windows and applying mechanical ventilation creates a strong airflow current. This ventilation regime is considered an inefficient decision in terms of energy consumption as it interrupts the energy balance that the mixing ventilation has created. The results of the air velocities per ventilation regime are shown in Figure 4.2.

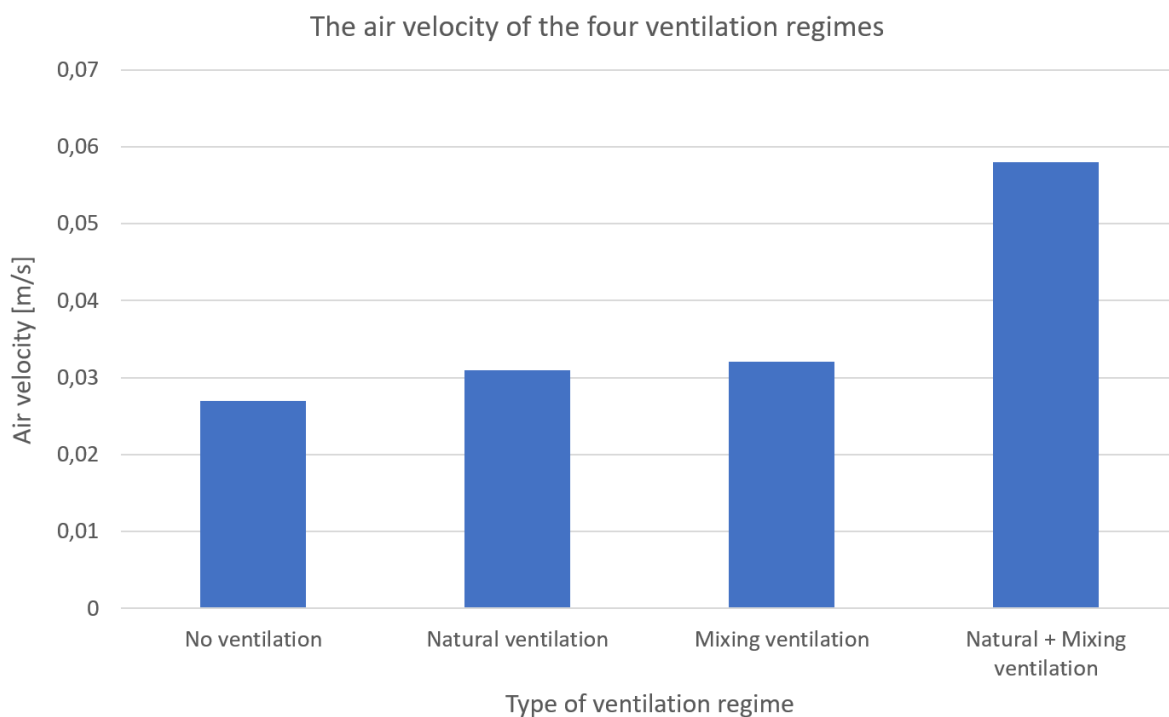


FIGURE 4.2: The average air velocities of the four ventilation regimes. The *no ventilation* regime has the lowest air velocity (0.027 m/s). The *natural + mixing ventilation* regime has the highest air velocity (0.058 m/s).

The analyse of the six locations resulted that location B has on average the lowest air velocity (0.028 m/s) and location C the highest (0.046 m/s). Both locations are influenced by the window and ceiling grilles. The air velocity at the right half of the experience room (location D, E and F) do not vary much with each other (0.002 m/s at most). The results are shown in Figure 4.3.

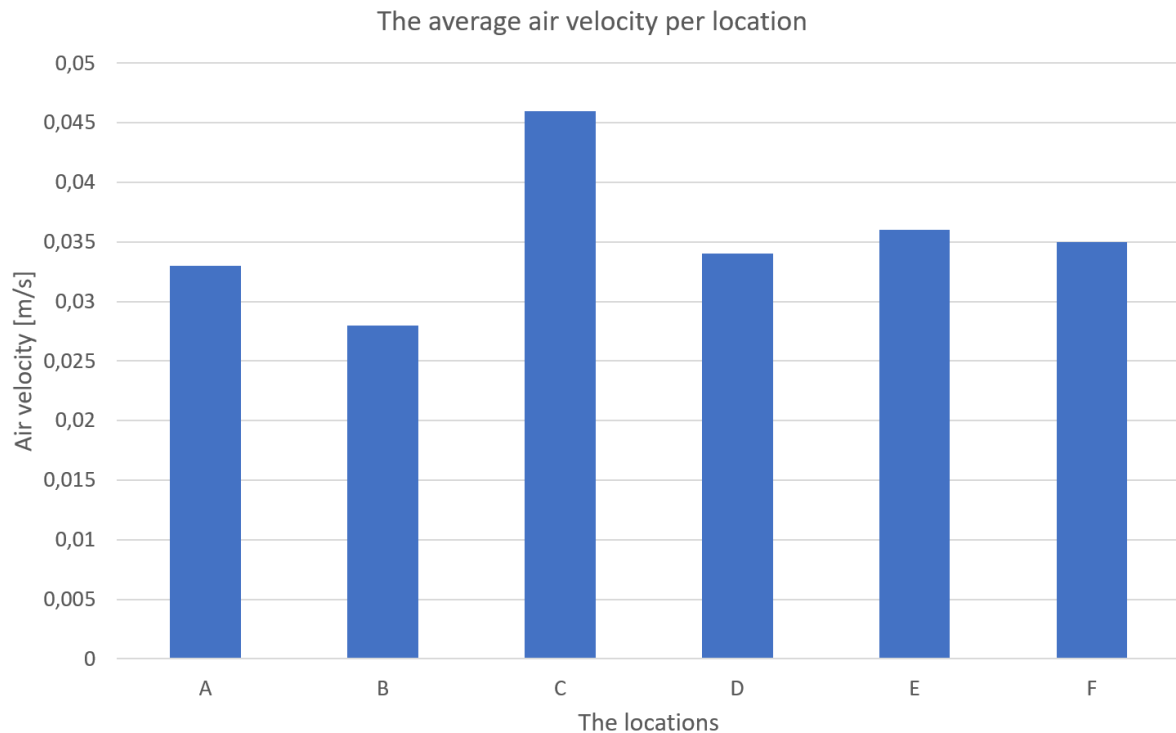


FIGURE 4.3: The average air velocity of all four ventilation regimes is 0.035 m/s . The lowest air velocity is found at location B (0.028 m/s) and the highest at location C (0.046 m/s).

The air velocity at three different heights was measured and the results can be seen in Figure 4.4. At the *natural ventilation* regime, the air velocity is the highest at 20 centimetres with a value of 0.038 m/s . The highest air velocity was 0.066 m/s at a height of 120 centimetres at the *natural + mixing ventilation* regime. The height of 180 centimetres has the lowest air velocity off all ventilation regimes. The lowest value is seen in the *natural ventilation* regime (0.026 m/s).

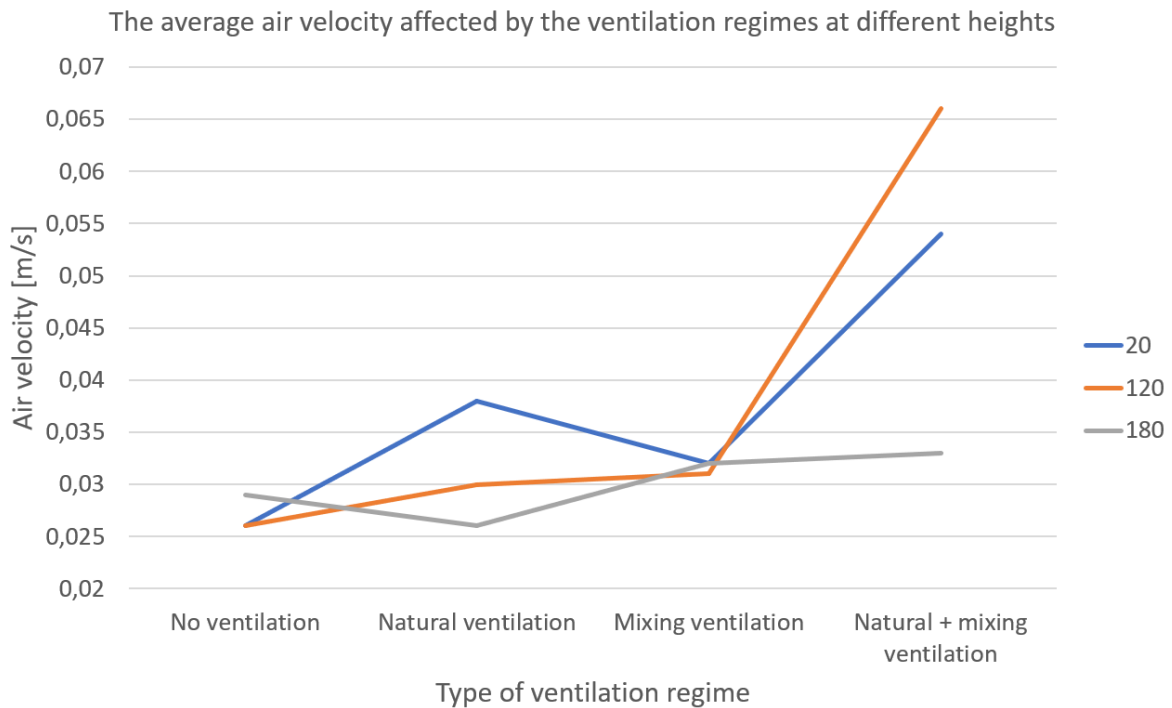


FIGURE 4.4: The overall air velocity is the highest at the *natural + mixing ventilation* regime. The air velocity is low at 180 centimetres compared to the other two heights in all ventilation regimes.

Furthermore, both heights of 20 and 120 centimetres has an average air velocity of 0.038 m/s . The lowest value is seen at 180 centimetres (0.030 m/s). The results of the heights are shown in Figure 4.5.

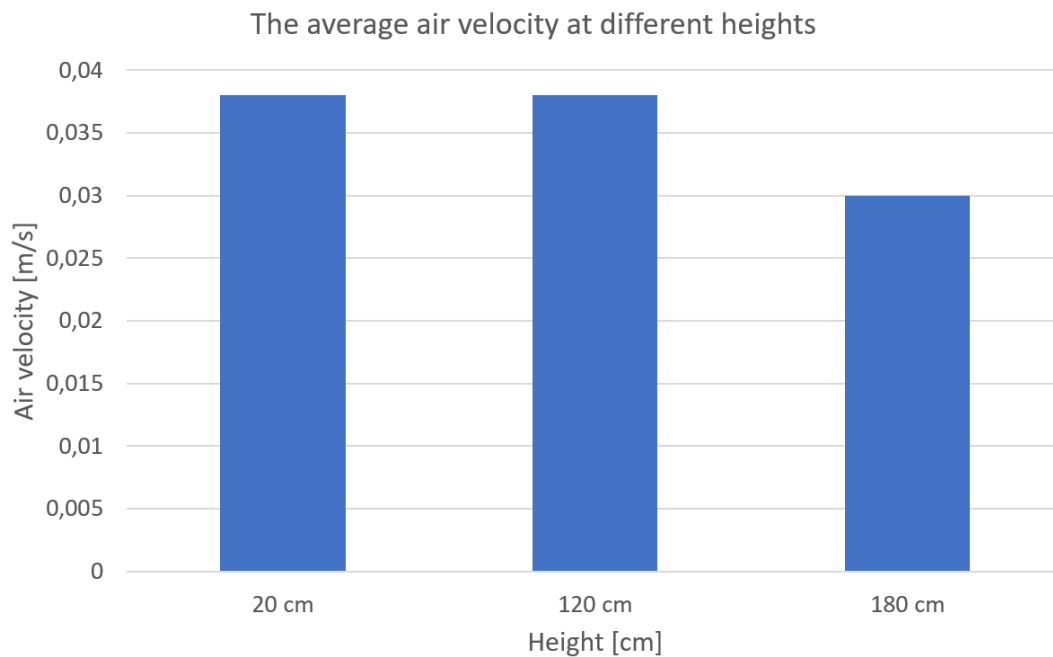


FIGURE 4.5: The air velocities at different heights. The values are the highest at 20 and 120 centimetres.

4.1.2 Temperature

The temperature was measured during the baseline measurements for each ventilation regime. The temperature fluctuated between 20.9—21.6°C. On the first day in the afternoon, the *no ventilation* had an average temperature of 21.4°C. By opening the windows during *natural ventilation* the temperature has risen to 21.6°C. On the second day in the morning, the temperature of the *mixing ventilation* was set to 21.0°C. The temperature during *natural + mixing ventilation* was 21.3°C. The average temperature of all four ventilation regimes is displayed in Figure 4.6.

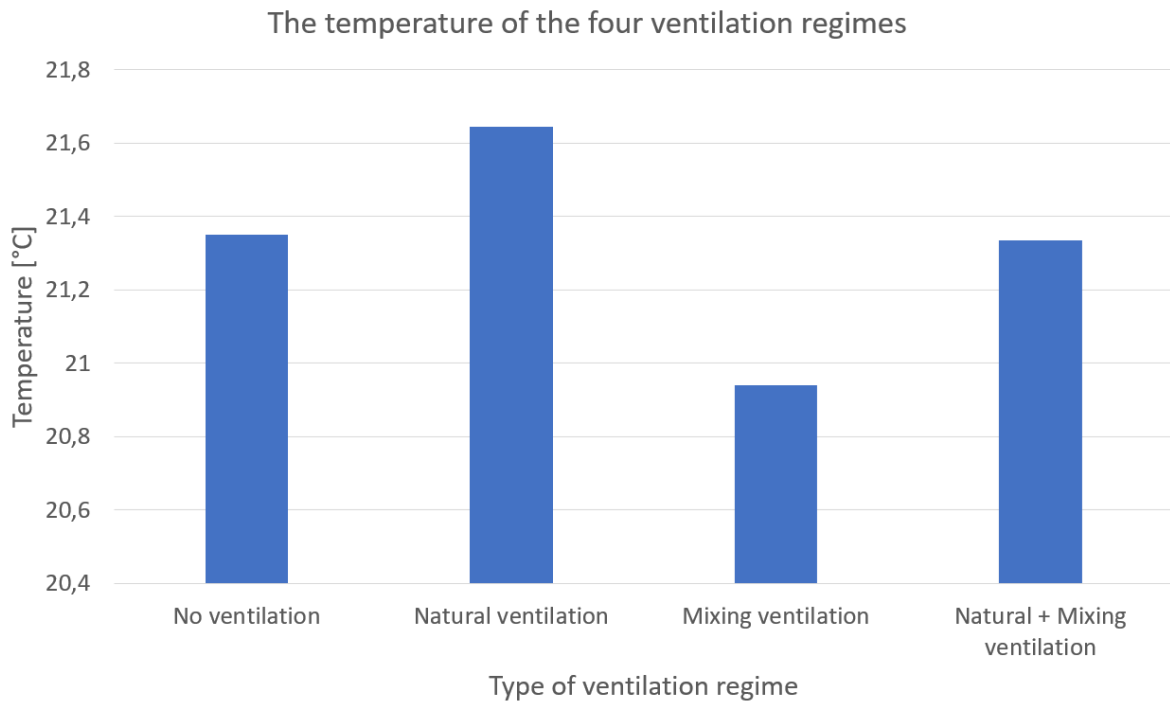


FIGURE 4.6: The temperature increases from 20.8 to 21.6°C. The heat of the machine and operators affected the indoor temperature of the room, gradually increasing the temperature.

The temperature drop between the natural ventilation and mixing ventilation is due to doing the measurement on two separate days. The heat of the machine and operators affected the indoor temperature of the room, gradually increasing the temperature during the measurements. The study results seem to indicate that there is no strong correlation between the temperature and the ventilation regimes.

4.1.3 Relative humidity

Unfortunately, only the relative humidity was measured on the second day. The results showed that RH decreased all the time during the measurements. The *mixing ventilation* regime had a RH of 31.74%. This value dropped to 27.83% at the *natural + mixing ventilation* regime.

4.2 Experiment: Airflow pattern visualisation

4.2.1 Duration

The operators in the experience room noticed during the experiment that the droplets stayed in the air longer than what was recorded in the video. Therefore, measurements were also timed during the experiment with a stopwatch. The mean value of the two attempts were taken for each ventilation regime. In the *no ventilation* regime, the droplets were able to form a plume and remained suspended in the air for 12.7 seconds in the video and 15.5 seconds in person. The fog plume in *natural ventilation* is less concentrated than in the previous ventilation regime. The droplets lingered in the air for 12.2 seconds in the recording and 13.8 seconds in person. It is important to note that not only both windows were opened, but also the door of the experience room. This was to analyse what the effect would be if the door was also open. In the regime of only *mixing ventilation*, the fog plume is less concentrated and dissipates in both the horizontal and vertical directions. The fog is being pushed down by the ventilation from the ceiling, causing it to drop down faster. It was visible for 9.5 seconds in the video and 11.2 seconds in person. The fog plume disappears the quickest at the *natural + mixing ventilation* regime. The droplets is travelling upwards and spread even faster when it almost reaches the ceiling with a lingering time of 5.4 seconds in the video and 7.2 seconds in person. An overview of the results is shown in Figure 4.7.

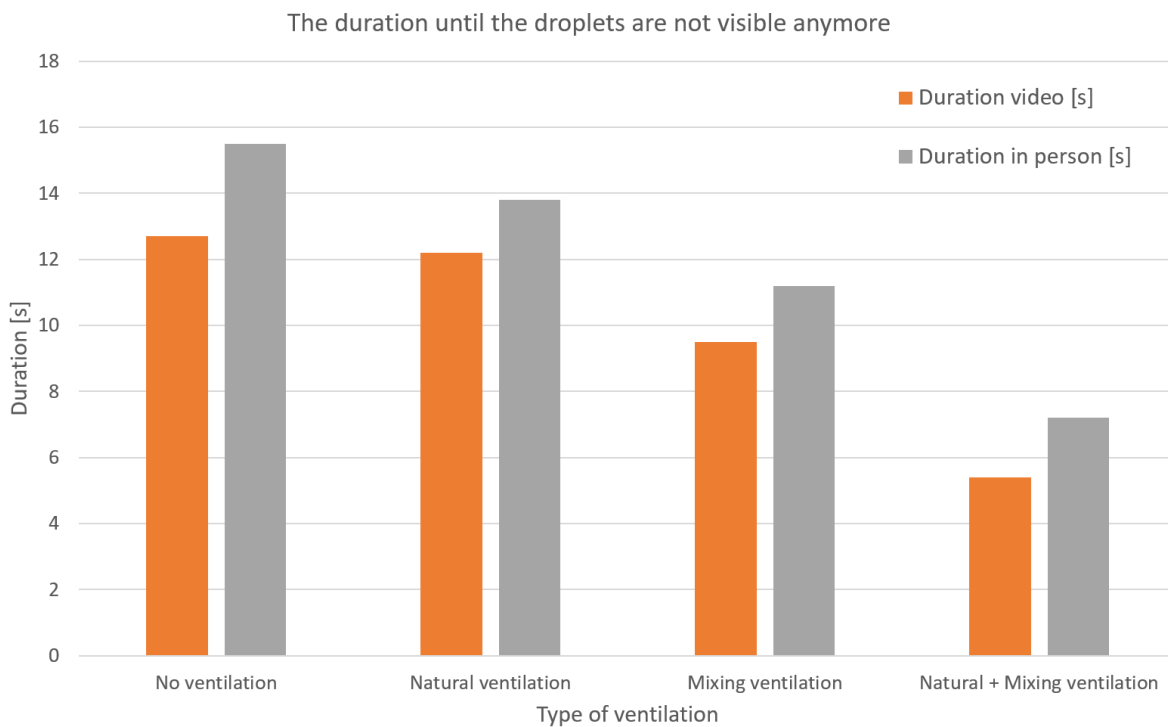


FIGURE 4.7: The droplets settled or evaporated faster in the recordings than with the naked eye. Any form of ventilation decreases the visibility of the droplets.

4.2.2 Distance

On average, the human eye cannot see particles smaller than $60 \mu\text{m}$. What was seen in the video or during the experiment is not a single droplet, but a collection of droplets. The results are shown in Figure 4.8. The corresponding frames of the video which were used to determine the distance can be found in **Appendix D**. The droplets reached a distance of 1.3

metres without any ventilation. By opening the windows and door in the *natural ventilation* regime, a distance of 1.8 metres was recorded. The door was behind the manikin, pushing the drops further into the classroom. Applying only mechanical ventilation in the *mixing ventilation* regime resulted that the droplets travelling 0.9 metres. The droplets reached the shortest distance of 0.5 metres in the *natural + mixing ventilation* regime.

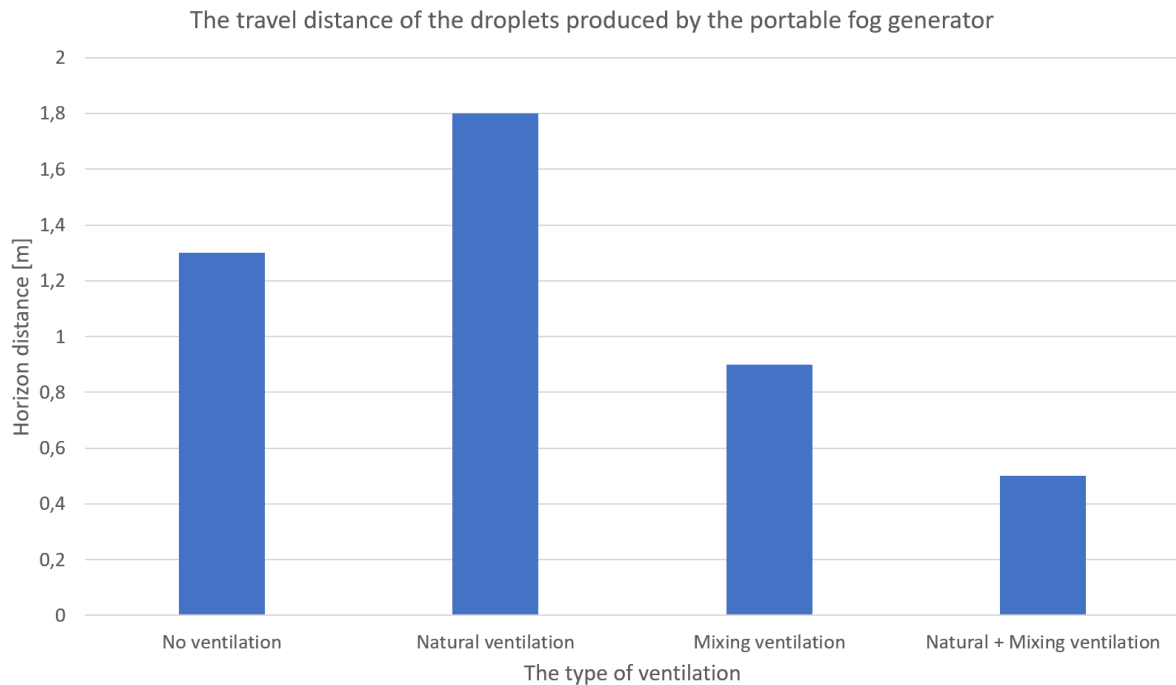


FIGURE 4.8: The droplets travelled furthest with *natural ventilation* (1.8 metres) and crusted with *natural + mixing ventilation* (0.5 metres).

4.2.3 Percentage of fog plume per ventilation regime

The value on the vertical axis indicates the mean grey intensity, which is the percentage of fog plume per frame. If the image were completely white, the mean grey intensity value would be 100% and 0% if it were completely black. The analysed images with only the fog plumes are mostly black pixels. This results in a low mean grey intensity value (0.41—1.56%). The pattern of the lines indicates the respiratory cycle for 60 seconds. The peak and valley indicate exhalation and inhalation, respectively. With all four ventilation regimes, the mean grey intensity increases in the beginning and decreases at the end (Figure 4.9). This is because the amount of fog in the buffer is decreasing during each exhalation. The *natural + mixing ventilation* regime has the lowest average mean grey intensity value (0.74%). The fog plume is immediately dispersed by the high air velocity caused by the open door, windows and the presence of mechanical ventilation. Therefore, the majority of the droplets are not detected by the laser. The average mean grey intensity of *no ventilation* and *natural ventilation* is 0.855% and 0.90%, respectively. More droplets are detected by the laser in *natural ventilation* as it passes a longer distance during *no ventilation*. The *mixing ventilation* regime has the highest value (1.22%). The fog plume is mainly dispersed horizontally, causing the total concentration of droplets per exhalation to spread out even more, thus making it easier for the lasers to reflect the droplets.

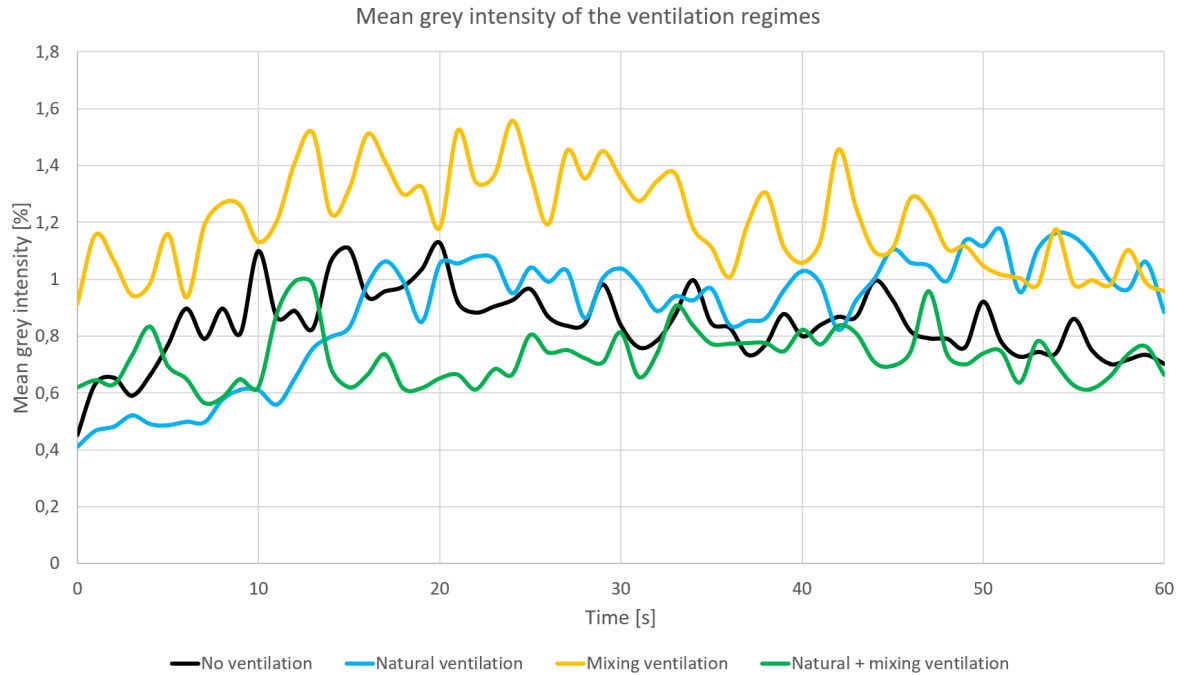


FIGURE 4.9: The respiratory cycle is represented in the graph with peaks and valleys. The mixing ventilation has the highest percentage of mean grey intensity. This means that the fog plume is more dispersed in comparison with the other ventilation regimes.

4.2.4 Basic indoor parameters

The temperature and relative humidity during the experiment is shown in Table 4.1. The temperature fluctuated between 24.3—24.4°C. The relative humidity started at 53.3% and dropped to 48.1% at the end of the experiment.

Ventilation regime	Temperature [°C]	Relative humidity [%]
No	24.3	53.3
Natural	24.3	52.3
Mixing	24.3	50.1
Natural + mixing	24.4	48.1

TABLE 4.1: The temperature and relative humidity during the airflow pattern visualisation experiment.

4.3 Theoretical results

4.3.1 Duration

To determine how long it takes for a particle to fall from a specific height in calm air (<0.2 m/s), the settling velocity needs to be calculated. The settling velocity between 0.1—100 μm were computed by using the Stokes' law in subsection 2.1.6. The basic indoor parameters of the airflow pattern visualisation experiment were used for the calculations. For this example, the settling velocity with a particle diameter of 1 μm was calculated. The first step is to use Sutherland's equation (eq. 4.1) to determine the dynamic viscosity:

$$\mu = \mu_0 \left(\frac{T}{T_0} \right)^{3/2} \left(\frac{T + S}{T_0 + S} \right) \quad (4.1)$$

where:

μ = dynamic viscosity [$Pa \cdot s$]
 μ_0 = reference viscosity [$Pa \cdot s$]
 T = reference temperature [K]
 T_0 = temperature at 273.15 Kelvin [K]
 S = Sutherland constant for the gas [K]

The average room temperature at the experience room was $24.30^\circ C = 297.45 K$. The reference viscosity at that specific temperature is $1.716 \times 10^{-5} Pa \cdot s$. The Sutherland constant of air at that specific temperature is 110.4 K. The dynamic viscosity is equal to 1.83×10^{-5} .

$$\mu = 1.716 \times 10^{-5} \left(\frac{294.45}{273.15} \right)^{3/2} \left(\frac{294.45 + 110.4}{273.15 + 110.4} \right) = 1.83 \times 10^{-5}$$

The Cunningham correction factor becomes even more relevant if the particle diameter is $< 15 \mu m$. The Cunningham correction factor for air in standard condition can be calculated with the following Equation 4.2:

$$C = 1 + \frac{0.167 \times 10^{-6}}{d} \quad (4.2)$$

where:

C = Cunningham correction factor
 d = particle diameter [m]

By applying the d with $1 \mu m$, the Cunningham correction factor can be computed.

$$C = 1 + \frac{0.167 \times 10^{-6}}{1 \times 10^{-6}} = 1.167$$

Now that all unknown values are calculated, the settling velocity can be computed with Stokes' law. Assume the particle density to water, which is equal to $1000 kg/m^3$. The Cunningham correction factor is 1.167 and dynamic viscosity is 1.83×10^{-5} . The settling velocity with a particle diameter $1 \mu m$ is $3.52 \times 10^{-2} m/s$.

$$v = \frac{9.81 \cdot (1.0 \times 10^{-6})^2 \cdot 1000 \cdot 1.167}{18 \cdot 1.83 \times 10^{-5}} = 3.52 \times 10^{-2} [m/s]$$

Table 4.2 indicates the dynamic viscosity, mean free path, Cunningham correction factor and settling velocities for particles ranging from 0.1 to $100 \mu m$.

TABLE 4.2: Settling velocity for particle diameters from 0.1 to 100 μm based on the temperature of the experience room.

Diameter d [μm]	Dynamic Viscosity μ	Correction Factor C_s	Settling Velocity v_{settling} [m/s]
0.1	1.83E-05	2.670	8.60E-07
0.5	1.83E-05	1.334	9.93E-06
1	1.83E-05	1.167	3.52E-05
5	1.83E-05	1.033	7.70E-04
10	1.83E-05	1.017	0.003
50	1.83E-05	1.003	0.075
100	1.83E-05	1.002	0.299

Based on the values of Table 4.2, various with different particle diameters are plotted from a height of 120 centimetres in **Appendix E** (0.1—100 μm). The portable fog generator system produces particles from 1—10 μm . This is shown in Figure 4.10.

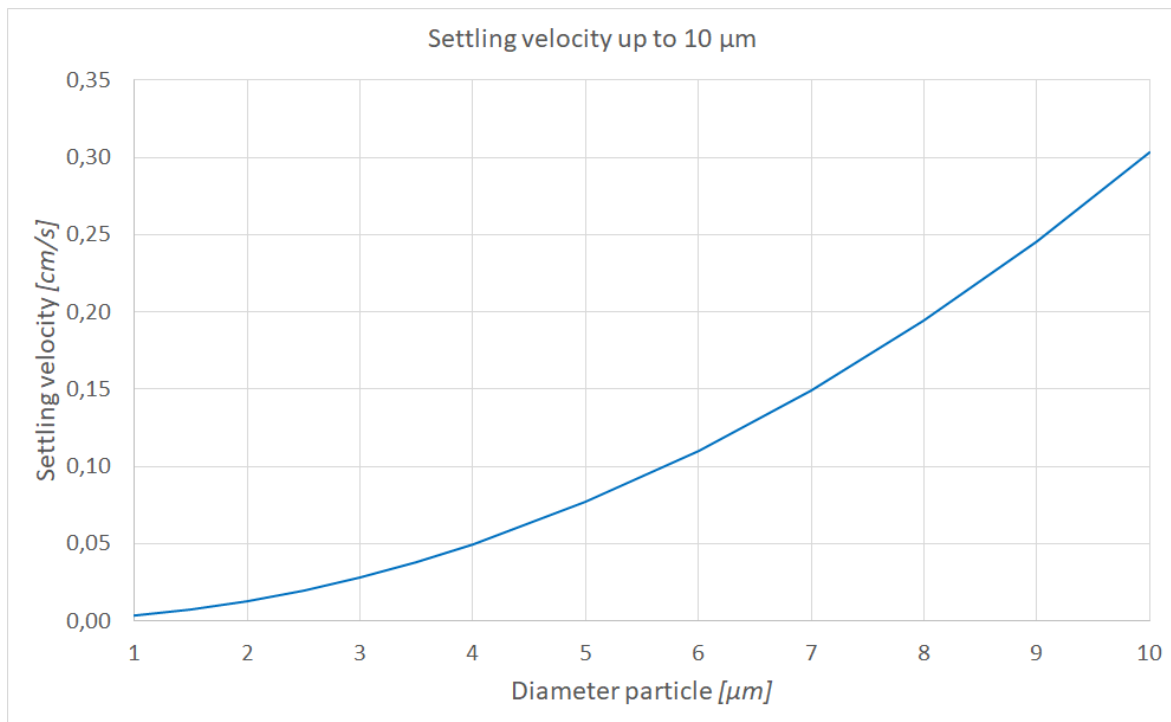


FIGURE 4.10: The settling velocity with a particle diameter from 0.1—10 μm at 297.45 K.

The duration until the droplets settles from that specific height is shown in Figure 4.11. It can take up to hours until the particles fall on the ground.

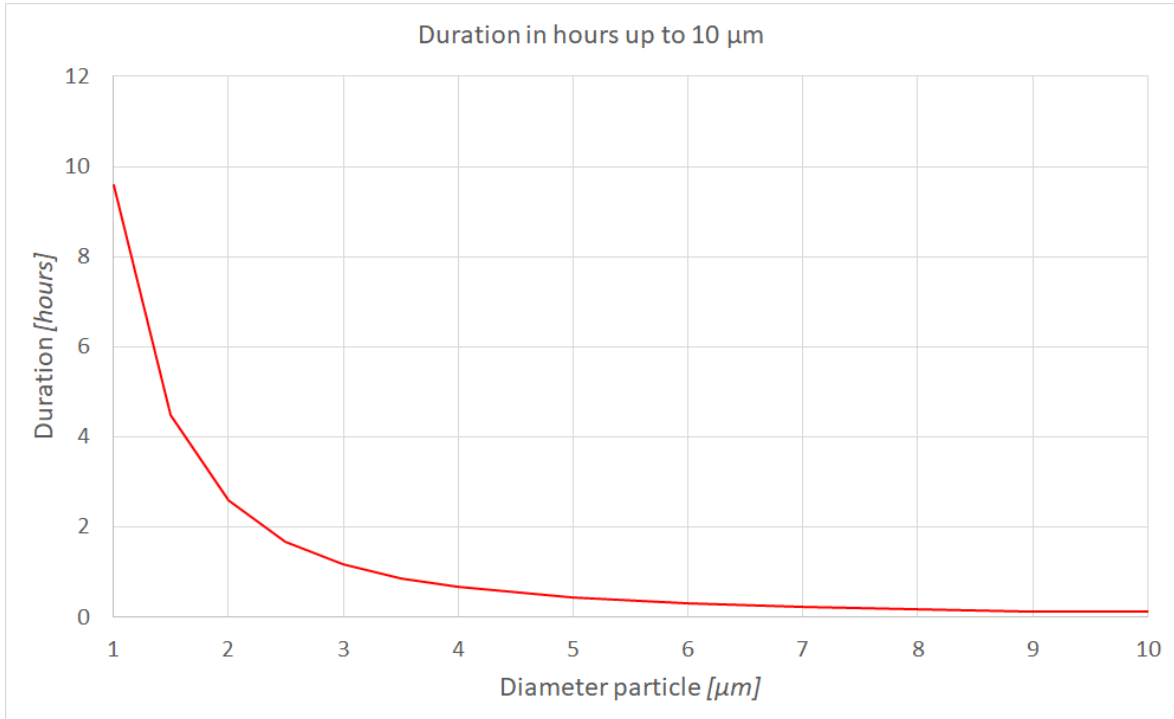


FIGURE 4.11: The duration in hours with a particle diameter between 0.1—10 μm at 297.45 K.

4.3.2 Distance

A simplified MATLAB model from Wang et al. was used to determine the distance the respiratory droplets travels after exhalation (Wang et al., 2020). For the MATLAB script, one can refer to **Appendix F**. The equation of Newton's second law and Köhler's evaporation model is applied. The following assumptions are made:

- the respiratory droplets are fully saturated with water;
- the random motions of particles in the air (Brownian motion) are neglected;
- the fluctuations of temperature and relative humidity are ignored;
- the pressure force is omitted to simplify the calculation process.

Newton's second law

The main factors acting on the respiratory droplet in the air are the drag, pressure and gravitational forces. By applying Newton's second law yield the following (eq. 4.3):

$$m_d \frac{du}{dt} = F_{drag} + F_{pressure} + F_{gravity} \quad (4.3)$$

where:

m_d = mass of the droplet estimated with $\frac{1}{6}\pi\rho_d d^3$ [g]

u = velocity of the droplet [m/s]

t = time [s]

The forces F_{drag} , $F_{pressure}$ and $F_{gravity}$ are respectively given by Equation (4.4, 4.5, 4.6):

$$F_{drag} = \frac{1}{2} C_a \rho_a A_d |u_a - u_d| (u_a - u_d) \quad (4.4)$$

$$F_{pressure} = -V_d \nabla p \quad (4.5)$$

$$F_{gravity} = V_d (\rho_d - \rho_a) g \quad (4.6)$$

where:

C_a = drag coefficient

ρ_a = density of the fluid [kg/m^3]

A_d = reference area estimated with $\pi \left(\frac{d}{2}\right)^2$ [m^2]

V_d = volume of the droplet [m^3]

The subscript d and a denotes droplets and air, respectively. The drag coefficient is calculated with Equation 4.7:

$$C_a = \frac{24}{Re} + \frac{6}{1 + \sqrt{Re}} + 0.4 \quad (4.7)$$

And the Reynolds number can be calculated with Equation 4.8:

$$Re = \frac{\rho_a |u_a - u_d| d}{\mu_a} \quad (4.8)$$

Evaporation model

The respiratory droplets immediately shrink after exhalation, primarily due to the difference in the relative humidity of the mouth and environment. It can become a droplet nuclei (<5 μm) and can linger in the air long enough for someone to inhale it. The equation of the decrease rate in the diameter due to evaporation was shown in subsection 2.1.2.

The height of the manikin's mouth is 120 centimetres above the floor. The temperature of the mouth and RH is assumed to be 25°C and 95%, respectively. The indoor temperature and RH of the experience room are 24.3°C and 50.3%, respectively. The indoor air velocity was 0.027 m/s (no ventilation). The breathing velocity is assumed to be 4.42 m/s (Mhetre and Abhyankar, 2017). Figure 4.12 shows the trajectories of droplets at different diameters during breathing. Although the portable fog generator system produces droplets up to 10 μm , the human respiratory droplets can go up to 500 μm (Gralton et al., 2011).

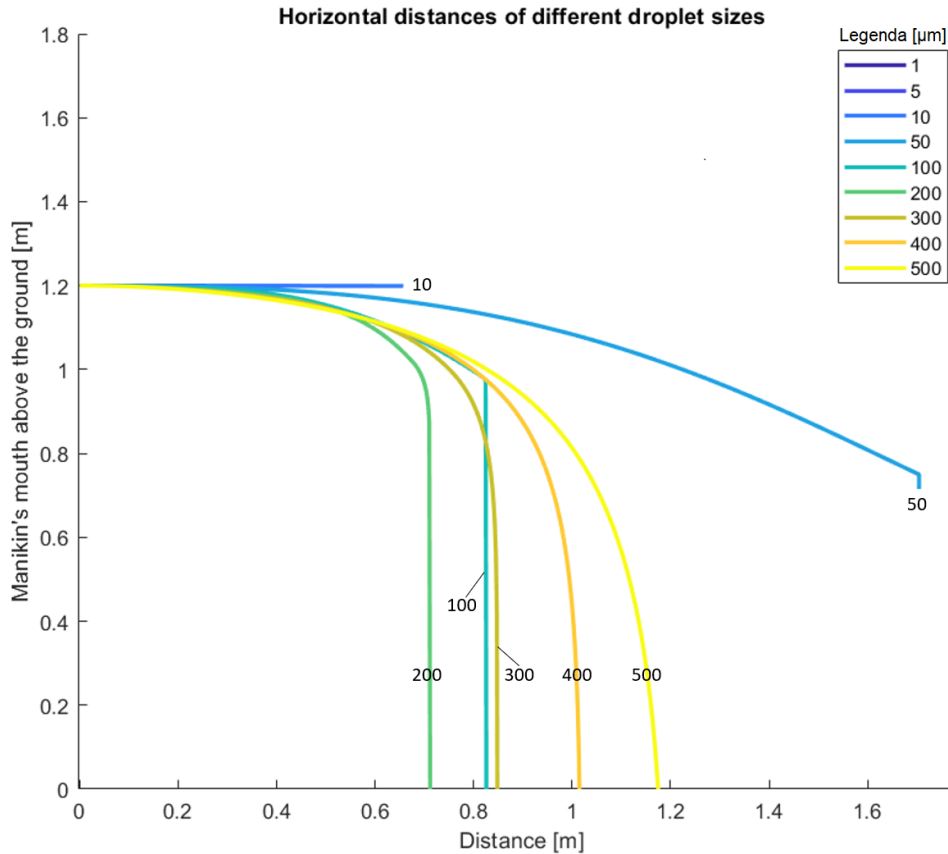


FIGURE 4.12: The trajectory of particle sizes from 1—500 μm based on the basic indoor parameters of the experience room during the experiment during breathing.

The smaller droplets ($<5 \mu\text{m}$) evaporate immediately and becomes droplet nuclei and it can take from minutes to hours before it settles on the ground. The 10 μm droplets reach a distance of 0.66 metres before it evaporates. The trajectory of a particle with a 50 μm diameter ends at 1.706 metres and settles due to gravity before evaporating. Droplets that are larger than 100 μm fall on the ground before they could completely evaporate due to the higher concentration of water. Adjusting the ventilation regime from *no ventilation* (0.027 m/s) to *natural + mixing ventilation* (0.058 m/s) had no effect on the trajectories of the droplets. There is a noticeable difference in the airflow pattern when the indoor air velocity is $>1.5 \text{ m/s}$. Such a high air velocity rate is often associated with drought and leads to the discomfort of the pupils in the room. The droplet size between 10—100 μm has been analysed. Between these ranges, the droplet has the highest horizontal travel distance. This is plotted in Figure 4.13.

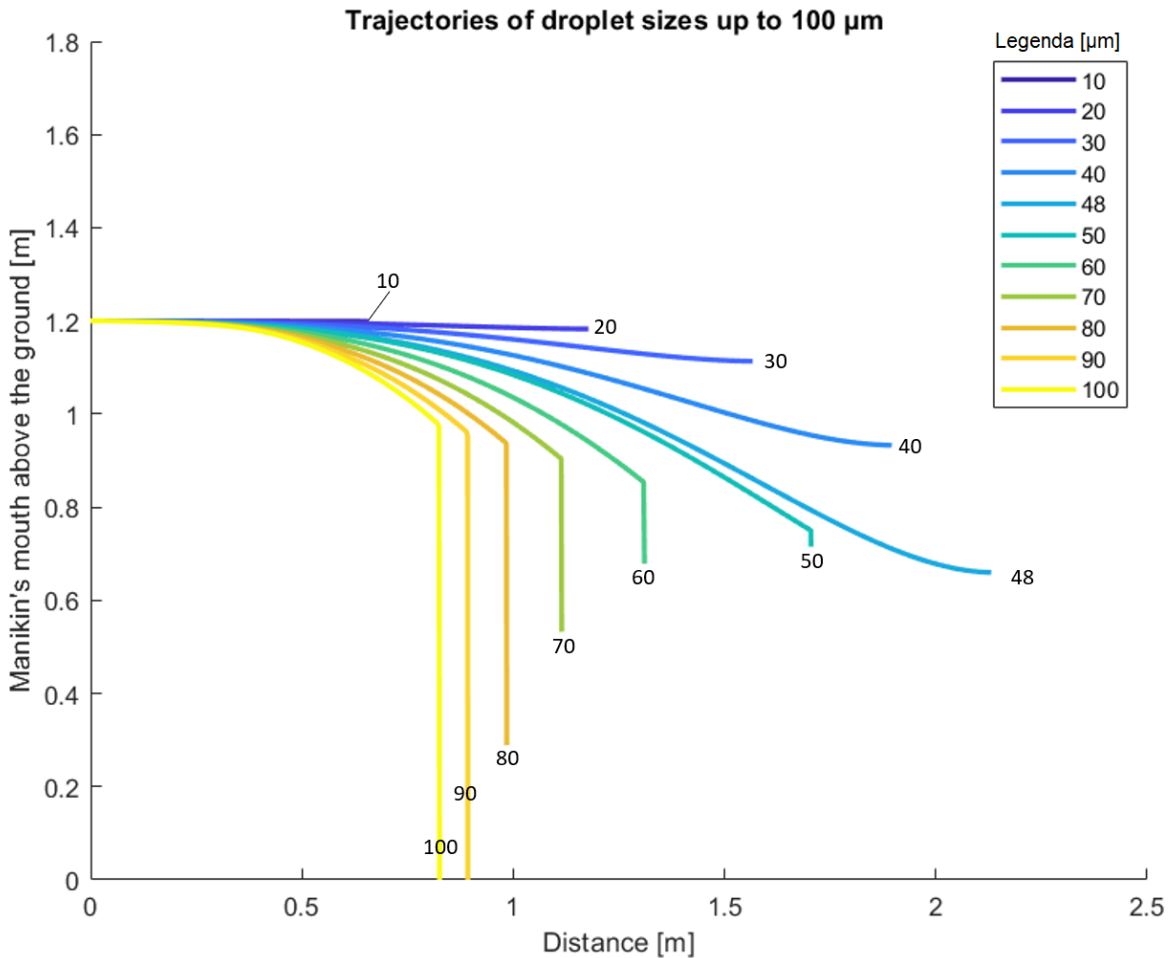


FIGURE 4.13: The trajectory of particle sizes from 10–100 μm based on the basic indoor parameters of the experience room during the experiment during breathing.

These particles linger long enough in the air to travel further with the airflow of the room. The results showed that a particle diameter of 48 μm reaches a distance of up to 2.13 metres and linger in the air for 17.4 seconds before evaporation plays a role. This goes along with the results of Xie et al. that the 'sweet spot' of droplets sizes is between 30 to 50 μm .

4.3.3 Basic indoor parameters

The results of the effect of the basic indoor parameters are found in **Appendix G**. A comparison was made with two different values of air velocity exiting the manikin's mouth. The results were compared with breathing (4.42 m/s). By simulating a cough (10.6 m/s) the most noticeable differences were that droplets starting from 200 μm reached a greater distance in comparison with breathing (Kwon et al., 2012). Droplets of 500 μm reached a distance of 1.58 metres (+0.46 m). The velocity of sneezing was 46 m/s (Jennison, 1942). An increment of the horizontal distance was noticed starting from 90 μm . A droplet of 500 μm reached a distance of 2.65 metres (+1.53 m).

In general, increasing the indoor temperature speeds up the evaporation process, while decreasing the temperature does the opposite. Three different temperatures were compared with the temperature of the airflow pattern experiment (24.3°C). At that temperature,

droplets $<100 \mu\text{m}$ tend to notice the effect of the temperature change. Especially with a particle diameter of 80 and $90 \mu\text{m}$. Both evaporates at a temperature of 0.29 and 0 m above the ground, respectively. Decreasing the temperature to 19.4°C has only an effect on the particle diameter of $80 \mu\text{m}$. It evaporates 0.17 metres above the ground. Increasing the temperature to 29.4°C results that both 80 and $90 \mu\text{m}$ evaporates sooner at 0.38 and 0.08 m , respectively. Another increment of 5°C results in both the particles evaporating at 0.45 and 0.19 m above the ground, respectively.

Adjusting in relative humidity primarily affects droplets smaller than $100 \mu\text{m}$. Due to the small volume, it can evaporate much quicker. The RH at 50.7% is set as the base value. At a RH of 10.7% , the $100 \mu\text{m}$ droplet evaporates at a height of 0.24 metres. At 30.7% , this affects only the droplets with a diameter of 80 and $90 \mu\text{m}$. Both evaporate at 0.21 and 0.28 metres, respectively. At a RH of 70.7% only the droplet size of $50 \mu\text{m}$ is influenced by the increment. It will evaporate 0.69 metres above the ground. Once again, only the $50 \mu\text{m}$ is affected at a RH of 90.7% as it will evaporate 0.55 metres above the surface.

4.4 Comparison between the results of the portable fog generator system and the theory

By adding the threshold distances of the airflow pattern visualisation experiment in the analytical model, a comparison can be made. Firstly, the differences from $1\text{--}500 \mu\text{m}$ are shown in Figure 4.14. Particles $>10 \mu\text{m}$ in diameter are visible at *natural + mixing ventilation*. The same applies for *mixing ventilation* with the difference that the droplets between $100\text{--}300 \mu\text{m}$ has fallen on the ground. At the *no ventilation* regime, both 400 and $500 \mu\text{m}$ have settled as well due to gravity. Finally, the $50 \mu\text{m}$ droplets have evaporated near the threshold of the *natural ventilation* regime. In theory, all larger droplets sizes have been recorded by the camera, albeit it is unknown from which threshold size the droplets are recorded.

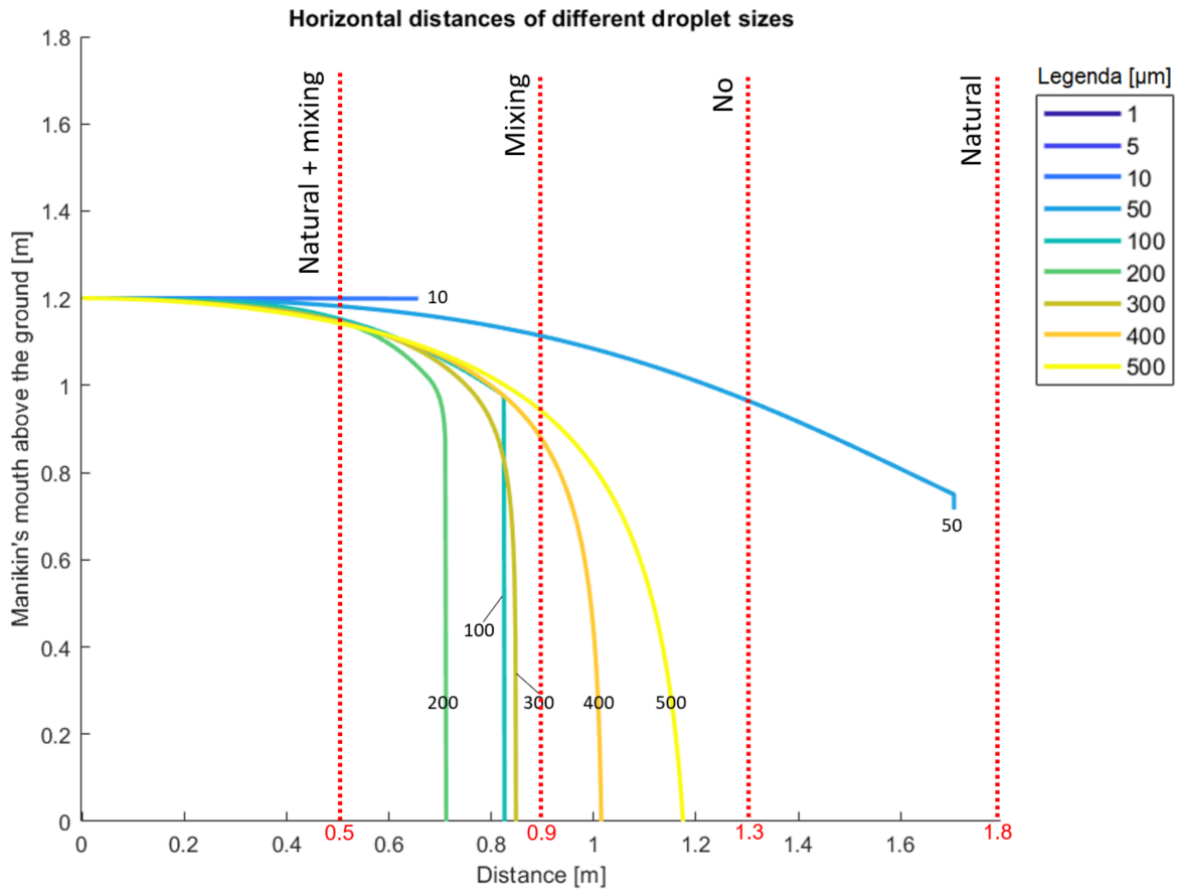


FIGURE 4.14: The trajectory of particle sizes from 1–500 μm during breathing, with the results of the airflow visualisation experiment in vertical dotted lines.

Interesting is to analyse what happened in the range between 10–100 μm , which can be seen in Figure 4.15. The main difference is that the droplets between 40–48 μm can travel much further than the *natural ventilation* regime. This was not visible while analysing the video images.

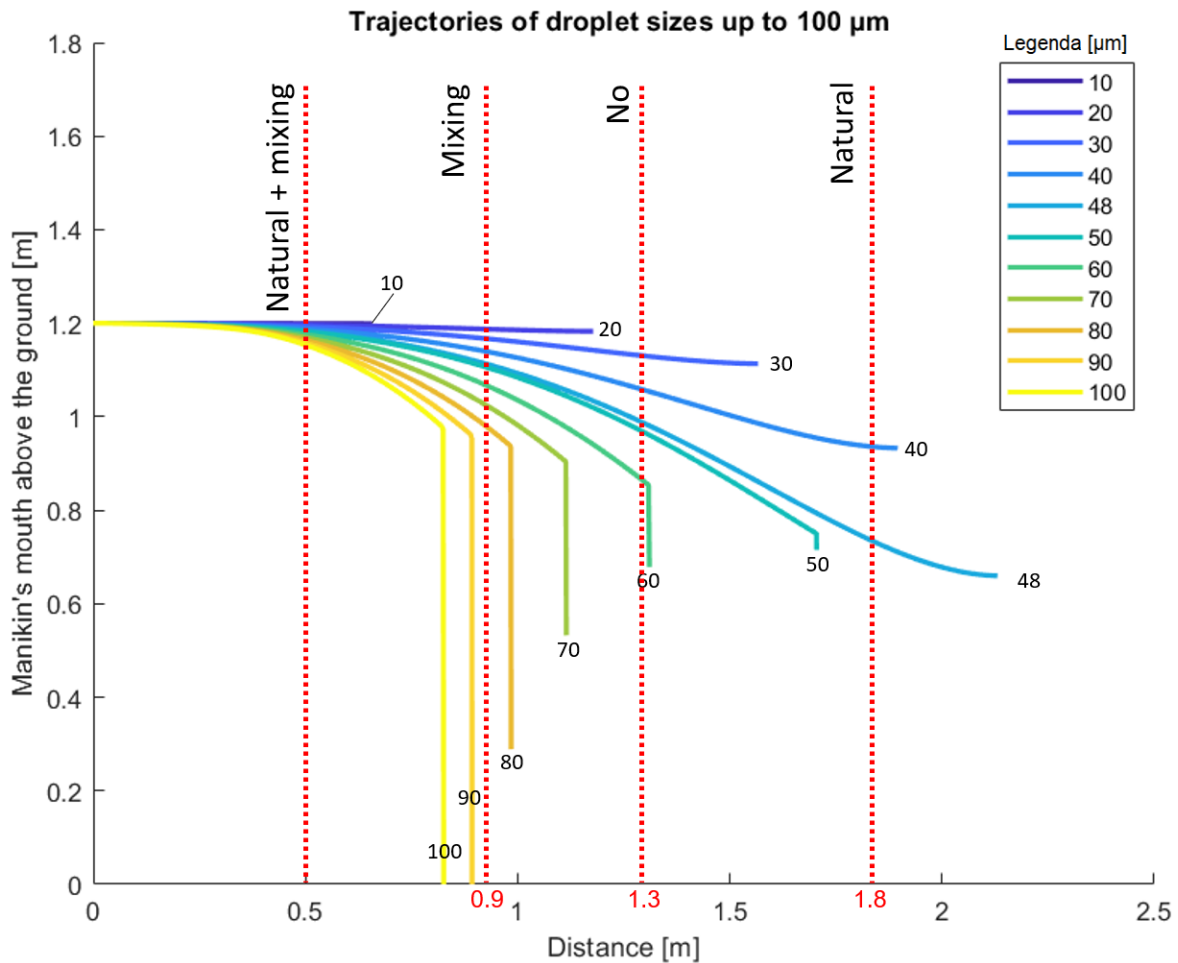


FIGURE 4.15: The trajectory of particle sizes from 10—100 μm during breathing, with the results of the airflow visualisation experiment in vertical dotted lines.

4.5 Conclusion

Baseline measurements

The objective was to research how the basic indoor parameters (temperature, air velocity and relative humidity) are affected by the ventilation regimes by comparing the *no ventilation* with the rest of the ventilation regimes. Based on the results of the measurement data, applying any type of ventilation increases the air velocity of the experience room. The breathing velocity of the manikin had little effect on the result. The air velocity was the lowest at *no ventilation* (0.027 m/s) and the highest at *natural + mixing ventilation* (0.058 m/s). The six different locations have shown that location B has the lowest mean air velocity (0.028 m/s) and location C the highest (0.046 m/s). A remarkable result was that there was a measurement of 0.21 m/s at location C at a height of 120 centimetres. Furthermore, the air velocity is more affected at a height of 20 and 120 centimetres than 180 centimetres with a value of 0.038 m/s and 0.030 m/s , respectively. The temperature of the room was set to 21°C. There is no strong correlation between the temperature and the different ventilation regimes as the value fluctuated between 20.9—21.6°C. The relative humidity decreased during the measurements from 27.83—31.74%.

Experiment: Airflow pattern visualisation

The goal was to determine how the different ventilation regimes affect the airflow pattern of the droplets. Three features were studied: the duration it lingers in the air, the travel distance and the percentage of fog plume per respiratory cycle. The fog plume was more visible with the naked eye than in the recordings (about 2 seconds longer). The camera has more difficulty recording the footage when there is insufficient lighting. The human eye captures the droplets better because the eye adapts more easily in the dark. It can see up particles up to $60 \mu\text{m}$. What was perceived in the recording of the experiment is a collection of smaller droplets together. The droplets lingered longest in the air when there was no ventilation (12.7 seconds in the video) and the shortest in the *natural + mixing ventilation* regime (5.4 seconds). It also reached the shortest distance (0.5 metres) due to the higher air velocity value in comparison with the other three ventilation regimes. The results of the percentage data of fog plume per ventilation regime showed that *mixing ventilation* causes the fog plume to disperse the most with an average percentage of 1.22% per respiratory cycle in comparison with all the other ventilation regimes, thus decreasing the concentration of droplets per breath.

Theoretical results

The larger the particle diameter, the longer it can remain in the air before falling due to gravity. A particle diameter of $100 \mu\text{m}$ (human hair) takes about 2.8 seconds to fall from a height of 1.2 metres. A particle diameter of $1 \mu\text{m}$ takes 34560 seconds to reach the ground from the same height. The results showed that a single aerosol smaller than $5 \mu\text{m}$ immediately evaporate after exhalation. When evaporated it becomes a droplet nuclei, which is even smaller and can linger in the air for much longer before it settles on a surface. Droplet sizes up to $50 \mu\text{m}$ evaporate before it can settle on the ground and also reaches the furthest distance (up to 2.13 metres). From 50—90 μm gravity plays a significant role, although the aerosol evaporates before reaching the ground. Particles with a diameter larger than $100 \mu\text{m}$ will fall on the surface before evaporating. Changing the ventilation regimes in the experience room has little influence on the results due to the low air velocity value (maximum of 0.058 m/s in the *natural + mixing ventilation* regime). However, coughing and sneezing will increase the horizontal distance of the droplets.

Chapter 5

Discussion

This section describes the relevance and meaning of the results. Firstly, we interpret the results with regard to the basic indoor parameters (air velocity, temperature and relative humidity). Secondly, the implications highlight the strengths and the importance of the research. Thirdly, the limitations describe what can or could not be concluded from the results to have a better understanding of the research. Finally, recommendations are made to improve the knowledge concerning the airflow pattern of droplets.

5.1 Interpretation

The findings from this thesis suggest that there is a strong correlation between the lifespan and the airflow pattern of droplets when ventilation is applied. This correlation depends on the values of the basic indoor parameters.

5.1.1 Air velocity

The results show that the exhaled droplets from the portable fog generator system tend to reach a shorter distance from the source when the indoor air velocity increases. The airflow pattern becomes more turbulent (characterised by chaotic movements and contains swirling regions), which is visible in the recordings. The air velocity at the ceiling grilles is larger (0.28—0.47 m/s) in comparison with the windows (0.16—0.27 m/s). This causes the airflow pattern of the droplets to disperse in all directions, making it easier for the laser to detect in the *mixing ventilation* regime. This is also the reason why this ventilation regime has the highest mean grey intensity (1.22%). The baseline measurements show the highest air velocity is up to 120 centimetres above the ground. Somewhat surprisingly, the droplets travelled the furthest in *natural ventilation* even though the indoor average air velocity in the *natural + mixing ventilation* regime was almost twice as high. Indeed, the locations where the airflow enters (e.g. door or window) determine the direction in which the droplets spread. This likely causes the droplets to be 'pushed' much further to the end of the classroom, thus increasing the distance the droplets spread.

5.1.2 Temperature

There is no evidence of a significant effect on the indoor temperature by changing the ventilation regimes. Nonetheless, there is a pronounced trend for the temperature increase through the presence of the operators, heat of the fog machine and incoming sunlight. The longer the measurements took, the warmer it got in the experience room. As expected, increasing the temperature speeds up the evaporation process, as shown in the analytical models. Droplets with a diameter of up to 90 μm tend to evaporate before falling on the ground,

whereas larger droplets ($> 100 \mu\text{m}$) fall on the ground quickly and are not transported by the airflow current in the horizontal direction. Although the influence of the temperature on the evaporation rate of the respiratory droplets has been widely documented (Biryukov et al., 2020, Lynch and Goring, 2020, Raines, Doniach, and Bhanot, 2021), the effect of how it affects the activity of the virus is still largely unknown. This is due to its strong correlation with the other basic indoor parameters, primarily relative humidity.

5.1.3 Relative humidity

The relative humidity decreased during measurements in both the baseline measurements and airflow pattern visualisation experiment when changing the ventilation regime. It is possible that it affected the lifespan of the droplet. While the evaporation rate increases with the decrease of the relative humidity, the distance the droplets travel before they are fully evaporated, which corresponds strongly with the other basic indoor parameters before becoming droplet nuclei. This is confirmed with the analytical model, where only the RH is adjusted. By decreasing the RH from 50.7% to 10.7% has the greatest effect between droplets diameters of 80—100 μm , resulting in them evaporating before it hits the ground. Alternatively, increasing the RH to 90.7% makes the droplets more likely to fall on the ground before they can completely evaporate.

5.1.4 portable fog generator system

Applying different ventilation regimes (i.e. different air velocity values) does not affect the results of the analytical model for the maximum travel distance of the droplets. In the recordings, different ventilation regimes do provide a more dramatic difference. This is likely due to the very low indoor average air velocity per ventilation regime (0.027—0.058 m/s). A distinct difference in the results is only noticeable from 1.5 m/s . One must question the contrast between the air velocity happening globally (affecting the whole environment on a large scale) and locally (affecting only certain areas on a smaller scale). The results of the baseline measurements showed that there are quite some differences in air velocity depending on the location and altitude. Ideally, these values at various locations should be implemented in the model to create more valid results.

5.1.5 Airborne transmission through breathing in schools

The chances of getting infected with diseases through airborne transmission are especially high in low ventilation enclosed environments. In such environments, respiratory droplets immediately shrink after exhalation and become droplet nuclei. The majority of the respiratory droplets are smaller than 75 μm and according to Stokes' law, droplets of these sizes can linger in the air from a few seconds to many hours in rooms with low indoor air velocity while holding viable infectious virions (Xie et al., 2009). The results of the airflow pattern visualisation show that the droplets can reach much further than the 1.5 metres guidelines in *natural ventilation* (1.8 metres). Simultaneously, the droplets lingered the longest in the air. Unfortunately, a third of the Dutch schools only have this type of ventilation, which is often not sufficient to provide adequate indoor air quality for the whole school day (LCVS, 2020). Various research has shown the importance of adequate ventilation in rooms with a high amount of occupants (Somsen et al., 2020, Miller et al., 2020, Schijven et al., 2021).

5.2 Implications

In this thesis, the visualisations of the portable fog generator system provide a quick method in understanding the duration and distance the droplets travel before they settle down. Visualisation studies mostly occurred in hospitals or dental clinics, of which the results were reviewed with numerical studies (Teichert-Filho et al., 2020, Bhattacharyya et al., 2020, Andersson et al., 1983 and Bivolarova et al., 2017). Others used a more practical approach to examine how well face masks obstruct the respiratory jets (Verma, Dhanak, and Frankenfield, 2020 and Arumuru et al., 2021). This research contributed to the understanding of how the aerosols and droplets disperse after exhalation under different air velocities. Firstly, it provides awareness and gives direct feedback on the effect of how droplets disperse at different ventilation regimes. Secondly, the fact that the setup is portable creates the convenience of taking it anywhere to visualise the airflow pattern of the droplets. Thirdly, the materials are accessible everywhere and relatively easy to assemble.

5.3 Limitations

5.3.1 Layout

The results obtained in this study may not apply to classrooms with a different layout of the experience room.

5.3.2 Manually operated

The reliability of the portable fog generator system may be constrained by the fact that it needs to be manually operated. This results in inconsistent outcomes as it depends on the skill of the operator to use the pump.

5.3.3 The presence of the operators

The machine and each person in the room is a heat island with a vertical plume they create drawing in surrounding air from nearer the floor, affecting the basic indoor parameters.

5.3.4 Low budget

An upgrade of the instruments, thus a larger budget, would increase the accuracy of the results. The respiratory system is overly simplified with the buffer, pump and styrofoam head. The temperature of the exhaled fog is 10–15°C lower compared to actual human breath.

5.3.5 Errors during the measurements

The door was opened during the airflow pattern visualisation experiment of the *natural ventilation* regime and *natural + mixing ventilation* regime but was closed during the baseline measurements of the experience room.

5.3.6 Unable to identify the droplet size

Although we captured the essence of the airflow pattern of the droplets in the recordings, we were unable to record all of the exhaled fog plumes. The camera cannot capture single droplets, only clouds of multiple droplets. This makes it impossible to determine the actual droplet sizes from the recordings. The same applies to estimating the time it took for the

droplets to evaporate or disappear in the video. Also, timing the experiment with the stopwatch likely caused inaccuracy in time measurements due to human reaction time to mainly start and stop the stopwatch.

5.3.7 Time

Due to limited time (the SenseLab was moved), the chance to repeat the airflow pattern visualisation experiment was not possible (only 2—3 recordings were made per ventilation regime). Repeating the experiment on another occasion would like result in different results.

5.3.8 No control on the other variables

Furthermore, the possibility to control one of the basic indoor parameters (the temperature or relative humidity) would provide more accurate results. Because now they all fluctuate during the measurements.

5.4 Recommendations for further research

Research on the effect on respiratory droplets at local levels where airflow enter or exit (e.g. windows, door, ceiling grilles and outlets) is somewhat lacking. By applying computational fluid dynamics (CFD), a result involving fluid flows can be given to a certain degree of accuracy. The effects of other types of ventilation regimes (e.g. displacement ventilation, personal ventilation, or combinations with multiple ventilation regimes) should also be considered. Furthermore, automating the process of the portable fog generator system and improving the instruments to understand the airflow pattern of the droplets. Improvements can be made by using a thermal manikin, a mechanical pump with adjustable breathing velocity or a more complex application of the buffer system. To better understand the airflow pattern visualisation future studies could also address coughing, sneezing or exhaling through the nose. Lastly, understanding what the capabilities and the limitations are of the camera, in particular, the minimum droplet diameter size it can record, can help to understand the airflow pattern of a droplet in practice. Particle Image Velocimetry (PIV) allows the option to record the flow visualisation more accurately with a high-speed camera. This can be employed by using a single light sheet, zoomed in to a region (e.g. $5 \times 5 \text{ cm}^2$) instead of filming the whole airflow pattern region.

Chapter 6

Conclusion

The goal of this study is to design and assemble a portable fog generator system to visualise the airflow pattern by using glycol. The system mimics the human breath to see how far the 'respiratory' droplets travel and linger in the air before they settle on the ground. The research question formulated at beginning of the thesis was:

'How is the airflow pattern of 'exhaled' droplets affected in a classroom under different ventilation regimes?'

Succinctly put, it strongly depends on three basic indoor parameters: temperature, relative humidity and air velocity. There is a strong coherence between the temperature and relative humidity. This can be considered as the lifespan of the droplets. Both basic indoor parameters affect the rate of how quickly the droplets form into particles smaller than $5\ \mu\text{m}$. According to Stokes' law, from this diameter, it can linger in the air for many hours before it settles on the ground. The ventilation regime influences the indoor air velocity. This defines how the droplets disperse, but mainly the distance it travels. To answer the research question in its entirety, five sub-questions were derived and are answered in this chapter.

6.1 Instruments

#1. Which instruments are needed to assemble a portable system mimicking the human breath?

The **fog generator** generates fog and allows the setup to be portable. The more expensive models can produce droplets starting from $0.2\ \mu\text{m}$. The next step is to decide the **medium** of the fog fluid, which is either oil-based or glycol. The latter option is much more suited to visualise the airflow pattern as the density of the fog droplets is high enough to be seen. The fog is transferred to the **buffer** to be accumulated. By using a larger volume, more fog can be stored and less time is needed to refill it during the experiments. The **pump** acts as the respiratory system to transport the fog from the buffer to the manikin. The volume of the pump must be comparable to that of a pupil (between 0.4—0.5 litres) and must be able to inhale and exhale. The styrofoam **manikin** is intended to mimic the characteristics of a human mouth. The material was cost-effective and the internal can be easily adjusted with a screwdriver. All the instruments are connected through **pipes** of various diameters (25 and 49 mm) and elbow tubes. Using a transparent pipe makes it possible to see how the fog is being transferred from one material to another.

6.2 Visualisation technique

#2. How can one record and analyse the visualisation of the exhaled droplets?

The recommended ratio of glycol and demineralised water is 9:1 to produce thick fog and the environment should be as dark as possible. The visibility of the airflow pattern in dimmed

environments increases by using multiple lasers. One should be placed in the back and pointed at the manikin's mouth. Several lasers are placed under the area where the fog comes out and the visuals should be recorded with a high-speed camera. These lasers must be aimed at the ceiling. It is necessary to extract at least one frame per second of the video to analyse the droplets, preferably more for an accurate result. With the program Fiji ¹, the images can be compared with each other to distinguish the percentage of fog per ventilation regime.

6.3 Ventilation regimes

#3. *How do different ventilation regimes affect the airflow pattern?*

The values of the average air velocity for each ventilation regime are minimal, albeit there are large differences on a local level (e.g. the location and height). The results show that *no ventilation* has the lowest indoor air velocity (0.027 m/s). The lack of adequate ventilation causes the droplets to linger in the air for much longer. What is striking in the *natural ventilation* regime, is that the droplets travelled the furthest distance (1.8 metres). This has most likely to do that the door was open and 'pushed' the droplets even further. The high air velocity rate at the ceiling grills in the *mixing ventilation* regime, caused the droplets to disperse the most. The *natural + mixing ventilation* regime creates the highest indoor air velocity (0.058 m/s). As a result, the droplets are dispersed almost immediately after exhalation.

6.4 The optimal method to reduce the aerosol spread

#4. *What is the most efficient method to reduce the spread of aerosols in classrooms through ventilation?*

The results contribute to a clearer understanding of the effect of various ventilation regimes on the fog plume distribution in the experience room. High indoor air velocity prevents the droplets to accumulate in the room. It is suggested that applying any type of ventilation improves the airflow and decreases the concentration of droplets in the indoor environment. While *natural ventilation* applies to most educational buildings, there is no control over the temperature and relative humidity that enters the room. Opening the windows during the colder periods is not pleasant for users. The low temperature and relative humidity that enters the room makes the viruses in the aerosols more likely to survive. Conversely, *mixing ventilation* is recommended as the user can control the basic indoor parameters. Although the occupants must be informed beforehand because they do not necessarily know that the ventilation system is turned on. In some cases, users will open the window to ventilate, thus increasing energy use. Personalised ventilation is a possible method to reduce the chance of airborne infection and improve indoor air quality.

6.5 The value of the portable fog generator system

#5. *What is the added value of this portable system in airborne transmission control at educational buildings?*

The most important value of the portable fog generator system is that it provides direct results by showing in which direction the droplets disperse, but also in how far they can

¹See subsection 3.4.3.

reach. Results of numerical or analytical models may not be correct at all, as not all the data are available. The crux mainly lies in the fact that the values of the basic indoor parameter vary continuously. Furthermore, with the portable fog generator system, the user gets a general impression of the density and concentration of the aerosol in the proximity of the emitter. It makes the user aware of the importance of adequate ventilation and actions can be taken immediately such as increasing the ventilation rate or applying face masks to prevent the aerosols to spread.

Appendix A

Invoice of the materials for the portable fog generator

Folder	Name	Price	Description
1. Fluid	Invoice_5liter100%glycol	€ 34,45	100% pure glycol
	Invoice_SmokeFluid	€ 18,40	2 bottles of 1L different smoke fluid
2. Machine	Invoice_SmokeMachine	€ 80,00	Ayra WSM Black 01 smoke machine
3. Pump	Invoice_ManualPump+tube	€ 58,65	0,4L pump + 19mm reinforced tube
4. Buffer	Invoice_2x70LiterAirtightBox	€ 37,99	2 airtight boxes of 70L
	Invoice_BlokkerBufferx2+4lids	€ 19,94	Blokker storage box (20L) and several lids. Most of them are damaged by drilling
5. Tubes	Invoice_25mmTube_reinforced	€ 21,80	25mm PVC reinforced tube (3 meter)
	Invoice_25mmTube+miniclamp+tiewraps	€ 20,19	25mm transparent tube + weight + tie wraps
	Invoice_40mmtube+25mmtube	€ 37,61	25mm and 49mm transparent tube
	Invoice_ConnectionPieces	€ 9,19	Various type of connection tube to connect to the manikin's neck
	Invoice_CornerTube+45degreeTubes	€ 6,95	Corner tubes to connect the tubes (GAMMA)
	Invoice_LidTube50mm	€ 4,79	A lid to place on top of the 49mm tube (GAMMA)
	Invoice-CornerTUBE-25mm	€ 9,20	Another corner tube for the small one (25mm)
6. Manikin	Invoice_ManikinHeadx4	€ 23,75	
7. Lasers and Battery	Invoice-BatteryAAS	€ 4,59	Battery for the laser
	Invoice-5-Lasers	€ 299,95	5 sets of lasers from Huepar
	Invoice-GAMMA-50mmCorner+wingnuts	€ 37,88	Wingnuts to tight the tube
	Total price	€ 725,33	

FIGURE A.1: Invoice of the materials for the portable fog generator.

Appendix B

Logbook

The events of the experiments from February 28 to June 4 are described in this **Appendix**. The aim was to develop a portable fog generator and to record it with video equipment so that it can be analyzed afterwards. Each logbook includes the following elements:

The date of the experiment
<p>Goal The objective of the experiment.</p>
<p>Summary A summary of the procedures of the experiment and anything interesting happened during that day.</p>
<p>Failure points Features of the experiments that did not work.</p>
<p>Improvements for next time</p> <ul style="list-style-type: none"> • Item #1 that can be improved for the next experiment. • Item #2 that can be improved for the next experiment. • Et cetera.
<p>Setup A picture of the setup, if available.</p>

February 24

Goal

Assemble all the equipment together for a first test run.

Summary

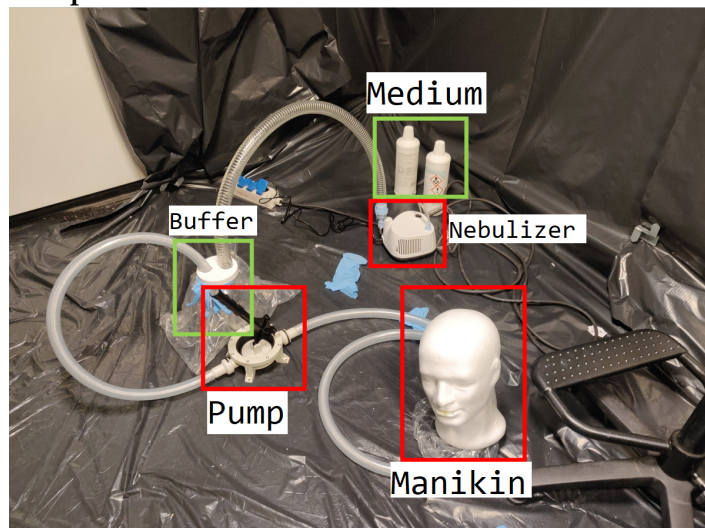
I connected a reinforced PVC pipe from the nebulizer to the buffer. The two holes at the buffer's lid were cut with a small saw. The part where the pipe and the holes met were sealed with tape to prevent leaks. I also used a plastic bag and blue glove to cover seal the buffer more tightly. The second pipe was connected to the manual pump. This is connected to the neck of the manikin. The fog plume exiting the mouth of the manikin was weak and disappears in a few seconds. However, it showed that the concept worked.

Failure points

Leaks were found near the two holes at the buffer's lid and also at the neck of the manikin. The fog came out of the manikin's mouth while the machine was turned on. The nebulizer was not powerful enough to create a sufficient amount of fog. The capacity of the buffer was too small as it was necessary to refill it after a few pumps. I used two different fog fluid: Eurolite ROOKVLOEISTOF DSA (medium density) and Eurolite ROOKVLOEISTOF DSA (high density). The last medium causes the fog to be more visible and linger longer in the room due to its higher density value. The tubes are curved and very stiff, making it difficult to move them around without tipping the nebulizer, buffer, manual pump or manikin.

Improvements for next time

- Get a larger buffer.
- Find a more powerful fog machine.
- Use 100% glycol.
- Find a method to make the pipes less stiff.

Setup

An overview of the setup in the test chamber of the SenseLab. The room was covered with black garbage bags to make the fog more visible.

March 4

Goal

Evaluate the upgraded setup.

Summary

The fog machine, buffer and reinforced PVC pipe have been replaced with a bigger pipe. The fog machine needs a few minutes to heat up before usage. An operator is needed to hold the big pipe in front of the nozzle of the fog machine. The fog goes through this pipe to the new buffer (20 litres). The machine is turned off after accumulation and the operator starts to pump. The fog is much more visible with this new setup.

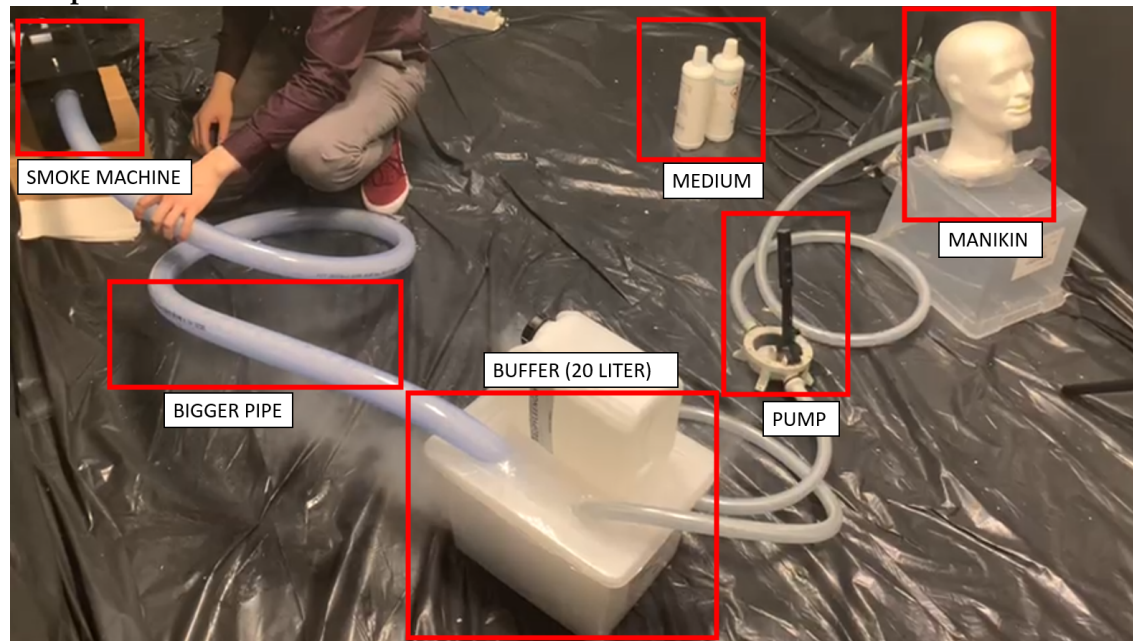
Failure points

The fog becomes very hot, which causes the temperature of the nozzle and the big pipe to rise as well. Lots of condensation with the big pipe. There were leaks on the lid of the buffer. fog leaks were seen at the lid of the buffer. Confirming it was not tightly sealed, even with the use of duct tape.

Improvements

- Shorten the length of both the pipes due to condensation.
- Drill the holes with more accuracy to prevent leaks.
- Stabilize the manikin during use.

Setup



Second setup with a new fog machine, bigger pipe and buffer.

March 8

Goal

Replace the fog machine with the nebulizer.

Summary

The nebulizer is small enough to fit inside the buffer. As a result, one less tube is required. Which makes the setup more portable.

Failure points

The output of the nebulizer is insufficient for the buffer to accumulate the fog. The result is the same as the setup on February 24.

Improvements for next time

- Stop using the nebulizer.
- Put the manikin on a tripod.

Setup



The nebulizer is inside the buffer.

March 9**Goal**

Use the laser to cut the holes on the lid.

Summary

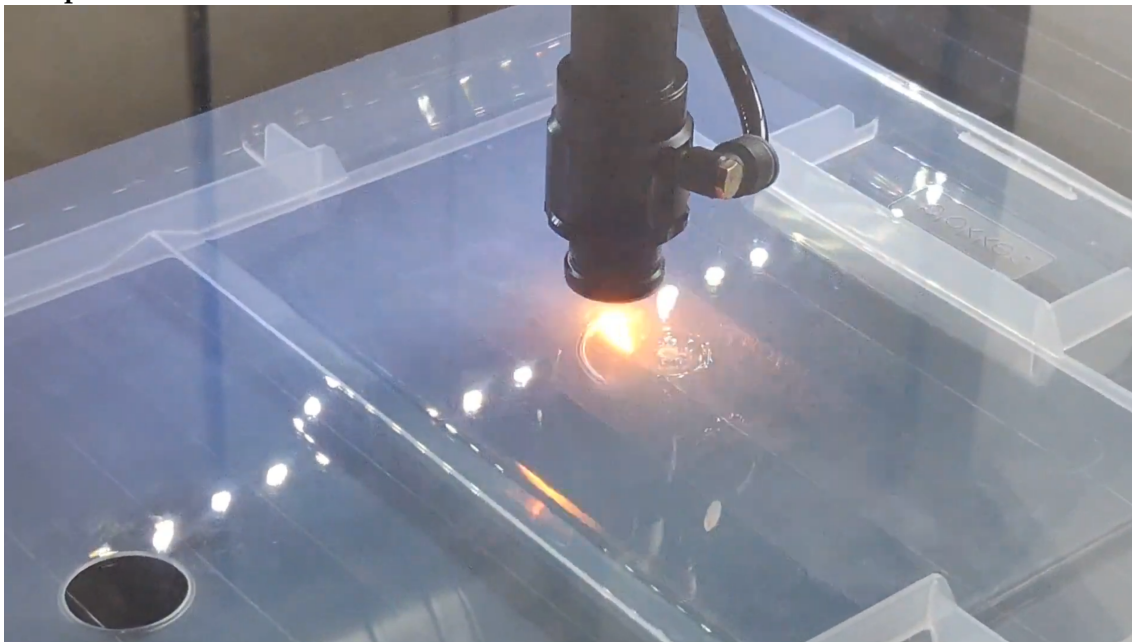
There is a workshop inside the Science Center. An acquaintance of mine has access to the laser cutter and assisted me in cutting the holes on the lid. The process is much faster and precise than drilling it by hand.

Failure points

The diameter of the pipes was 25 mm and 48 mm. We tried to cut the holes with the same size, but it was too large. Ultimately we the perfect sizes are 24.5 mm and 47.5 mm.

Improvements for next time

- Still leaks from the buffer, use an airtight lid.

Setup

Cutting two holes with a laser cutter on a lid.

March 12**Goal**

Prepare a new manikin and laser cut the new airtight lid.

Summary

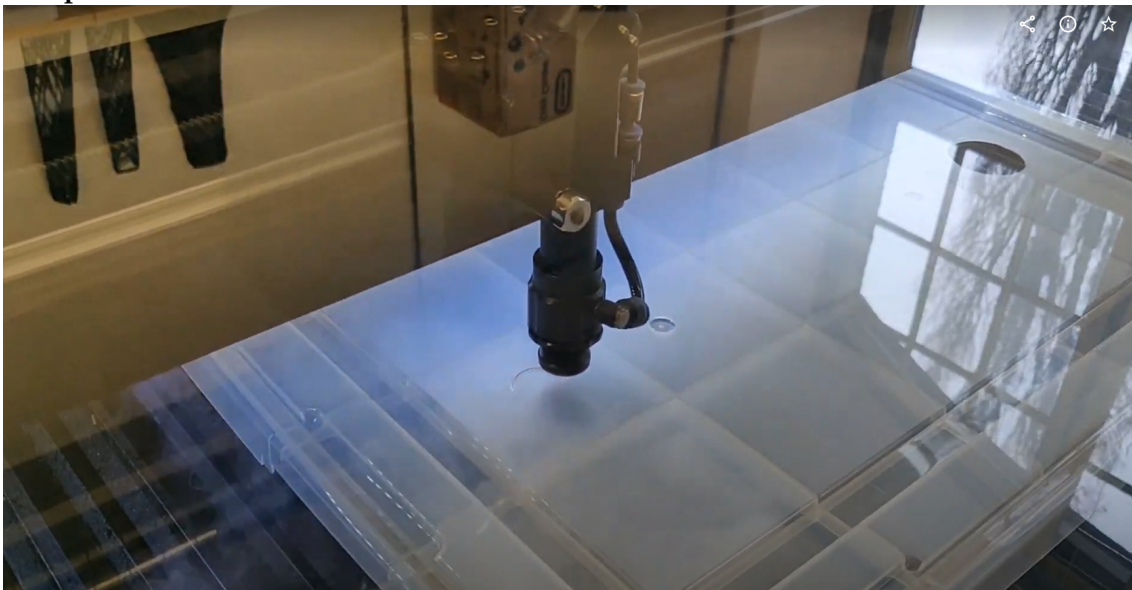
A bigger buffer arrived which has an airtight lid (IRIS Airtight Box opbergbox - 50L). The laser-cut two holes with a dimension of 24.5 mm and 47,5 mm. Till now I have been using an old styrofoam manikin from older experiments, but luckily a new styrofoam manikin is on its way.

Failure points

None

Improvements for next time

- None

Setup

Cutting holes on the airtight lid.

March 15

Goal

Validate if the air velocity of the manikin's mouth is comparable with a human subject.

Summary

The air velocity was measured for the manual pump, reinforced pipe (25mm) and manikin's mouth at three different distances: 2 cm, 10 cm and 25 cm. The measurement device was fixed with a clamp-on a chair. The operator pumped the air of the manual pump for one minute long (on average 15 exhalations per minute). The results were compared with a study where they measured the air velocity of 10 different human subjects. Distances of 5, 10, 15, 20 and 25 cm from the nose were measured (Ivanov, 2019). Important to note, I put the fog machine inside the buffer during use. Without knowing it, this will have a detrimental effect on the fog machine in later experiments.

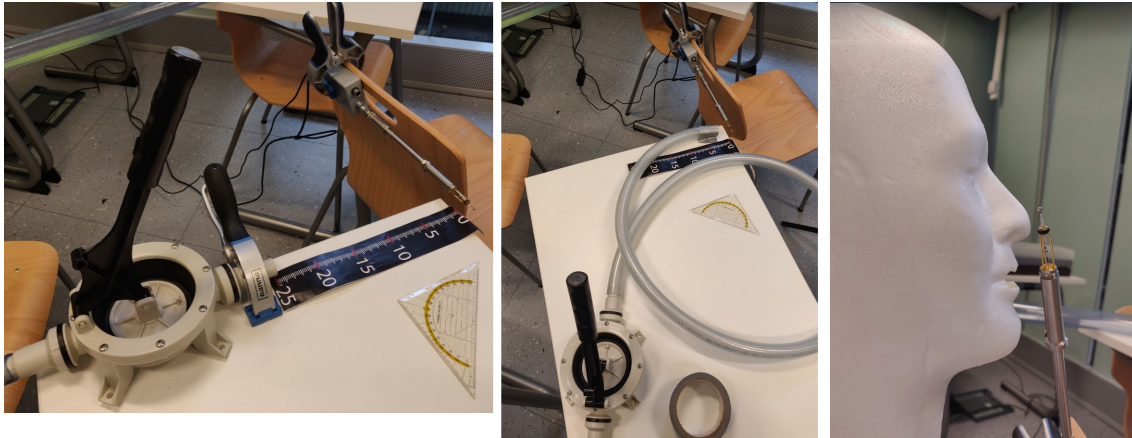
Failure points

The results of this experiment showed that the air velocity of the manikin's mouth is almost twice as high as the experiment of Ivanov (0.06 m/s vs 0.036833 m/s at 25 cm distance from the mouth). This is due to the difference in the mouth's surface area in comparison with a human's mouth. This will be corrected when the new manikin arrives.

Improvements for next time

- Make the opening of the manikin's mouth similar to a human subject.
- Results of the manual pump and pipe are not relevant.

Setup



Measurement of the air velocity of the manual pump (left), pipe (middle) and manikin (right). The measurement device (clamped on a chair) can be seen here as well.

March 16**Goal**

Install a plastic tube at the back of the manikin. Carve out the mouth and nostrils.

Summary

The new manikins have arrived. The neck of the styrofoam manikin gets damaged a little bit each time the pipes are inserted or removed. The solution for this is to glue a plastic tube behind the neck. From now on, you only have to connect the pipe with the tube without using too much force. The holes of the nose and mouth were carved out with a screwdriver. The area of the nostrils and mouth are 45 mm^2 and 180 mm^2 , respectively (Grymer et al., 1991).

Failure points

Styrofoam gets damaged easily. A part of the nose broke off but was fixed with glue.

Improvements for next time

- Print 3D manikin with a cavity, if there is enough time.

Setup

The styrofoam manikin with the mouth and nostrils carved out (left). Plastic tube behind the neck to connect the pipe (right).

March 17

Goal Validate if the temperature and relative humidity of the exhaled breath is comparable with a human subject.

Summary

Two Onset HOBO MX1102 data loggers were used to measure the temperature (and relative humidity (RH)). One was placed inside the buffer and the other one near the manikin's mouth. This was done to see if the values were decreasing in the buffer while the operator was doing the pumping. The procedure was as follow:

20 seconds to fill the buffer of seventy litres.

10 minutes to let the fog settle inside the buffer.

Five minutes of pumping.

This was done three times (manual pump, pipe and manikin).

The temperature inside the buffer kept increasing during the whole experiment. It started at 16,80°C and ended at 27,3°C. The RH was around 89% and decreased during pumping. The result for the manual pump, pipe and manikin were:

Equipment	Temperature [°C]	RH [%]
Pump	18.40	79.67
Pipe	18.41	73.27
Manikin	18.69	61.64

Failure points

The RH value was within the acceptable range of 41.9—88,6%. However, the temperature is much lower than a human's breath, which should be between 31.4—35.4°C (Mansour et al., 2020). This is because the device was measured 10 centimetres from the equipment. The breath is cooled by the indoor temperature before it reaches the data logger. The best method is to measure directly in front of the manikin's mouth by putting a mouthpiece inside the mouth.


Improvements for next time

- Let the temperature inside the buffer increase more.
- Use shorter pipes (due to condensation).
- Measure it directly in front of the equipment (by using a mouthpiece).
- Figure out why fog comes out of the fog machine when not in use .
- Keep track of how many pumps can be pumped before refilling the buffer.

Setup



Setup to measure the temperature and the RH of the manual pump (left) and for the manikin (right).

March 22	
Goal	Visualise the airflow pattern in an occupied classroom with natural + mixing ventilation.
Summary	
Failure points	The manikin is tilted slightly and this caused the plume to go more upwards. The airflow pattern was only visible with an opaque background. It was overall less visible than expected.
Improvements for next time	<ul style="list-style-type: none">• Keep the manikin's mouth horizontally (it was under an angle).• Improve the visibility with laser.• Measure the particle size of the fog with a particle counter.
Setup	 <p>The manikin was not mounted correctly (blue dotted line). A part of the fog is made clearer with red lines.</p>

March 23

Goal

Test if the lasers make the fog more visible.

Summary

The fog coming out of the manikin was getting weaker after each experiment. We went back to the test chamber and tried if pointing a laser at the manikin would be more visible. A couple of similar experiments was conducted this way, so the expectations were high (Jiang et al., 2017), (Verma, Dhanak, and Frankenfield, 2020). Unfortunately, the results of those studies could not be replicated.

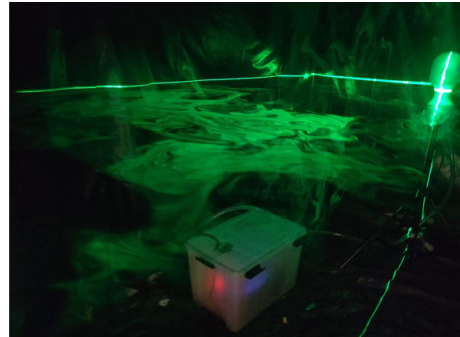
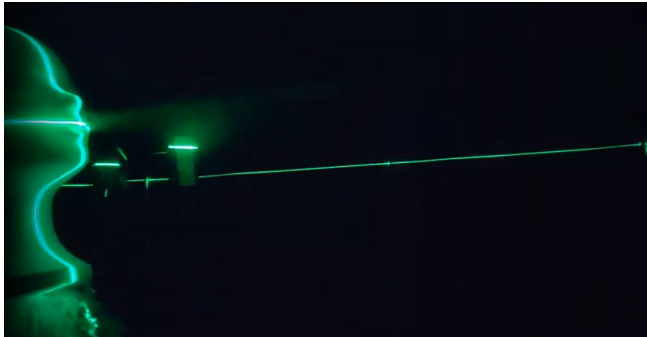
Failure points

It seems that the volume of the manual pump (400 ml) produces too few fog particles for the laser to deflect. Only when the entire room is filled with fog, the laser deflects the fog particles to their full potential. The airflow pattern was not visible from the side view. However, it can be seen if you stood behind the manikin. The laser seems not strong enough. It needs to be pointed perfectly at a straight line at the mouth. Otherwise, the visibility decreases tremendously.

Improvements for next time

- Improve visibility with the laser.
- Try different fog fluids.
- Try with a different laser.
- Figure out why the fog machine produces less fog.

Setup



The exhaled fog could only be seen at the first few centimetres from the manikin (left). After filling the whole room with fog, the visuals of the airflow pattern was much better (right).

March 26

Goal

Clean the machine to do the laser test, again.

Summary

After the fog was machine-turned, it immediately started to squirt the liquid. Normally it takes 4 to 5 minutes for the fog machine to heat up before it starts producing fog. After an attempt to clean the machine by using demineralised water, the machine still did not work accordingly. The machine has been sent back for reparations.

Failure points

After reading the manual, the most obvious reason is that the heating element of the fog machine malfunctioned. The machine has been inside the buffer the whole time during each experiment and has not been cooled down properly.

Improvements for next time

- Keep the fog machine outside the buffer.
- After a few sessions, use demineralised water to clean the nozzles to avoid clogging.

Setup



The fog machine was brought outside to be cleaned. It immediately started spraying the fluid.

March 31

Goal

Brainstorm a new setup without implementing the fog machine inside the buffer and how to use the experiment for the CFD study.

Summary

The fog machine will be put outside the buffer, just like in the early experiments. The idea is to make a hole on one side of the buffer so that a pipe can fit through and connects the machine's nozzle. This prevents the fog machine from overheating and keeps it clean from all the fog residue.

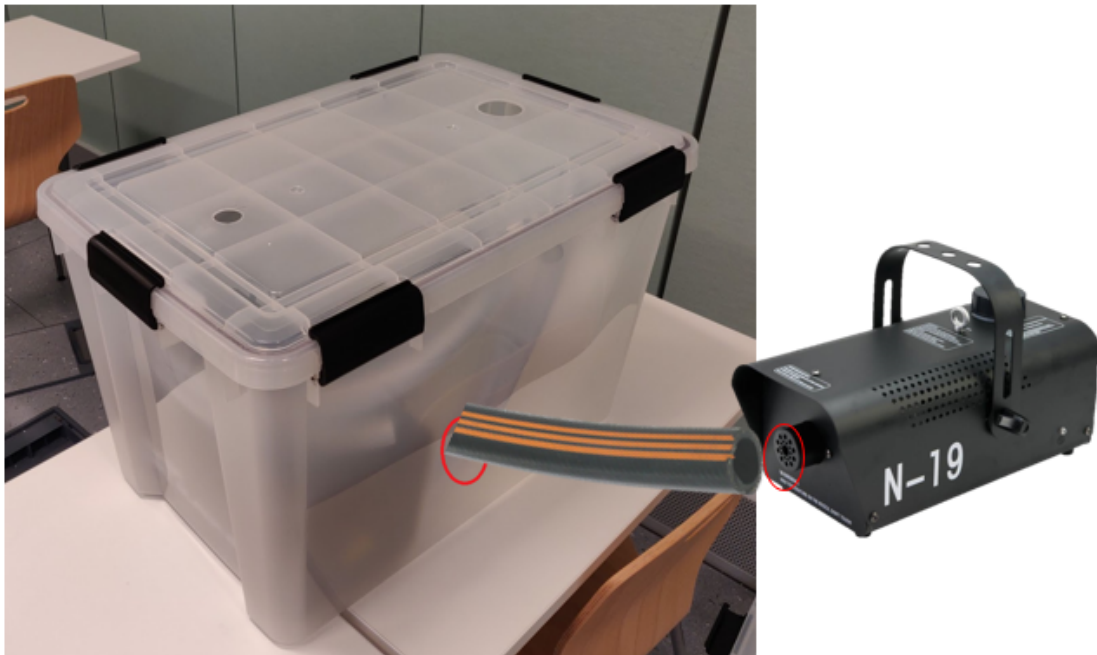
Prepare an idea on how to use this experimental study for the CFD study. The different type of ventilation regimes plays an important role at schools. For now, the idea is to test it in the SenseLab with natural ventilation, mixing ventilation and a combination of those two.

Failure points

None.

Improvements for next time

- Take good care of the equipment.

Setup

A sketch of connecting the nozzle with the side of the buffer.

April 6

Goal

Make a new hole directly behind the manikin's mouth and measure the travel distance of the fog.

Summary

Received the fog machine to continue with the experiments. For today's attempt, the old pipe (diameter of 49 mm) was used. The idea for the upcoming experiments is to put the machine on top of the buffer and use an elbow pipe to direct the fog in the buffer to eliminate the use of an extra pipe.

A person exhales either through the nostrils or mouth. The latter option is the most common, therefore the nose of the manikin has been stuffed with adhesive putty.

A new hole was drilled directly behind the manikin's mouth. This allows the pipe to be placed just behind the mouth. The plastic tube is not used anymore and has also been stuffed with adhesive putty.

The particle counter (Trotec PC220) was used to measure the particle size of the fog. This is to give a preliminary indication of the size distribution. A new particle counter will be purchased in the future.

The test chamber has been taped with several coloured tapes (20 cm from each). The fog plume reaches 80 cm. The laser will be used next time.

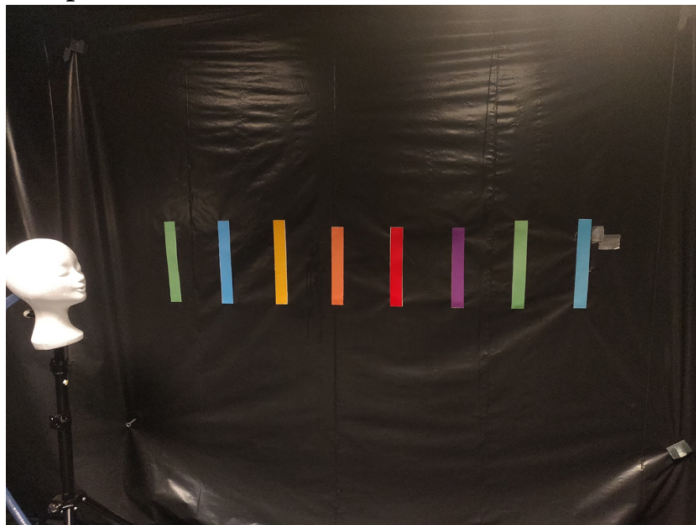
Failure points

Do not connect the nozzle inside the pipe when producing fog in the buffer as this cause a vacuum effect. The fog will barely go through the pipe

Improvements for next time

- Use an elbow tube to direct the fog into the buffer.
- Use the same setup, but with a laser to measure the distance and lingering time in the dark.

Setup



The new setup with the tube going directly behind the same height as the manikin's mouth (left). The result of the particle counter after the experiment (right).

April 9

Goal

Implement a new setup with an elbow tube and test with the laser.

Summary

Purchased an elbow tube (and corresponding lid) and implemented it with the new setup. The nozzle needs to be a few centimetres away from the pipe in order for the fog to reach inside the buffer. The lid must be put on the pipe to create a closed environment for the buffer before pumping. Otherwise, the fog will escape through the pipe (connected with the elbow tube) during 'exhalation'.

The laser seems to work the best in a dark environment when aligned perfectly with the manikin's mouth. It is difficult to record a video in the dark.

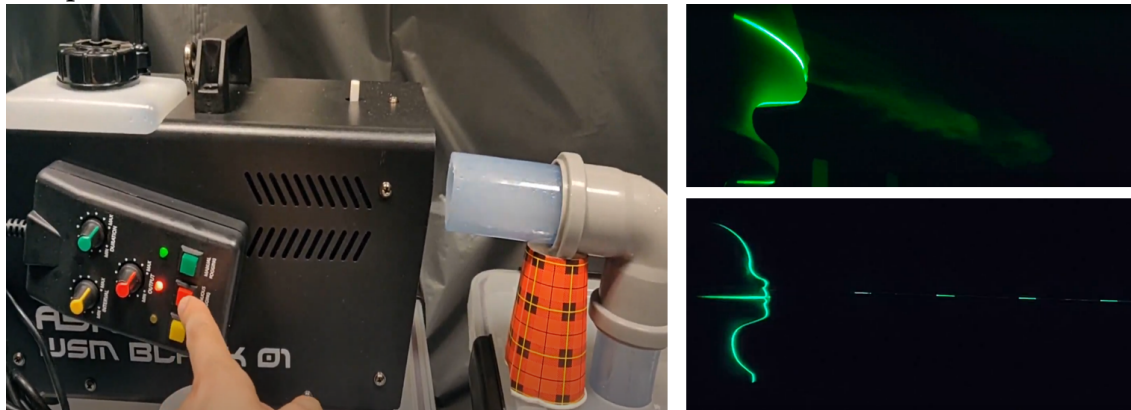
Failure points

Currently, it is not possible to put the fog machine on top of the buffer. It will block the other hole where it is connected with the manual pump. A new hole needs to be made. It is difficult to capture the airflow pattern of the fog with the side view. However, it is much more visible when filmed behind the back.

Improvements for next time

- Find a method to view the airflow pattern from the side
- Make a new hole on the lid so that the fog machine does not block another hole
- Make the pipe longer so that the support of the paper cup is not needed
- Improve visibility with different ratios of glycol

Setup



The pipe needs to be placed a few centimetres away from the nozzle so that it can let through the fog and is supported on a paper cup (left). The airflow pattern is much more visible behind the manikin (top-right). Not visible when viewing from the side (bottom-right).

April 20

Goal

Use different ratios of glycol and add ice cubes to improve the visibility of the fog.

Summary

A new hole was laser cut at the corner of the lid. The fog machine can be placed on top of the buffer. The height of the pipe (connected to the elbow tube) is long enough to reach the bottom of the buffer, the paper cup is not needed anymore.

A medium was used consisting of 30% glycol and 70% demineralised water. The fog was much more visible than ever before. It reaches a distance of 120 centimetres. The use of ice cubes did not affect the visibility.

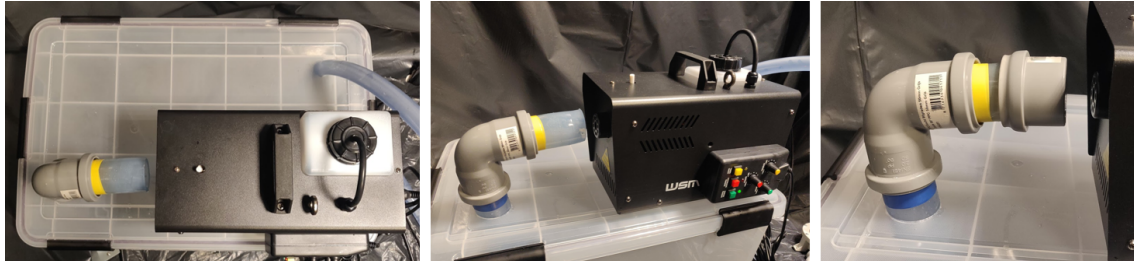
Failure points

Dry ice must be used instead of regular ice. However, it is dangerous due to its low temperature of -78.5°C and must be handled with care. Therefore, this method will not be considered anymore.

Improvements for next time

- Try different ratios of glycol and demineralised water.
- Test the setup with the laser.
- Order more elbow tubes for the section between the manual pump and manikin.
- Further testing to be done at the SenseLab.

Setup



The fog machine can be placed on the lid of the buffer (left). The nozzle is placed two centimetres away from the pipe so that the fog can go in the buffer, without creating a vacuum environment. The paper cup is removed, as the pipe is long enough to reach the bottom of the buffer (middle). The lid is placed on the pipe to prevent the fog from escaping during pumping (right).

April 26

Goal

Test the setup with the laser and different percentages of glycol at the SenseLab.

Summary

The setup is pretty much complete and has been moved to the SenseLab for further experiments. The elbow pipes for the smaller pipe arrived and has been applied in the setup, making the pipe less rigid and easier to adjust its position.

A total of five different medium was made with different percentage of glycol and demineralised water. Starting from 10/90 (glycol/demineralised water) to 90/10 (with increments of 20% glycol each time). The amount of glycol determines the degree of visibility, while the demineralised water dilutes the viscosity. Making it easier for the fog to come out of the fog machine and prevent it from getting clogged. This is the reason why most fog fluid is sold with at least 50% glycol. During the experiments, it seems that the medium with 70% has the best visual results. Tomorrow the 90% and 100% glycol will be tested.+

Failure points

It is still not visible to see the airflow pattern from the side. Maybe this can be solved by placing more lasers at different angles pointing towards the manikin.

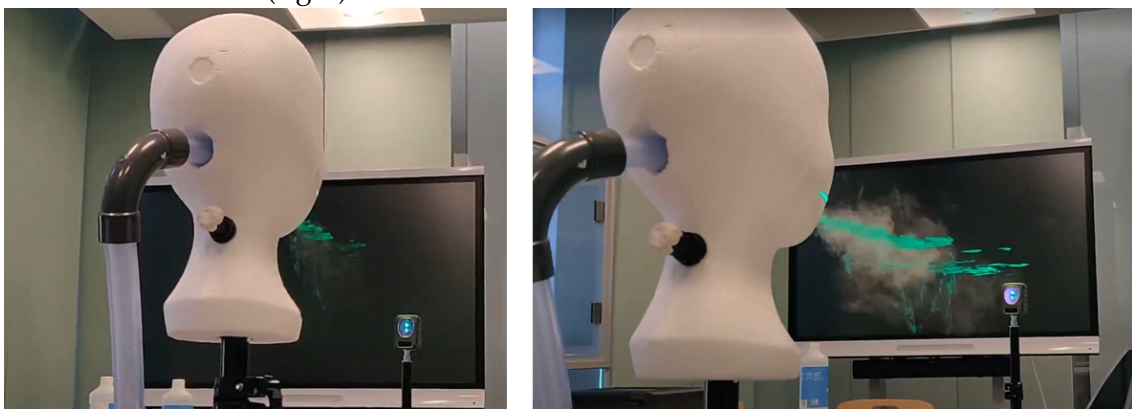
Improvements for next time

- Test the setup with 90% and 100% glycol.
- Purchase more lasers to get a side view of the airflow pattern.

Setup



The whole setup in the experience room. The fog machine lies on top of the buffer (left) with a pipe connected to the manual pump (middle). Another pipe is connected to the back of the manikin (right).



Using 10% glycol (left) and using 70% glycol (right). The visibility is much better with a higher percentage of glycol.

April 27

Goal

Test the setup with 90% and 100% glycol.

Summary

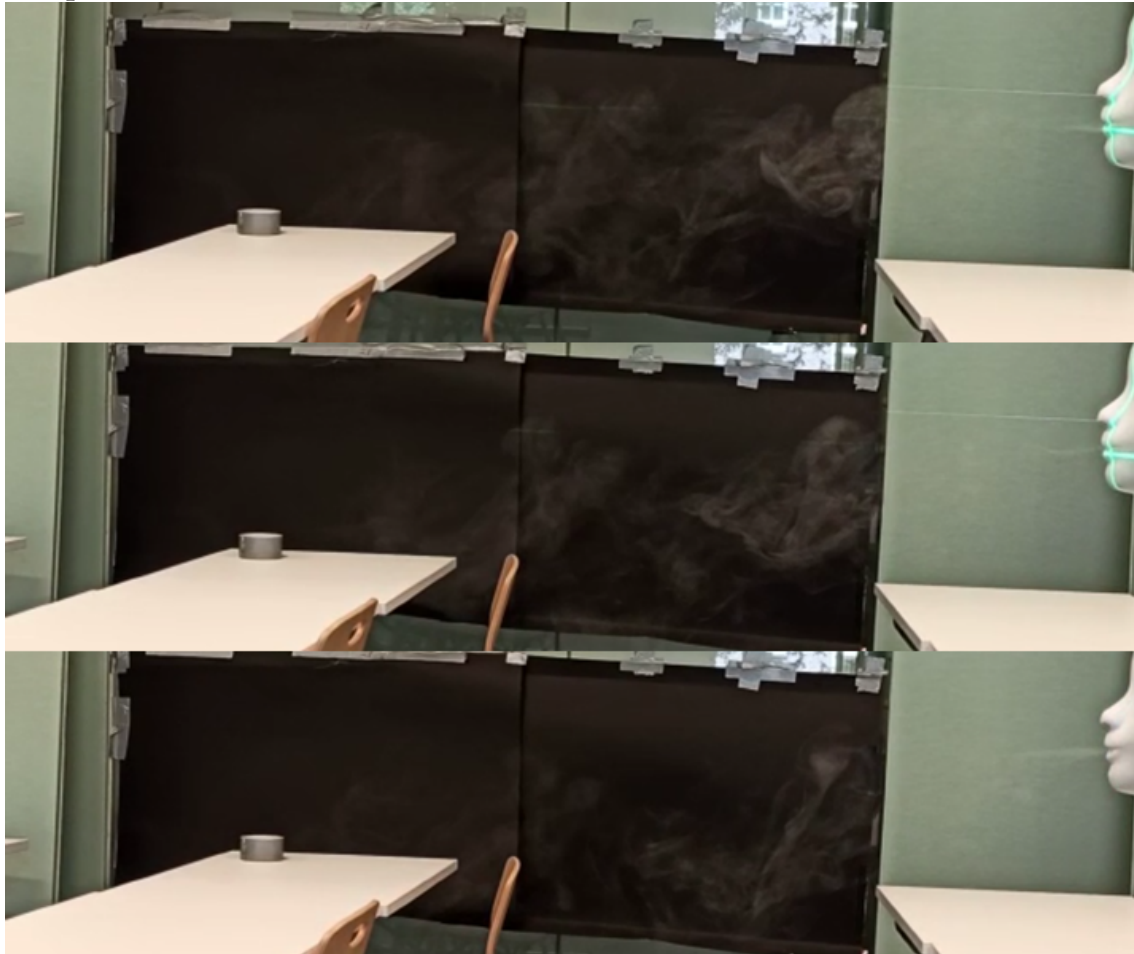
The airflow pattern is much more visible with a black background. It reaches about 150 cm. There was no noticeable difference between 90% and 100% glycol.

Failure points

None.

Improvements for next time

- Redo the setup with more lasers.

Setup

The airflow pattern with 90% glycol. Three different snapshots were taken to see the fog reaching about 150 centimetres.

May 21

Goal

Visualize the airflow pattern from the side with multiple lasers.

Summary

I was asked to apply my setup with another experiment where they used fluorescent ink as the medium. I was working on that from April 28th till May 10th. Meanwhile, several lasers had been tested and we finally found one that was strong enough to be used. One laser was placed from a distance and five others were placed on the table facing upwards. The travel distance and lingering time were measured for normal breathing and coughing.

Failure points

Difficult to note how far the fog travels from the back view of the manikin.

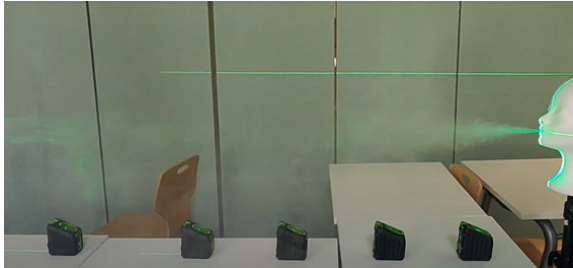
Improvements for next time

- Use a black background.

Setup



The setup with the six lasers and a measurement tape (left). The lasers when they are turned on (right).



The visibility of the airflow pattern at the side view has been improved (left). The back view remains the best perspective to see the airflow pattern (right).

June 2

Goal

Compare the breath of a manikin with a human subject.

Summary

I redid the experiment of March 17 to validate the temperature, relative humidity and air velocity of the manikin's breath with a human subject. Two female participants of **ask their ages** were asked to sit on a chair and breath through their mouth for one minute with a thirty-second rest afterwards. This was repeated three times. The air velocity and particle counter were used for measurement. It was placed as close to the mouth as possible. The settings for the experience room were: no ventilation regime, an indoor temperature of 22.4°C and relative humidity of 47.4%. The results were compared with the manikin.

	Average air velocity [m/s]	Temperature [°C]	Relative humidity [%]
Human	0.23	26.06	50.98
Manikin	0.00 — 0.64	25.63	40.23

It is possible to match the air velocity of the manikin with the human subjects, although it requires skill for the operator to find the sweet spot during pumping. The temperatures are similar. **don't know why the relative humidity is different**

Failure points

Difficult to match the air velocity of the pump with the human breath air velocity.

Improvements for next time

- Using a mouthpiece in the mouth would have a much accurate result.

Setup



Manikin with the air velocity (left) and particle counter (middle). Human subject breathing through her mouth (right).

June 4

Goal

Record the airflow pattern.

Summary

We recorded the airflow pattern in four different ventilation regimes while breathing and coughing. The indoor temperature was between 22.4—23,8°C and the relative humidity varied from 57.4—61.4% during the experiment. We noticed that the plume was more concentrated if there was no ventilation, while the spread is the largest at natural + mixing ventilation.

Failure points

Because the manikin was placed almost underneath the exhaust, the airflow pattern was heavily influenced by that. The tube inside the manikin needs to be adjusted carefully so that the fog plume goes into a straight line instead of deviating to the left or right. The video quality captured with our mobile phone was good enough to analyze the airflow pattern. It is better to use a camera to record it.

Improvements for next time

- Place the setup in the centre back of the room.
- Align the lasers properly.
- The tube needs to be placed in the centre of the manikin.
- Use a (professional) camera.

Setup



The lasers were not aligned properly (left). Different fluids were tested, above 50% glycol has the best result (right).

Appendix C

Baseline measurement data

The baseline measurement data is shown in the figures below. The average velocity values per ventilation regime are colored from low (green) to high (red). Furthermore, the 6 locations (A, B, C, D, E, F) are indicated and the height (1=20 cm, 2=120 cm and 3=180 cm). As an example, A2 means that it was measured at location A at 120 centimeters above the ground.

Regime	Location	Date Time	avg temp	Velocity [m/s]	Velocity Min. [m/s]	Velocity Max. [m/s]	Velocity Deviation [m/s]
No ventilation	A2	12-Apr-21 2:51:14 PM	20,1	0,02584	0,01	0,04	0,01
No ventilation	A1	12-Apr-21 2:56:02 PM	20,25	0,02576	0,02	0,06	0,01
No ventilation	A3	12-Apr-21 2:59:52 PM	20,45	0,02717	0,02	0,06	0,01
No ventilation	B2	12-Apr-21 3:06:58 PM	21,1	0,02723	0,02	0,05	0,01
No ventilation	B1	12-Apr-21 3:09:19 PM	21,05	0,02939	0,01	0,04	0,01
No ventilation	B3	12-Apr-21 3:12:01 PM	21,1	0,02803	0,02	0,04	0,01
No ventilation	C2	12-Apr-21 3:15:01 PM	21,35	0,02735	0,01	0,06	0,01
No ventilation	C1	12-Apr-21 3:17:54 PM	21,35	0,03591	0,01	0,08	0,02
No ventilation	C3	12-Apr-21 3:20:23 PM	21,35	0,03179	0,02	0,06	0,01
No ventilation	D2	12-Apr-21 3:28:33 PM	21,75	0,02047	0,01	0,05	0,01
No ventilation	D1	12-Apr-21 3:30:59 PM	21,55	0,02157	0,01	0,04	0,01
No ventilation	D3	12-Apr-21 3:33:53 PM	21,55	0,02157	0,01	0,04	0,01
No ventilation	E2	12-Apr-21 3:36:38 PM	21,7	0,02546	0,02	0,05	0,01
No ventilation	E1	12-Apr-21 3:38:53 PM	21,7	0,02272	0,01	0,03	0,01
No ventilation	E3	12-Apr-21 3:41:37 PM	21,85	0,02676	0,02	0,04	0,01
No ventilation	F2	12-Apr-21 3:44:00 PM	21,95	0,02749	0,01	0,05	0,01
No ventilation	F1	12-Apr-21 3:46:34 PM	21,95	0,02272	0,01	0,03	0,01
No ventilation	F3	12-Apr-21 3:49:11 PM	22	0,03534	0,02	0,07	0,01
			0	0,00416			
Manikin (10 cm)	Manikin (10 cm)	12-Apr-21 3:56:57 PM	10,7	0,55	0,01	2,47	0,77
Window left	Window left	12-Apr-21 4:02:08 PM	10,95	0,16	0,00	0,79	0,11
Window right	Window right	12-Apr-21 4:04:32 PM	10,9	0,20	0,04	0,41	0,05
			0				
Natural ventilation	A2	12-Apr-21 4:09:52 PM	21,4	0,04144	0,02	0,07	0,01
Natural ventilation	A1	12-Apr-21 4:12:37 PM	21,4	0,02536	0,00	0,08	0,01
Natural ventilation	A3	12-Apr-21 4:15:30 PM	21,45	0,01850	0,01	0,03	0,01
Natural ventilation	B2	12-Apr-21 4:18:02 PM	21,7	0,02909	0,00	0,07	0,02
Natural ventilation	B1	12-Apr-21 4:20:25 PM	21,65	0,03066	0,00	0,11	0,02
Natural ventilation	B3	12-Apr-21 4:23:31 PM	21,7	0,02354	0,01	0,04	0,01
Natural ventilation	C2	12-Apr-21 4:26:03 PM	21,75	0,02059	0,00	0,20	0,04
Natural ventilation	C1	12-Apr-21 4:28:34 PM	21,55	0,01422	0,00	0,13	0,03
Natural ventilation	C3	12-Apr-21 4:31:11 PM	21,45	0,01165	0,00	0,06	0,02
Natural ventilation	D2	12-Apr-21 4:43:04 PM	21,65	0,02402	0,01	0,06	0,01
Natural ventilation	D1	12-Apr-21 4:45:32 PM	21,55	0,04150	0,01	0,13	0,02
Natural ventilation	D3	12-Apr-21 4:48:02 PM	21,55	0,02662	0,01	0,04	0,01
Natural ventilation	E2	12-Apr-21 4:50:56 PM	21,8	0,03756	0,02	0,06	0,01
Natural ventilation	E1	12-Apr-21 4:53:48 PM	21,7	0,05737	0,03	0,10	0,01
Natural ventilation	E3	12-Apr-21 4:56:31 PM	21,7	0,03026	0,01	0,05	0,01
Natural ventilation	F2	12-Apr-21 4:59:01 PM	21,85	0,02868	0,01	0,08	0,01
Natural ventilation	F1	12-Apr-21 5:01:16 PM	21,85	0,06062	0,02	0,13	0,02
Natural ventilation	F3	12-Apr-21 5:03:49 PM	21,9	0,04275	0,02	0,10	0,02

FIGURE C.1: Baseline measurements: The velocity of *no ventilation* and *natural ventilation*.

Regime	Location	Date Time	Turbulence Intensity [%]	Draught Rate [%]	Temperature [begin]	Temperature [end]
No ventilation	A2	12-Apr-21 2:51:14 PM	22,27	0,00	20,1	20,1
No ventilation	A1	12-Apr-21 2:56:02 PM	22,05	0,00	20,3	20,2
No ventilation	A3	12-Apr-21 2:59:52 PM	24,52	0,00	20,4	20,5
No ventilation	B2	12-Apr-21 3:06:58 PM	25,45	0,00	21,1	21,1
No ventilation	B1	12-Apr-21 3:09:19 PM	28,65	0,00	21,1	21
No ventilation	B3	12-Apr-21 3:12:01 PM	17,86	0,00	21,1	21,1
No ventilation	C2	12-Apr-21 3:15:01 PM	27,78	0,00	21,3	21,4
No ventilation	C1	12-Apr-21 3:17:54 PM	58,54	0,00	21,4	21,3
No ventilation	C3	12-Apr-21 3:20:23 PM	27,08	0,00	21,3	21,4
No ventilation	D2	12-Apr-21 3:28:33 PM	31,09	0,00	21,7	21,8
No ventilation	D1	12-Apr-21 3:30:59 PM	36,93	0,00	21,6	21,5
No ventilation	D3	12-Apr-21 3:33:53 PM	18,92	0,00	21,6	21,8
No ventilation	E2	12-Apr-21 3:36:38 PM	29,68	0,00	21,8	21,8
No ventilation	E1	12-Apr-21 3:38:53 PM	27,89	0,00	21,7	21,7
No ventilation	E3	12-Apr-21 3:41:37 PM	21,15	0,00	21,8	21,9
No ventilation	F2	12-Apr-21 3:44:00 PM	30,66	0,00	21,9	22
No ventilation	F1	12-Apr-21 3:46:34 PM	31,91	0,00	22	21,9
No ventilation	F3	12-Apr-21 3:49:11 PM	27,18	0,00	21,9	22,1
Manikin (10 cm)	Manikin (10 cm)	12-Apr-21 3:56:57 PM	139,02	705,00	21,4	
Window left	Window left	12-Apr-21 4:02:08 PM	71,61	61,63	21,9	
Window right	Window right	12-Apr-21 4:04:32 PM	25,83	51,84	21,8	
Natural ventilation	A2	12-Apr-21 4:09:52 PM	25,17	0,00	21,4	21,4
Natural ventilation	A1	12-Apr-21 4:12:37 PM	48,54	0,00	21,4	21,4
Natural ventilation	A3	12-Apr-21 4:15:30 PM	31,46	0,00	21,4	21,5
Natural ventilation	B2	12-Apr-21 4:18:02 PM	52,68	0,00	21,7	21,7
Natural ventilation	B1	12-Apr-21 4:20:25 PM	68,24	0,00	21,7	21,6
Natural ventilation	B3	12-Apr-21 4:23:31 PM	26,19	0,00	21,6	21,8
Natural ventilation	C2	12-Apr-21 4:26:03 PM	180,69	0,00	21,8	21,7
Natural ventilation	C1	12-Apr-21 4:28:34 PM	212,41	0,00	21,7	21,4
Natural ventilation	C3	12-Apr-21 4:31:11 PM	144,67	0,00	21,4	21,5
Natural ventilation	D2	12-Apr-21 4:43:04 PM	43,44	0,00	21,6	21,7
Natural ventilation	D1	12-Apr-21 4:45:32 PM	50,67	0,00	21,6	21,5
Natural ventilation	D3	12-Apr-21 4:48:02 PM	25,21	0,00	21,5	21,6
Natural ventilation	E2	12-Apr-21 4:50:56 PM	31,00	0,00	21,8	21,8
Natural ventilation	E1	12-Apr-21 4:53:48 PM	25,62	5,96	21,8	21,6
Natural ventilation	E3	12-Apr-21 4:56:31 PM	24,78	0,00	21,6	21,8
Natural ventilation	F2	12-Apr-21 4:59:01 PM	50,42	0,00	21,8	21,9
Natural ventilation	F1	12-Apr-21 5:01:16 PM	40,16	8,21	21,9	21,8
Natural ventilation	F3	12-Apr-21 5:03:49 PM	41,98	0,00	21,9	21,9

FIGURE C.2: Baseline measurements: The turbulence intensity, draught rate, temperature, relative humidity and CO₂ of *no ventilation* and *natural ventilation*.

Regime	Location	Date Time	avg temp	Velocity [m/s]	Velocity Min. [m/s]	Velocity Max. [m/s]	Velocity Deviation [m/s]
Mixing ventilation (600 m3/h)	A2	14-Apr-21 9:44:13 AM	20,625	0,01968	0,00	0,06	0,01
Mixing ventilation (600 m3/h)	A2	14-Apr-21 9:49:06 AM	20,33	0,04930	0,00	0,13	0,03
Mixing ventilation (600 m3/h)	A1	14-Apr-21 9:52:34 AM	20,445	0,04384	0,00	0,10	0,02
Mixing ventilation (600 m3/h)	B2	14-Apr-21 9:54:48 AM	20,555	0,02590	0,01	0,06	0,01
Mixing ventilation (600 m3/h)	B1	14-Apr-21 9:57:31 AM	20,64	0,02420	0,01	0,05	0,01
Mixing ventilation (600 m3/h)	B3	14-Apr-21 10:00:21 AM	20,71	0,02725	0,02	0,05	0,01
Mixing ventilation (600 m3/h)	C2	14-Apr-21 10:03:13 AM	20,815	0,03200	0,01	0,08	0,01
Mixing ventilation (600 m3/h)	C1	14-Apr-21 10:05:30 AM	20,84	0,04345	0,00	0,12	0,02
Mixing ventilation (600 m3/h)	C3	14-Apr-21 10:08:26 AM	20,98	0,03160	0,01	0,07	0,01
Mixing ventilation (600 m3/h)	D2	14-Apr-21 10:11:17 AM	21,09	0,03444	0,02	0,09	0,01
Mixing ventilation (600 m3/h)	D1	14-Apr-21 10:14:03 AM	21,14	0,02355	0,01	0,04	0,01
Mixing ventilation (600 m3/h)	D3	14-Apr-21 10:16:43 AM	21,115	0,03094	0,01	0,09	0,01
Mixing ventilation (600 m3/h)	E2	14-Apr-21 10:20:09 AM	21,235	0,03880	0,02	0,07	0,01
Mixing ventilation (600 m3/h)	E1	14-Apr-21 10:22:26 AM	21,295	0,02231	0,01	0,05	0,01
Mixing ventilation (600 m3/h)	E3	14-Apr-21 10:25:11 AM	21,275	0,03237	0,02	0,06	0,01
Mixing ventilation (600 m3/h)	F2	14-Apr-21 10:28:12 AM	21,33	0,03475	0,00	0,09	0,02
Mixing ventilation (600 m3/h)	F1	14-Apr-21 10:31:29 AM	21,235	0,02818	0,01	0,05	0,01
Mixing ventilation (600 m3/h)	F3	14-Apr-21 10:34:27 AM	21,29	0,02622	0,00	0,05	0,01
Air supply	A	14-Apr-21 10:47:54 AM	10,56	0,28	0,06	0,52	0,15
Air supply	C	14-Apr-21 10:49:38 AM	10,61	0,45	0,30	0,57	0,09
Air supply	D	14-Apr-21 10:51:29 AM	10,58	0,47	0,32	0,63	0,11
Air supply	F	14-Apr-21 10:53:21 AM	10,615	0,33	0,09	0,62	0,17
Outlet	A	14-Apr-21 10:55:03 AM	10,555	0,17	0,07	0,26	0,04
Outlet	C	14-Apr-21 10:56:56 AM	10,585	0,18	0,15	0,22	0,02
Outlet	D	14-Apr-21 10:58:31 AM	10,615	0,19	0,16	0,28	0,02
Outlet	F	14-Apr-21 11:00:27 AM	10,635	0,15	0,06	0,26	0,04
Window left	Window left	14-Apr-21 11:06:03 AM	10,705	0,23	0,05	0,35	0,07
Window right	Window right	14-Apr-21 11:08:37 AM	10,68	0,27	0,12	0,43	0,07
Mixing + nat ventilation	A2	14-Apr-21 11:11:42 AM	21,17	0,03564	0,00	0,21	0,04
Mixing + nat ventilation	A1	14-Apr-21 11:14:12 AM	21,08	0,03571	0,00	0,10	0,02
Mixing + nat ventilation	A3	14-Apr-21 11:16:33 AM	21,17	0,04203	0,01	0,11	0,02
Mixing + nat ventilation	B2	14-Apr-21 11:19:37 AM	21,235	0,03579	0,00	0,10	0,02
Mixing + nat ventilation	B1	14-Apr-21 11:21:53 AM	21,22	0,02943	0,00	0,07	0,01
Mixing + nat ventilation	B3	14-Apr-21 11:24:14 AM	21,25	0,02308	0,01	0,05	0,01
Mixing + nat ventilation	C2	14-Apr-21 11:28:23 AM	21,34	0,21239	0,01	0,44	0,11
Mixing + nat ventilation	C1	14-Apr-21 11:31:11 AM	21,29	0,06324	0,01	0,22	0,04
Mixing + nat ventilation	C3	14-Apr-21 11:33:55 AM	21,32	0,02687	0,02	0,05	0,01
Mixing + nat ventilation	D2	14-Apr-21 11:36:35 AM	21,53	0,04195	0,02	0,10	0,02
Mixing + nat ventilation	D1	14-Apr-21 11:38:58 AM	21,48	0,06538	0,01	0,18	0,04
Mixing + nat ventilation	D3	14-Apr-21 11:41:57 AM	21,46	0,05265	0,02	0,13	0,03
Mixing + nat ventilation	E2	14-Apr-21 11:44:41 AM	21,41	0,03763	0,01	0,07	0,01
Mixing + nat ventilation	E1	14-Apr-21 11:46:43 AM	21,34	0,07372	0,03	0,14	0,03
Mixing + nat ventilation	E3	14-Apr-21 11:49:17 AM	21,39	0,02723	0,00	0,07	0,01
Mixing + nat ventilation	F2	14-Apr-21 11:51:47 AM	21,52	0,02996	0,01	0,06	0,01
Mixing + nat ventilation	F1	14-Apr-21 11:54:14 AM	21,41	0,05614	0,00	0,09	0,02
Mixing + nat ventilation	F3	14-Apr-21 11:56:45 AM	21,44	0,022495	0,01	0,05	0,01

FIGURE C.3: Baseline measurements: The velocity of *mixing ventilation* and *natural + mixing ventilation*.

Regime	Location	Date Time	Turbulence Intensity [%]	Draught Rate [%]	Temperature [begin]	Temperature [end]	RH	CO2
Mixing ventilation (600 m3/h)	A2	14-Apr-21 9:44:13 AM	57.16	0.00	20.1	21.15	34.3	499
Mixing ventilation (600 m3/h)	A1	14-Apr-21 9:49:06 AM	60.56	0.00	20.32	20.34	32.8	516
Mixing ventilation (600 m3/h)	A3	14-Apr-21 9:52:34 AM	51.44	0.00	20.41	20.48	32.8	516
Mixing ventilation (600 m3/h)	B2	14-Apr-21 9:54:48 AM	38.70	0.00	20.53	20.58	32.5	516
Mixing ventilation (600 m3/h)	B1	14-Apr-21 9:57:31 AM	34.90	0.00	20.58	20.7	32.2	521
Mixing ventilation (600 m3/h)	B3	14-Apr-21 10:00:21 AM	26.19	0.00	20.7	20.72	32.2	521
Mixing ventilation (600 m3/h)	C2	14-Apr-21 10:03:13 AM	39.10	0.00	20.79	20.84	31.9	516
Mixing ventilation (600 m3/h)	C1	14-Apr-21 10:05:30 AM	49.23	0.00	20.84	20.84	31.7	516
Mixing ventilation (600 m3/h)	C3	14-Apr-21 10:08:26 AM	46.81	0.00	20.98	20.98	31.8	518
Mixing ventilation (600 m3/h)	D2	14-Apr-21 10:11:17 AM	36.36	0.00	21.08	21.1	31.3	532
Mixing ventilation (600 m3/h)	D1	14-Apr-21 10:14:03 AM	28.67	0.00	21.15	21.13	31.2	532
Mixing ventilation (600 m3/h)	D3	14-Apr-21 10:16:43 AM	41.52	0.00	21.13	21.1	31.1	522
Mixing ventilation (600 m3/h)	E2	14-Apr-21 10:20:09 AM	28.61	0.00	21.22	21.25	31.1	522
Mixing ventilation (600 m3/h)	E1	14-Apr-21 10:22:26 AM	33.80	0.00	21.27	21.32	30.8	517
Mixing ventilation (600 m3/h)	E3	14-Apr-21 10:25:11 AM	27.65	0.00	21.27	21.28	30.8	517
Mixing ventilation (600 m3/h)	F2	14-Apr-21 10:28:12 AM	50.22	0.00	21.32	21.34	30.9	527
Mixing ventilation (600 m3/h)	F1	14-Apr-21 10:31:29 AM	28.92	0.00	21.25	21.22	30.8	518
Mixing ventilation (600 m3/h)	F3	14-Apr-21 10:34:27 AM	30.98	0.00	21.29	21.29	31.1	518
Air supply	A	14-Apr-21 10:47:54 AM	53.71	119.03	21.12			
Air supply	C	14-Apr-21 10:49:38 AM	20.94	127.43	21.22			
Air supply	D	14-Apr-21 10:51:29 AM	22.72	140.74	21.16			
Air supply	F	14-Apr-21 10:53:21 AM	52.49	147.23	21.23			
Outlet	A	14-Apr-21 10:55:03 AM	23.35	42.14	21.11			
Outlet	C	14-Apr-21 10:56:56 AM	9.19	36.24	21.17			
Outlet	D	14-Apr-21 10:58:31 AM	11.82	39.05	21.23			
Outlet	F	14-Apr-21 11:00:27 AM	23.66	36.17	21.27			
Window left	Window left	14-Apr-21 11:06:03 AM	30.12	66.12	21.41			
Window right	Window right	14-Apr-21 11:08:37 AM	24.68	76.17	21.36			
Mixing + nat ventilation	A2	14-Apr-21 11:11:42 AM	116.27	0.00	21.17		28.9	465
Mixing + nat ventilation	A1	14-Apr-21 11:14:12 AM	66.44	0.00	21.08		28.9	465
Mixing + nat ventilation	A3	14-Apr-21 11:16:33 AM	51.86	0.00	21.17		29.1	503
Mixing + nat ventilation	B2	14-Apr-21 11:19:37 AM	51.29	0.00	21.22	21.25	28.9	503
Mixing + nat ventilation	B1	14-Apr-21 11:21:53 AM	41.12	0.00	21.22		29	535
Mixing + nat ventilation	B3	14-Apr-21 11:24:14 AM	34.85	0.00	21.25		28.7	535
Mixing + nat ventilation	C2	14-Apr-21 11:28:23 AM	52.10	79.69	21.34		28.1	523
Mixing + nat ventilation	C1	14-Apr-21 11:31:11 AM	66.42	10.93	21.29		27.9	485
Mixing + nat ventilation	C3	14-Apr-21 11:33:55 AM	25.43	0.00	21.32		27.8	485
Mixing + nat ventilation	D2	14-Apr-21 11:36:35 AM	42.37	0.00	21.48	21.58	27.8	523
Mixing + nat ventilation	D1	14-Apr-21 11:38:58 AM	58.92	11.67	21.48		27.3	523
Mixing + nat ventilation	D3	14-Apr-21 11:41:57 AM	50.36	3.54	21.46		27	531
Mixing + nat ventilation	E2	14-Apr-21 11:44:41 AM	34.02	0.00	21.41		27	531
Mixing + nat ventilation	E1	14-Apr-21 11:46:43 AM	42.35	14.36	21.34		26.5	523
Mixing + nat ventilation	E3	14-Apr-21 11:49:17 AM	47.30	0.00	21.39		27.1	523
Mixing + nat ventilation	F2	14-Apr-21 11:51:47 AM	34.28	0.00	21.56	21.48	27	502
Mixing + nat ventilation	F1	14-Apr-21 11:54:14 AM	34.67	5.58	21.41		26.7	502
Mixing + nat ventilation	F3	14-Apr-21 11:56:45 AM	24.32	0.00	21.44		27.3	520

FIGURE C.4: Baseline measurements: The turbulence intensity, draught rate, temperature, relative humidity and CO₂ of *mixing ventilation* and *natural + mixing ventilation*.

Appendix D

Video frame of the maximum travel distance per ventilation regime

Airflow pattern of breathing under different ventilation regimes. The vertical lines are to show the distances. Each picture contains a white dot, indicating the furthest distance the droplet travelled that could be seen in the recording.

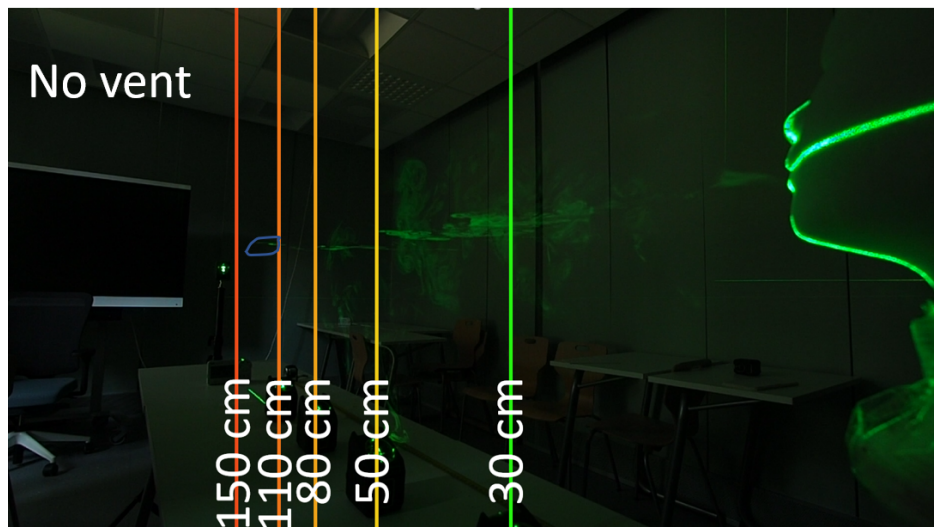


FIGURE D.1: No ventilation. Distance = 1.3 metres.

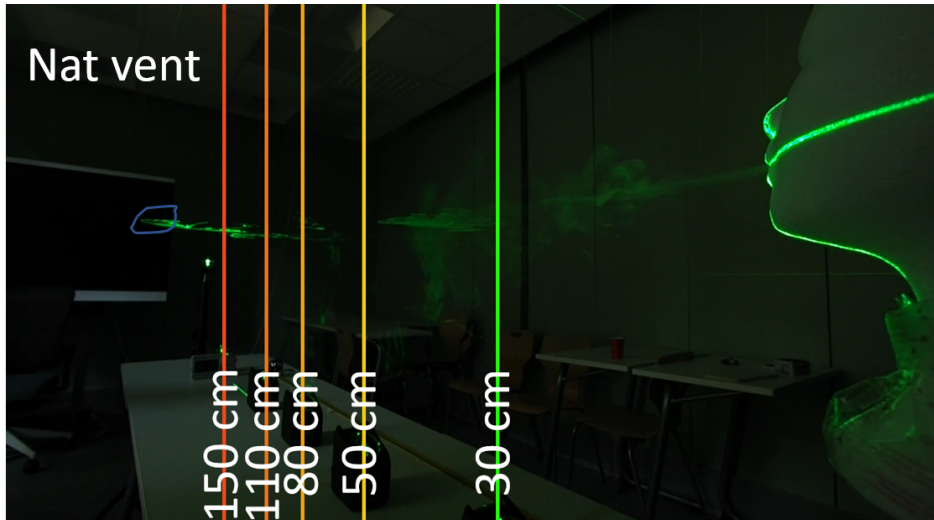


FIGURE D.2: Natural ventilation. Distance = 1.8 metres.

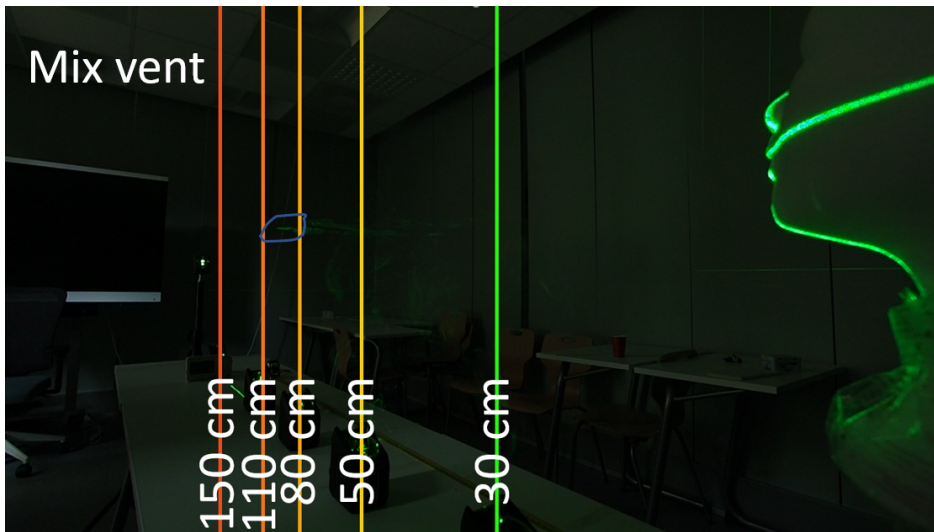


FIGURE D.3: Mixing ventilation. Distance = 0.9 metres.

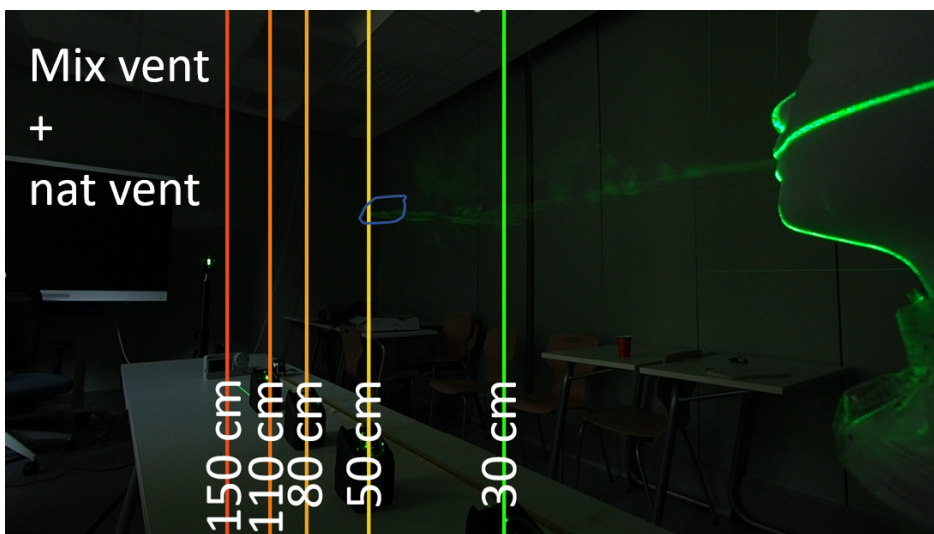


FIGURE D.4: Natural + mixing ventilation. Distance = 0.5 metres.

Appendix E

Settling velocity and duration

This Appendix contains the following figures:

- 0.1—100 μm .
- 0.1—1 μm .
- 10—50 μm (the duration is given in seconds).
- 50—100 μm (the duration is given in seconds).

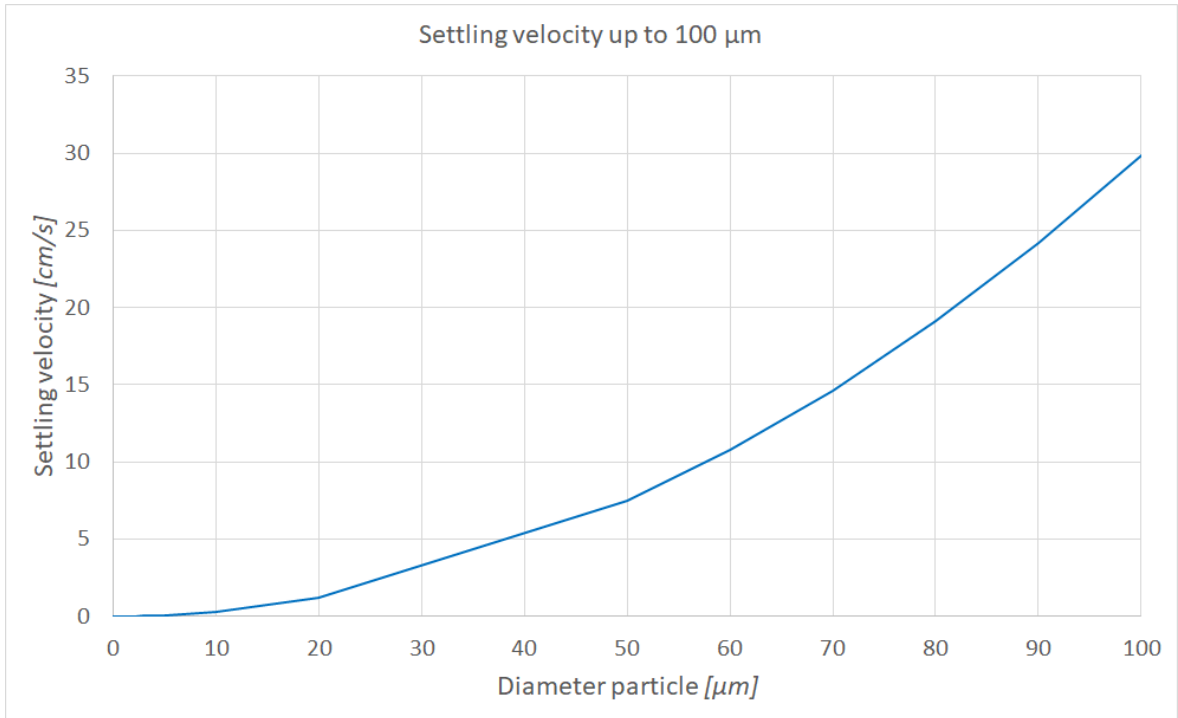


FIGURE E.1: The settling velocity with a particle diameter from 0.1—100 μm at 297.45 K.

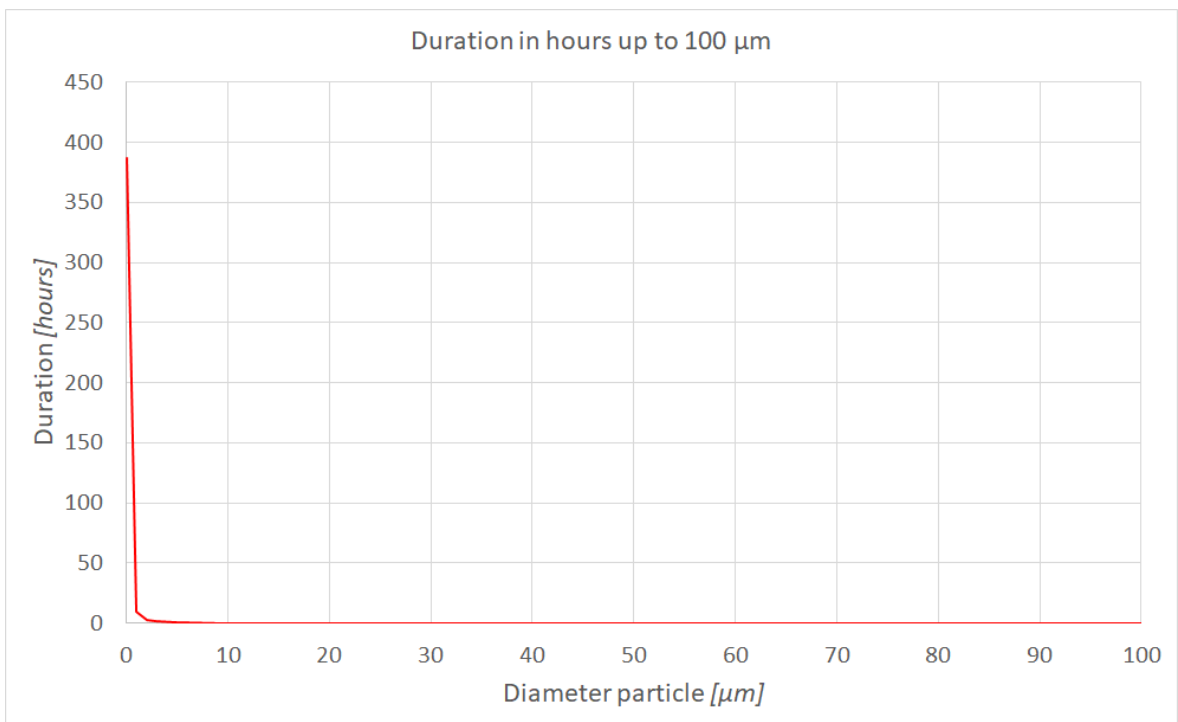


FIGURE E.2: The duration in hours with a particle diameter from 0.1—100 μm at 297.45 K.

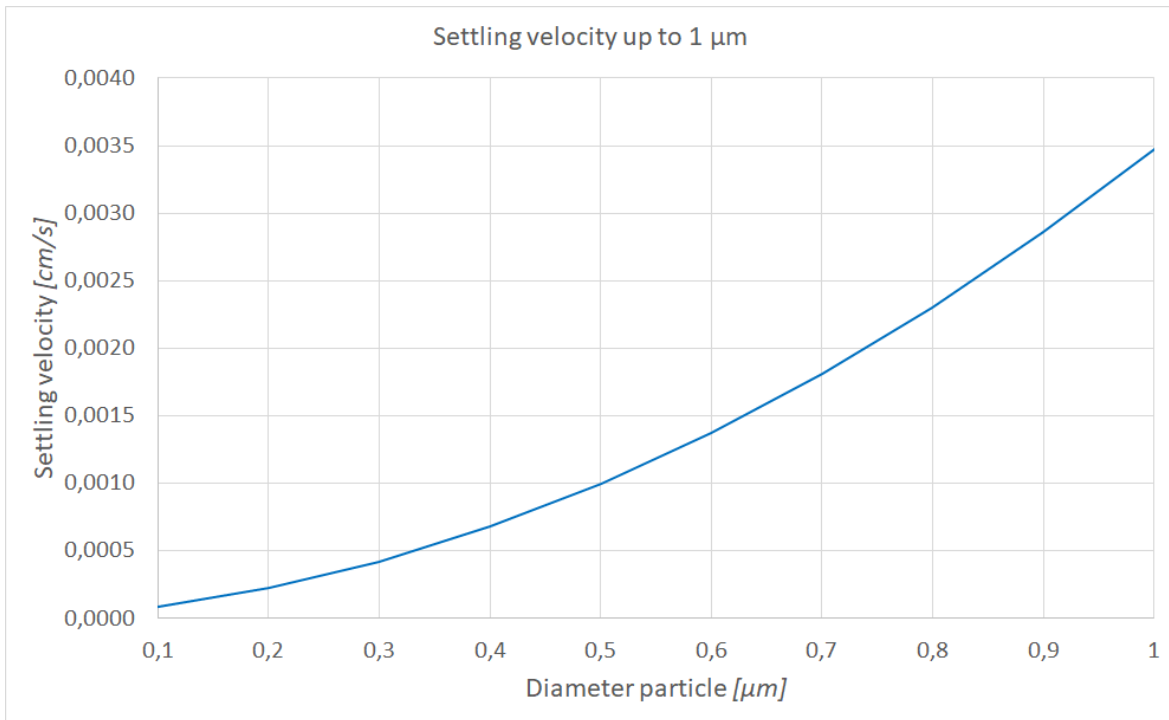


FIGURE E.3: The settling velocity with a particle diameter from 0.1—1 μm at 297.45 K.

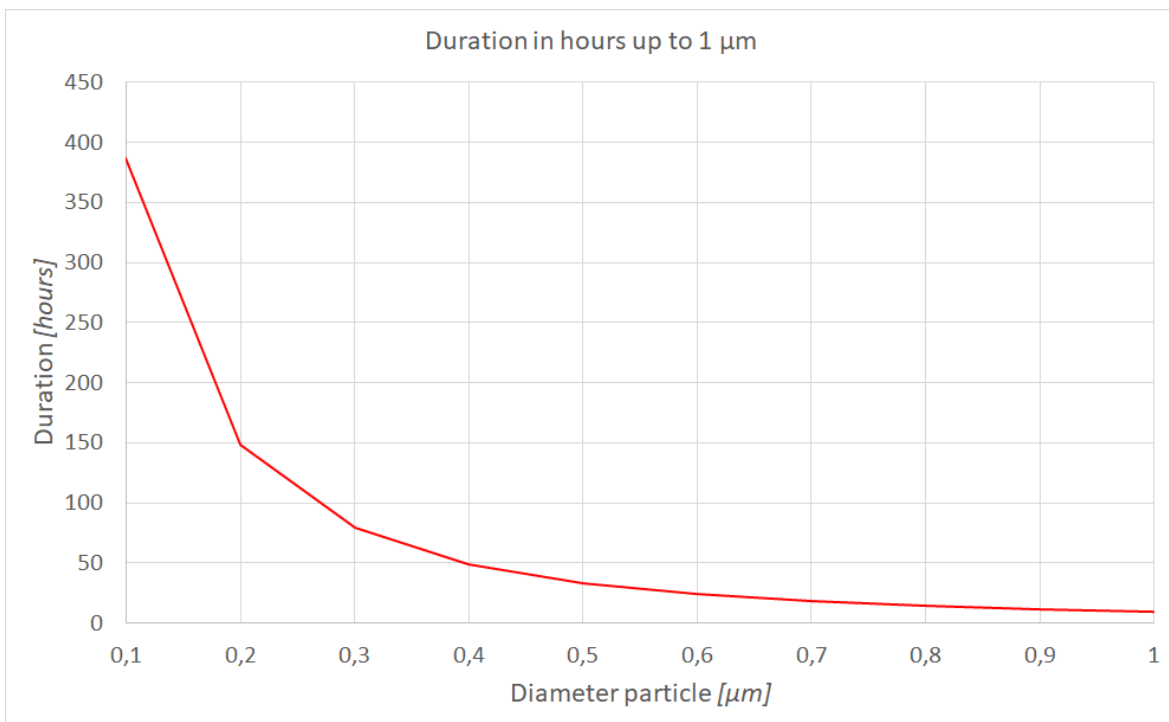


FIGURE E.4: The duration in hours with a particle diameter from 0.1—1 μm at 297.45 K.

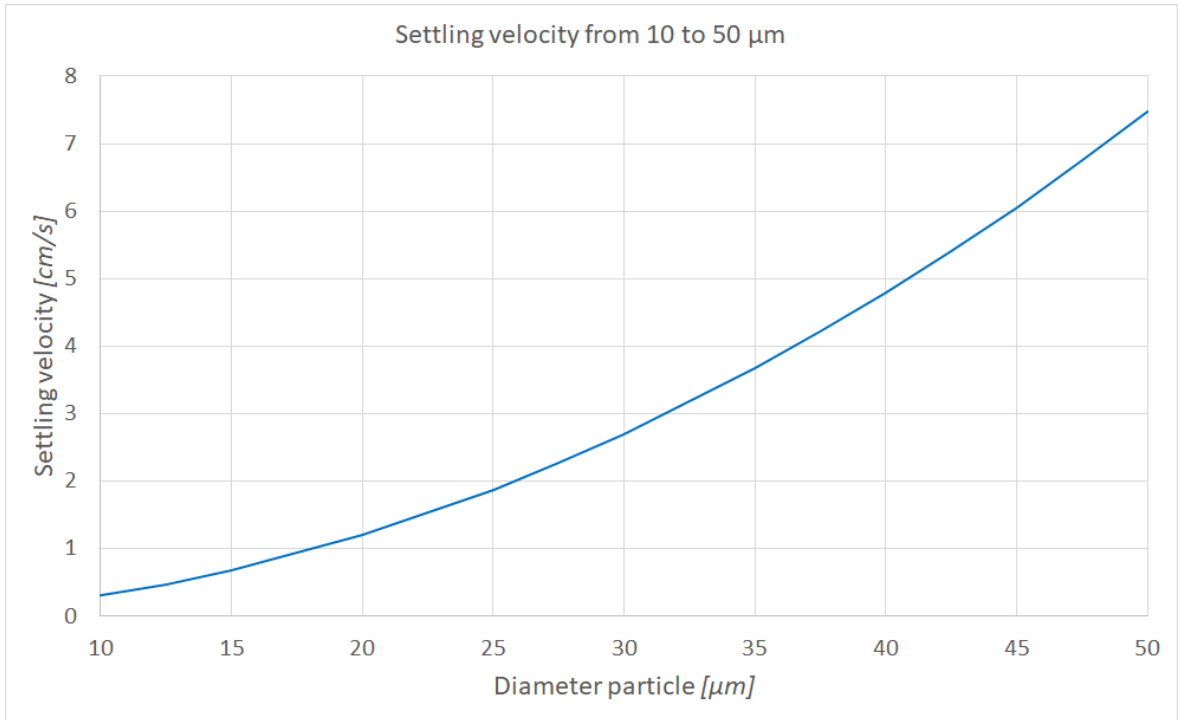


FIGURE E.5: The settling velocity with a particle diameter from 10—50 μm at 297.45 K.

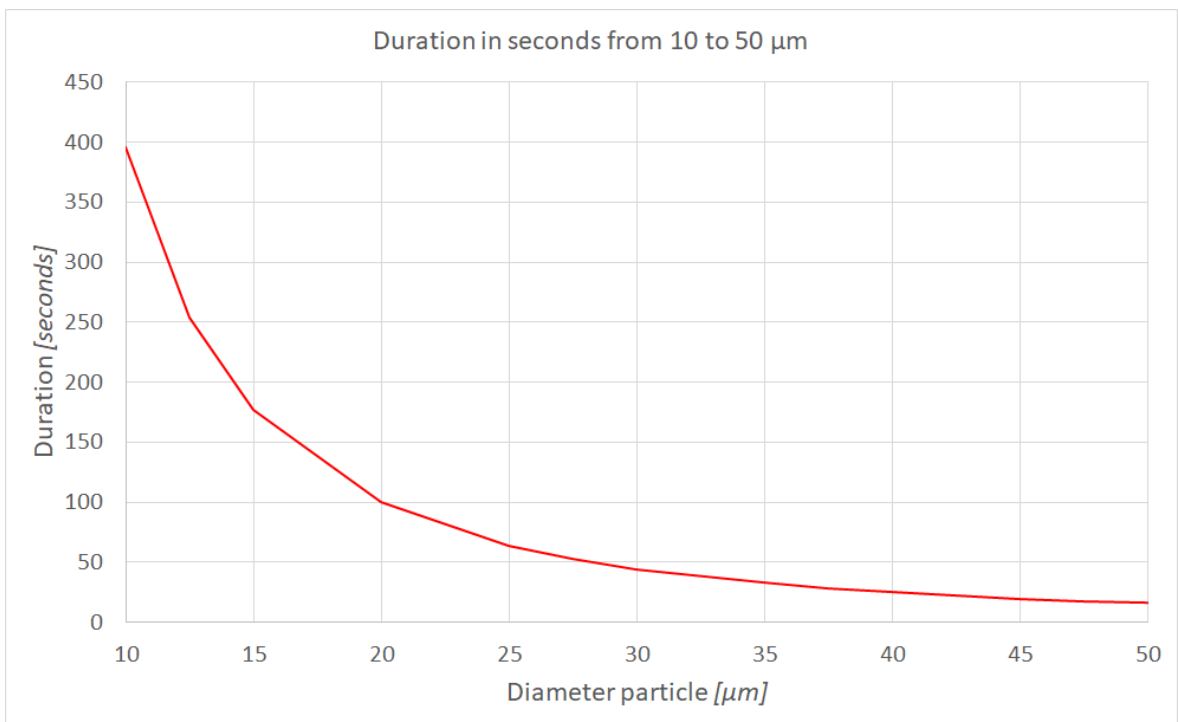


FIGURE E.6: The duration in seconds with a particle diameter from 10—50 μm at 297.45 K.

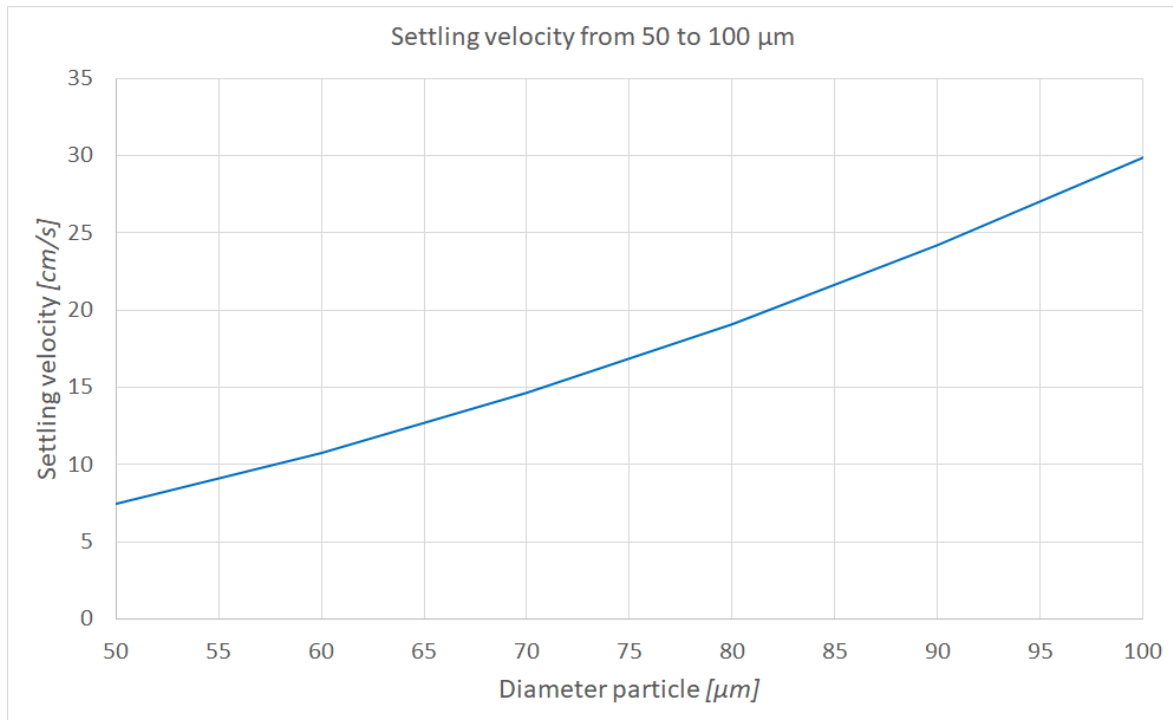


FIGURE E.7: The settling velocity with a particle diameter from 50—100 μm at 297.45 K.

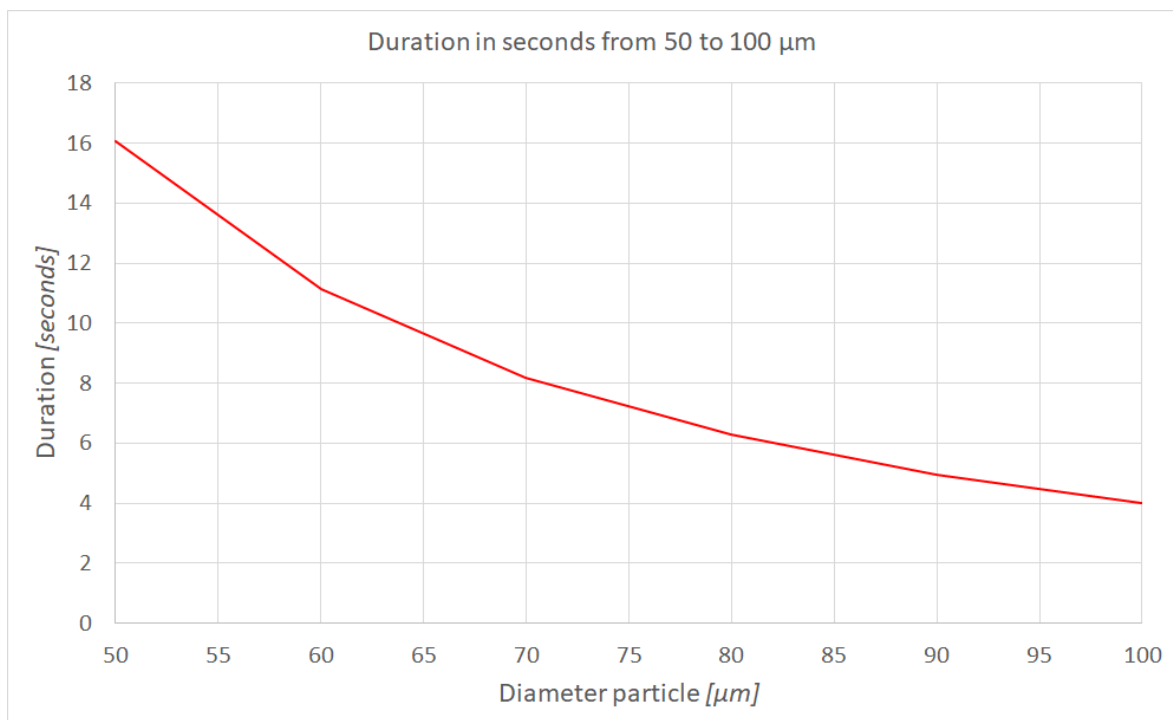


FIGURE E.8: The duration in seconds with a particle diameter from 50—100 μm at 297.45 K.

Appendix F

MATLAB script

```

% diameter of the droplets
D0 = [10;20;30;40;48;50;60;70;80;90;100];
% breathing velocity manikin
U0 = 4.42;
% the temperature of manikin's mouth
T_breath = 25;
% the temperature of the experience room
T_air = 24.3;
% the relative humidity of manikin's mouth (assume)
RH_breath = 90;
% the relative humidity of experience room (no ventilation regime)
RH_air = 53.3;
% the atmospheric pressure of the air
Pt = 101300;
% the air density at 24.3oC
rho_air = 1.187;
% the water density at 24.3oC
rho_sal = 997.225;
% gravitational acceleration
g = 9.81;
% the dynamic viscosity of the air from subsection 4.3.1
mu = 1.83*1e-5;
% the height of the mouth
height = 1.2;
% air velocity experience room (no ventilation)
u0_air = 0.0027;
% molecular weight of the evaporating liquid
ML = 0.018;
% gas constant 8.3144 J mol-1K-1
R = 8.3144;
% time interval
dt = 0.0001;

% Kinetics and evaporation of water drops in air, H.J. Holterman, 2003
% estimate the saturated vapor pressure at different temperature
getsaturatedpress = @(t) 610.7*10^(7.5*t/(t+237.3));
% estimate the wet-bulb temperature
getwetbulbtemp = @(t,rh) t-((5.1055+0.4295*t)+...
(-0.04703-0.005951*t)*rh+...

```

```

        (-4.005e-5+1.66e-5*t)*rh*rh);
% estimate the density of ambient air at different temperature
getairdensity = @(t) 1.2929*273.15/(t+273.15);
% estimate the dynamic viscosity of the air
getairvis = @(t) (17.1+0.067*t-0.0004*t*t)*1e-6;
% estimate the diffusion coefficient
getdiffusioncoeff = @(t) 21.2e-6*(1+0.0071*t);

% get the wet-bulb temperature of the breathing airflow
Tw_breath = getwetbulbtemp(T_breath,RH_breath);
% get the wet-bulb temperature of the ambient air
Tw_air = getwetbulbtemp(T_air,RH_air);

% plot
myc = parula(length(D0));
fig = figure('color','w');
gca1 = axes(fig); hold(gca1,'on');
tmps = 0:0.1:2;
tmpw = 0.523*tmps+0.0088;
ylim([0 1.8])

T = zeros(length(D0),length(U0));
S = zeros(length(D0),length(U0));
Y = zeros(length(D0),length(U0));
Dia = zeros(length(D0),length(U0));
Mark_EvapB = zeros(length(D0),length(U0));
Mark_EvapA = zeros(length(D0),length(U0));
for ii = 1:length(D0)
    for jj = 1:length(U0)
        fprintf('ii=%d, jj=%d.....\n',ii,jj);

        t = zeros(1000000,1);
        x = zeros(1000000,1);
        y = zeros(1000000,1);
        u_sal= zeros(1000000,1);
        v_sal = zeros(1000000,1);
        % record the diameter of droplets
        d_sal = zeros(1000000,1);
        % record the horizontal displacement of droplets
        s = zeros(1000000,1);
        % the width of the breathing airflow
        w = zeros(1000000,1);
        s(1) = 0;
        % Equation of: Phys. Fluids 32, 125102 (2020)
        w(1) = 0.523*s(1)+0.0088;
        x(1) = 0; y(1) = height;
        u_sal(1) = U0(jj); v_sal(1) = 0;
        d_sal(1) = D0(ii)*1e-6;
        t(1) = 0;
        iter = 1;
        % flag=0: fall to the ground; flag=1: evaporated

```

```

flag = 0;
while (y(iter)>0)
    iter = iter+1;
    u0_sal = u_sal(iter-1);
    v0_sal = v_sal(iter-1);
    d0_sal = d_sal(iter-1);
    x0 = x(iter-1);
    y0 = y(iter-1);

    vol_sal = 4/3*pi*(d0_sal/2)^3;
    m_sal = rho_sal*vol_sal;
    A_sal = pi*(d0_sal/2)^2;

    t(iter) = t(iter-1)+dt;
    if t(iter) < 0.0124
        s(iter) = u0_air*t(iter);
        w(iter) = 0.523*s(iter)+0.0088;
    elseif t(iter) >= 0.012
        s(iter) = t(iter)^0.3-0.188;
        w(iter) = 0.523*s(iter)+0.0088;
    end

    % check if the droplets in breathing airflow
    tmpw = 0.523*x0+0.0088;
    if y0 >= height-tmpw/2
        rho_air = getairdensity(T_breath);
        mu = getairvis(T_breath);
        Tf = T_breath;
        Dv = getdiffusioncoeff(T_breath);
        Pw_sat = getsaturatedpress(Tw_breath);
        Pd_sat = getsaturatedpress(T_breath);
        RH = RH_breath;

        if x0 <=0.08
            u_air = 6.48;
        else
            u_air = 0.3*(x0+0.188)^(-7/3);
        end
        v_air = 0;
        Mark_EvapA(ii,jj) = 1;
    else
        tmp_idx(2) = 1;
        rho_air = getairdensity(T_air);
        mu = getairvis(T_air);
        Tf = T_air;
        Dv = getdiffusioncoeff(T_air);
        Pw_sat = getsaturatedpress(Tw_air);
        Pd_sat = getsaturatedpress(T_air);
        RH = RH_air;
        u_air = 0;
        v_air = 0;
    end
end

```

```

        Mark_EvapA(ii,jj) = 0;
    end

    % Reynolds number
    du = u_air-u0_sal;
    dv = v_air-v0_sal;
    Re = sqrt(du*du+dv*dv)*rho_air*d0_sal/mu;

    % Sc number
    Sc = mu/rho_air/Dv;

    % drag coefficient
    if Re < 100*eps
        Cd = 1000;
    else
        Cd = 24/Re+6/(1+sqrt(Re))+0.4;
    end

    % force
    Fx = 0.5*Cd*rho_air*A_sal*du*sqrt(du*du+dv*dv);
    Fy = 0.5*Cd*rho_air*A_sal*dv*sqrt(du*du+dv*dv)-vol_sal*(rho_sal-rho_air)*g;

    % velocity
    u_sal(iter) = (Fx*dt)/m_sal+u0_sal;
    v_sal(iter) = (Fy*dt)/m_sal+v0_sal;

    % displacement
    x(iter) = x0+(u0_sal+u_sal(iter))/2*dt;
    y(iter) = y0+(v0_sal+v_sal(iter))/2*dt;

    % diameter
    tmp = 4*Pt*ML*Dv*(1+0.276*Re^(1/2)*Sc^(1/3))*log((Pt-Pw_sat)/
    (Pt-RH/100*Pd_sat))/d0_sal/rho_sal/R/(Tf+273.15);
    d_sal(iter) = (tmp*dt)+d0_sal;

    % check if the diameter is larger than 5 micron
    if d_sal(iter) <= 5e-6
        flag = 1;
        break;
    end
end
end
t(iter+1:end) = [];
x(iter+1:end) = [];
y(iter+1:end) = [];
u_sal(iter+1:end) = [];
v_sal(iter+1:end) = [];
d_sal(iter+1:end) = [];
s(iter+1:end) = [];
w(iter+1:end) = [];

T(ii,jj) = t(iter);

```

```
S(ii,jj) = x(iter);
Y(ii,jj) = y(iter);
Dia(ii,jj) = d_sal(iter);
Mark_EvapB(ii,jj) = flag;
plot(gca1,x(1:iter),y(1:iter),'color',myc(ii,:), 'linewidth',2);
end
end
```


Appendix G

Comparison of the basic indoor parameters with MATLAB

Air velocity

Particle diameter [μm]	Breathing [m]	Coughing [m]	Increase [%]
10	0.66	0.66	0
50	1.70	1.70	0
80	0.98	0.99	0
90	0.89	0.90	+1
100	0.83	0.83	0
200	0.71	0.78	+9
300	0.85	1.01	+20
400	1.00	1.30	+30
500	1.12	1.58	+41

TABLE G.1: The increase in horizontal distance when coughing (10.6 m/s).

Particle diameter [μm]	Breathing [m]	Sneezing [m]	Increase [%]
10	0.66	0.66	0
50	1.70	1.71	+1
80	0.98	1.00	+2
90	0.89	1.00	+12
100	0.83	0.92	+11
200	0.71	0.86	+21
300	0.85	1.49	+76
400	1.00	2.06	+107
500	1.12	2.65	+136

TABLE G.2: The increase in horizontal distance when sneezing (46 m/s).

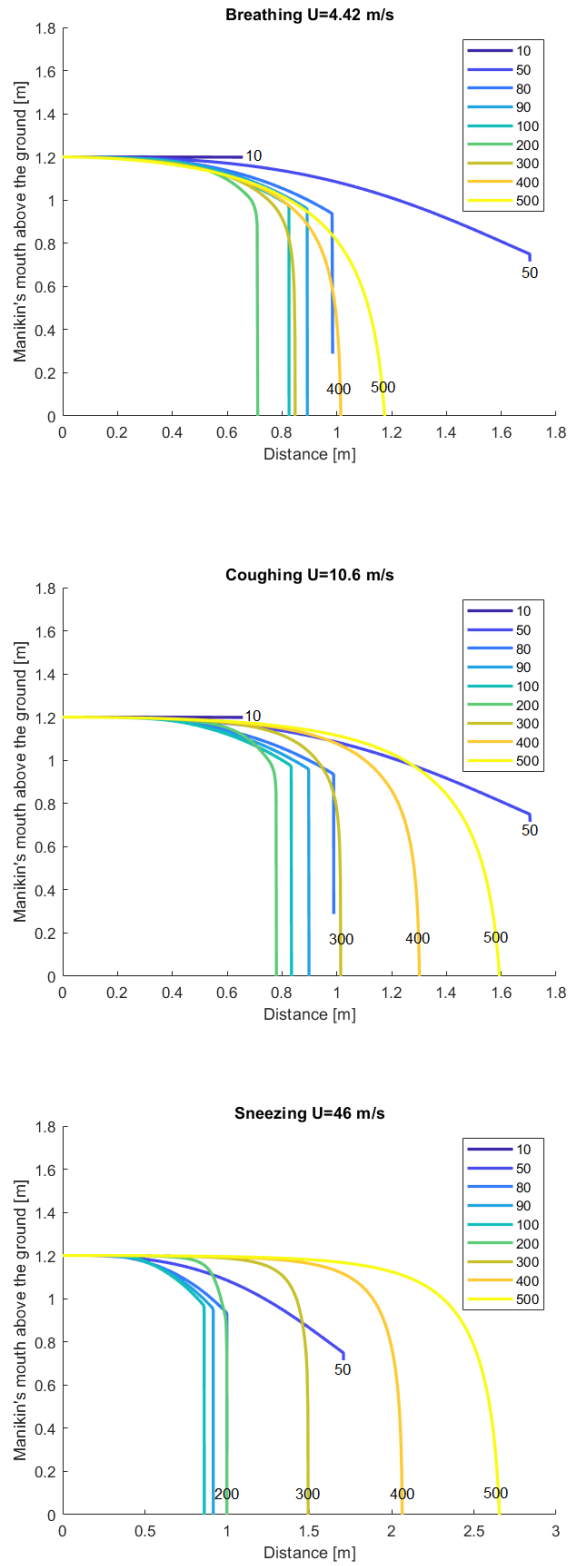


FIGURE G.1: Distance of the aerosols when breathing (4.42 m/s), coughing (10.6 m/s) and sneezing (46 m/s).

Temperature

Particle diameter [μm]	T = 24.3 °C [m]	T = 19.3 °C [m]	Difference [m]
80	0.29	0.17	+0.12
90	0	0	0

TABLE G.3: Height difference between T = 19.3—24.3 °C.

Particle diameter [μm]	T = 24.3 °C [m]	T = 29.3 °C [m]	Difference [m]
80	0.29	0.38	-0.09
90	0	0.08	-0.08

TABLE G.4: Height difference between T = 24.3—29.3 °C.

Particle diameter [μm]	T = 24.3 °C [m]	T = 34.3 °C [m]	Difference [m]
80	0.29	0.45	-0.16
90	0	0.19	-0.19

TABLE G.5: Height difference between T = 24.3—34.3 °C.

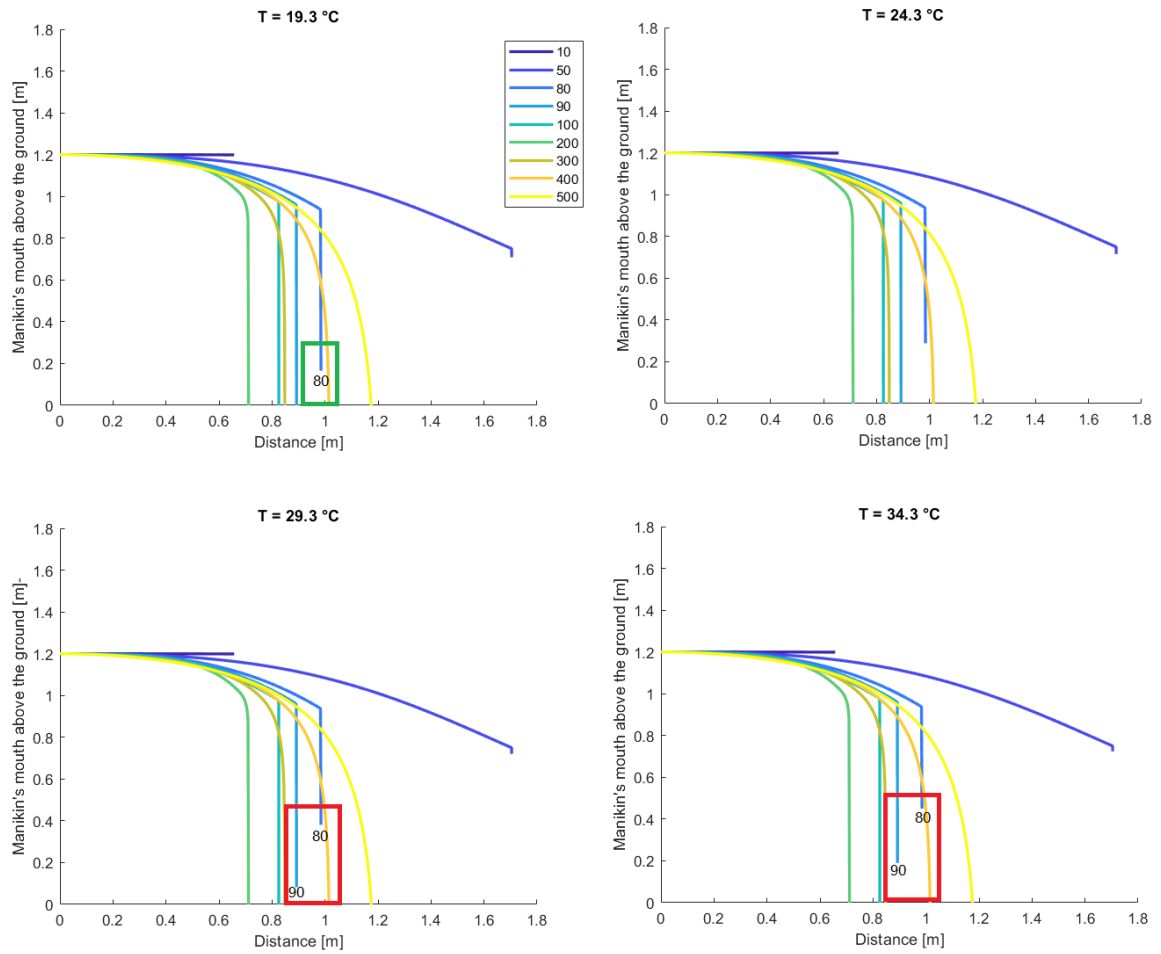


FIGURE G.2: Decreasing the temperature to 19.4 °C slows down the evaporation process, which is given in the green box. Increasing the temperature causes the droplets to evaporate at a faster rate (at both 29.4 and 34.4 °C).

Relative humidity

Particle diameter [μm]	Height at 50.7% [m]	Height at 10.7% [m]	Difference [m]
50	0.72	0.73	-0.01
80	0.29	0.62	-0.33
90	0	0.46	-0.46
100	0	0.24	-0.24

TABLE G.6: Height difference between RH = 10.7—50.7%.

Particle diameter [μm]	Height at 50.7% [m]	Height at 30.7% [m]	Difference [m]
50	0.72	0.73	-0.01
80	0.29	0.50	-0.21
90	0	0.28	-0.28
100	0	0	0

TABLE G.7: Height difference between RH = 30.7—50.7%.

Particle diameter [μm]	Height at 50.7% [m]	Height at 70.7% [m]	Difference [m]
50	0.72	0.69	+0.03
80	0.29	0	+0.29
90	0	0	0
100	0	0	0

TABLE G.8: Height difference between RH = 50.7—70.7%.

Particle diameter [μm]	Height at 50.7% [m]	Height at 90.7% [m]	Difference [m]
50	0.72	0.55	+0.17
80	0.29	0	+0.29
90	0	0	0
100	0	0	0

TABLE G.9: Height difference between RH = 50.7—90.7%.

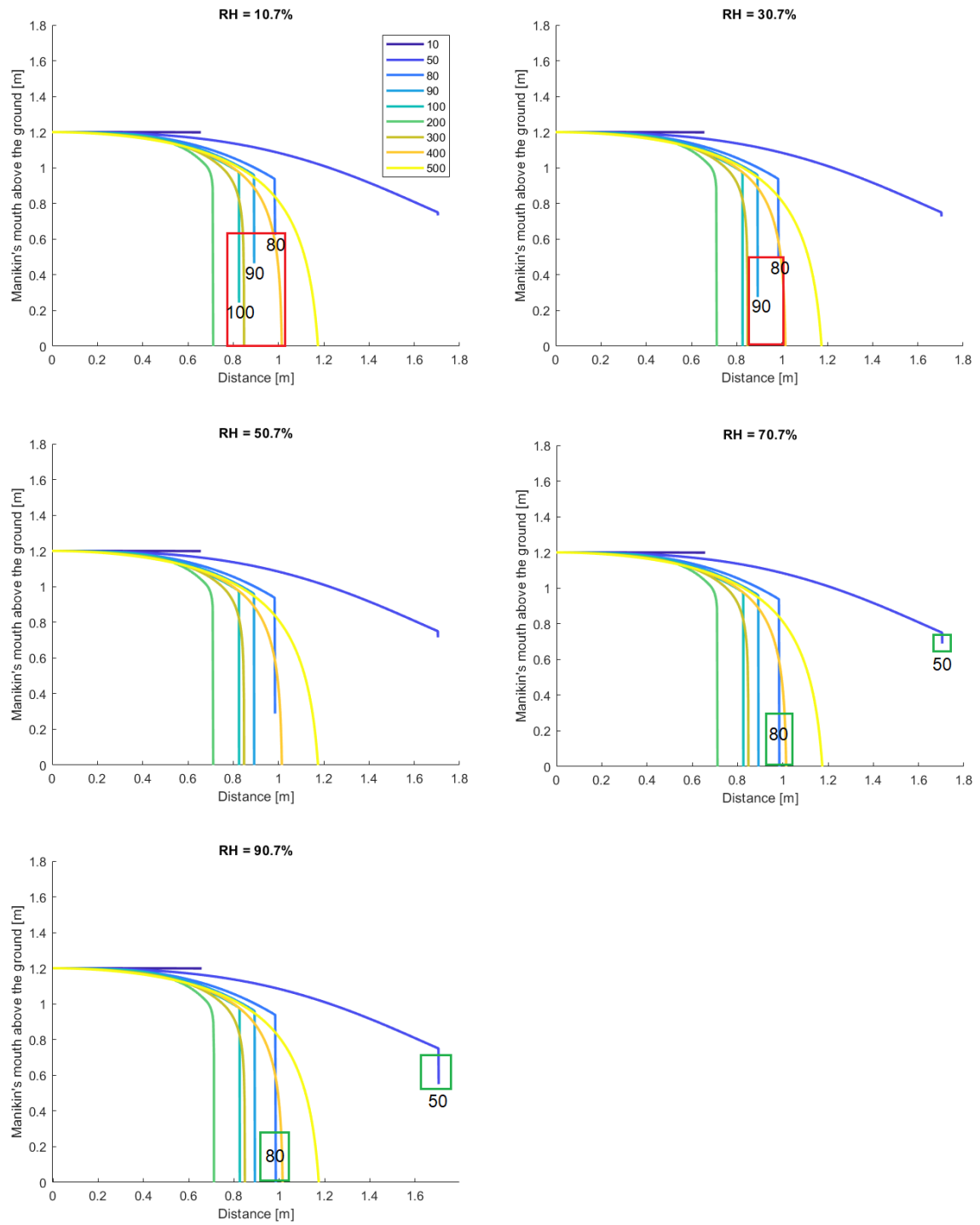


FIGURE G.3: Decreasing the RH makes the droplets evaporate faster. Increasing the RH makes the droplets more likely to fall on the surface before it evaporates and becomes a droplet nuclei.

Bibliography

- Andersson, Per-Arne et al. (Dec. 1983). "A comparison between tracer gas and tracer particle techniques in evaluating the efficiency of ventilation in operating theatres". In: *Journal of Hygiene* 91.3, pp. 509–519. DOI: [10.1017/s0022172400060551](https://doi.org/10.1017/s0022172400060551). URL: <https://doi.org/10.1017/s0022172400060551>.
- Arumuru, Venugopal et al. (Apr. 2021). "Breathing, virus transmission, and social distancing—An experimental visualization study". In: *AIP Advances* 11.4, p. 045205. DOI: [10.1063/5.0045582](https://doi.org/10.1063/5.0045582). URL: <https://doi.org/10.1063/5.0045582>.
- Bhattacharyya, Suvarjan et al. (Oct. 2020). "A novel CFD analysis to minimize the spread of COVID-19 virus in hospital isolation room". In: *Chaos, Solitons & Fractals* 139, p. 110294. DOI: [10.1016/j.chaos.2020.110294](https://doi.org/10.1016/j.chaos.2020.110294). URL: <https://doi.org/10.1016/j.chaos.2020.110294>.
- Biryukov, Jennifer et al. (Aug. 2020). "Increasing Temperature and Relative Humidity Accelerates Inactivation of SARS-CoV-2 on Surfaces". In: *mSphere* 5.4. Ed. by Matthew B. Frieman. DOI: [10.1128/msphere.00441-20](https://doi.org/10.1128/msphere.00441-20). URL: <https://doi.org/10.1128/msphere.00441-20>.
- Bivolarova, M. et al. (May 2017). "A comparison between tracer gas and aerosol particles distribution indoors: The impact of ventilation rate, interaction of airflows, and presence of objects". In: *Indoor Air* 27.6, pp. 1201–1212. DOI: [10.1111/ina.12388](https://doi.org/10.1111/ina.12388). URL: <https://doi.org/10.1111/ina.12388>.
- Bluyssen, Philomena M., Marco Ortiz, and Dadi Zhang (Jan. 2021). "The effect of a mobile HEPA filter system on 'infectious' aerosols, sound and air velocity in the SenseLab". In: *Building and Environment* 188, p. 107475. DOI: [10.1016/j.buildenv.2020.107475](https://doi.org/10.1016/j.buildenv.2020.107475). URL: <https://doi.org/10.1016/j.buildenv.2020.107475>.
- Bluyssen, Philomena M. et al. (June 2017). "The creation of SenseLab: a laboratory for testing and experiencing single and combinations of indoor environmental conditions". In: *Intelligent Buildings International* 10.1, pp. 5–18. DOI: [10.1080/17508975.2017.1330187](https://doi.org/10.1080/17508975.2017.1330187). URL: <https://doi.org/10.1080/17508975.2017.1330187>.
- Bourouiba, Lydia (Mar. 2020). "Turbulent Gas Clouds and Respiratory Pathogen Emissions". In: *JAMA*. DOI: [10.1001/jama.2020.4756](https://doi.org/10.1001/jama.2020.4756). URL: <https://doi.org/10.1001/jama.2020.4756>.
- Buonanno, G., L. Stabile, and L. Morawska (Aug. 2020). "Estimation of airborne viral emission: Quanta emission rate of SARS-CoV-2 for infection risk assessment". In: *Environment International* 141, p. 105794. DOI: [10.1016/j.envint.2020.105794](https://doi.org/10.1016/j.envint.2020.105794). URL: <https://doi.org/10.1016/j.envint.2020.105794>.
- Casanova, Lisa M. et al. (May 2010). "Effects of Air Temperature and Relative Humidity on Coronavirus Survival on Surfaces". In: *Applied and Environmental Microbiology* 76.9, pp. 2712–2717. DOI: [10.1128/aem.02291-09](https://doi.org/10.1128/aem.02291-09). URL: <https://doi.org/10.1128/aem.02291-09>.
- Dbouk, Talib and Dimitris Drikakis (May 2020). "On coughing and airborne droplet transmission to humans". In: *Physics of Fluids* 32.5, p. 053310. DOI: [10.1063/5.0011960](https://doi.org/10.1063/5.0011960). URL: <https://doi.org/10.1063/5.0011960>.

- Fehr, Anthony R. and Stanley Perlman (2015). "Coronaviruses: An Overview of Their Replication and Pathogenesis". In: *Coronaviruses*. Springer New York, pp. 1–23. DOI: [10.1007/978-1-4939-2438-7_1](https://doi.org/10.1007/978-1-4939-2438-7_1). URL: https://doi.org/10.1007/978-1-4939-2438-7_1.
- Gómez, José María Gómez et al. (July 2014). "Drying Bacterial Biosaline Patterns Capable of Vital Reanimation upon Rehydration: Novel Hibernating Biomineralogical Life Formations". In: *Astrobiology* 14.7, pp. 589–602. DOI: [10.1089/ast.2014.1162](https://doi.org/10.1089/ast.2014.1162). URL: <https://doi.org/10.1089/ast.2014.1162>.
- Gorbalenya, Alexander E. et al. (Feb. 2020). "Severe acute respiratory syndrome-related coronavirus: The species and its viruses – a statement of the Coronavirus Study Group". In: DOI: [10.1101/2020.02.07.937862](https://doi.org/10.1101/2020.02.07.937862). URL: <https://doi.org/10.1101/2020.02.07.937862>.
- GOV (2021). *Coronavirus: how to stay safe and help prevent the spread*. URL: <https://www.gov.uk/guidance/covid-19-coronavirus-restrictions-what-you-can-and-cannot-do>.
- Gralton, Jan et al. (Jan. 2011). "The role of particle size in aerosolised pathogen transmission: A review". In: 62.1, pp. 1–13. DOI: [10.1016/j.jinf.2010.11.010](https://doi.org/10.1016/j.jinf.2010.11.010). URL: <https://doi.org/10.1016/j.jinf.2010.11.010>.
- Grymer, L F et al. (Mar. 1991). "Acoustic rhinometry: values from adults with subjective normal nasal patency". English. In: *Rhinology* 29.1, pp. 35–47. ISSN: 0300-0729.
- Hamner, Lea et al. (May 2020). "High SARS-CoV-2 Attack Rate Following Exposure at a Choir Practice — Skagit County, Washington, March 2020". In: *MMWR. Morbidity and Mortality Weekly Report* 69.19, pp. 606–610. DOI: [10.15585/mmwr.mm6919e6](https://doi.org/10.15585/mmwr.mm6919e6). URL: <https://doi.org/10.15585/mmwr.mm6919e6>.
- Holterman, H.J. (2003). *Kinetics and evaporation of water drops in air*. English. IMAG rapport 2003-12. IMAG. ISBN: 9789054062349.
- Huang, Chaolin et al. (Feb. 2020). "Clinical features of patients infected with 2019 novel coronavirus in Wuhan, China". In: *The Lancet* 395.10223, pp. 497–506. DOI: [10.1016/s0140-6736\(20\)30183-5](https://doi.org/10.1016/s0140-6736(20)30183-5). URL: [https://doi.org/10.1016/s0140-6736\(20\)30183-5](https://doi.org/10.1016/s0140-6736(20)30183-5).
- Ivanov, Martin (2019). "Exhaled air speed measurements of respiratory air flow, generated by ten different human subjects, under uncontrolled conditions". In: *E3S Web of Conferences* 111. Ed. by S.I Tanabe et al., p. 02074. DOI: [10.1051/e3sconf/201911102074](https://doi.org/10.1051/e3sconf/201911102074). URL: <https://doi.org/10.1051/e3sconf/201911102074>.
- Jennison, Marshall W (1942). "Atomizing of mouth and nose secretions into the air as revealed by high-speed photography". In: *Aerobiology* 17, pp. 106–128.
- Jiang, Nan et al. (Oct. 2017). "Experimental study on flow behavior of breathing activity produced by a thermal manikin". In: *Building and Environment* 123, pp. 200–210. DOI: [10.1016/j.buildenv.2017.07.004](https://doi.org/10.1016/j.buildenv.2017.07.004). URL: <https://doi.org/10.1016/j.buildenv.2017.07.004>.
- Kudo, Eriko et al. (May 2019). "Low ambient humidity impairs barrier function and innate resistance against influenza infection". In: *Proceedings of the National Academy of Sciences* 116.22, pp. 10905–10910. DOI: [10.1073/pnas.1902840116](https://doi.org/10.1073/pnas.1902840116). URL: <https://doi.org/10.1073/pnas.1902840116>.
- Kulkarni, Pramod (2011). *Aerosol measurement : principles, techniques, and applications*. Hoboken, N.J: Wiley. ISBN: 978-0-470-38741-2.
- Kwon, Soon-Bark et al. (June 2012). "Study on the initial velocity distribution of exhaled air from coughing and speaking". In: *Chemosphere* 87.11, pp. 1260–1264. DOI: [10.1016/j.chemosphere.2012.01.032](https://doi.org/10.1016/j.chemosphere.2012.01.032). URL: <https://doi.org/10.1016/j.chemosphere.2012.01.032>.
- LCVS (2020). URL: <https://www.rijksoverheid.nl/documenten/rapporten/2020/10/01/eindrapport-landelijk-coördinatieteam-ventilatie-op-scholen>.

- Lu, Jianyun et al. (July 2020). "COVID-19 Outbreak Associated with Air Conditioning in Restaurant, Guangzhou, China, 2020". In: *Emerging Infectious Diseases* 26.7, pp. 1628–1631. DOI: [10.3201/eid2607.200764](https://doi.org/10.3201/eid2607.200764). URL: <https://doi.org/10.3201/eid2607.200764>.
- Lynch, Richard M. and Reginald Goring (July 2020). "Practical Steps to Improve Air Flow in Long-Term Care Resident Rooms to Reduce COVID-19 Infection Risk". In: *Journal of the American Medical Directors Association* 21.7, pp. 893–894. DOI: [10.1016/j.jamda.2020.04.001](https://doi.org/10.1016/j.jamda.2020.04.001). URL: <https://doi.org/10.1016/j.jamda.2020.04.001>.
- Mansour, Elias et al. (Feb. 2020). "Measurement of temperature and relative humidity in exhaled breath". In: *Sensors and Actuators B: Chemical* 304, p. 127371. DOI: [10.1016/j.snb.2019.127371](https://doi.org/10.1016/j.snb.2019.127371). URL: <https://doi.org/10.1016/j.snb.2019.127371>.
- Masters, Paul S. (2006). "The Molecular Biology of Coronaviruses". In: pp. 193–292. DOI: [10.1016/s0065-3527\(06\)66005-3](https://doi.org/10.1016/s0065-3527(06)66005-3). URL: [https://doi.org/10.1016/s0065-3527\(06\)66005-3](https://doi.org/10.1016/s0065-3527(06)66005-3).
- Mhetre, Manisha Rajesh and Hemant Keshav Abhyankar (Feb. 2017). "Human exhaled air energy harvesting with specific reference to PVDF film". In: 20.1, pp. 332–339. DOI: [10.1016/j.jestch.2016.06.012](https://doi.org/10.1016/j.jestch.2016.06.012). URL: <https://doi.org/10.1016/j.jestch.2016.06.012>.
- Miller, Shelly L. et al. (Oct. 2020). "Transmission of SARS-CoV-2 by inhalation of respiratory aerosol in the Skagit Valley Chorale superspreading event". In: *Indoor Air* 31.2, pp. 314–323. DOI: [10.1111/ina.12751](https://doi.org/10.1111/ina.12751). URL: <https://doi.org/10.1111/ina.12751>.
- Min, Long and Qiu Sun (Apr. 2021). "Antibodies and Vaccines Target RBD of SARS-CoV-2". In: *Frontiers in Molecular Biosciences* 8. DOI: [10.3389/fmolb.2021.671633](https://doi.org/10.3389/fmolb.2021.671633). URL: <https://doi.org/10.3389/fmolb.2021.671633>.
- Morawska, Lidia et al. (May 2021). "A paradigm shift to combat indoor respiratory infection". In: *Science* 372.6543, pp. 689–691. DOI: [10.1126/science.abg2025](https://doi.org/10.1126/science.abg2025). URL: <https://doi.org/10.1126/science.abg2025>.
- Nielsen, Peter V. (Sept. 2009). "Control of airborne infectious diseases in ventilated spaces". In: *Journal of The Royal Society Interface* 6.suppl_6. DOI: [10.1098/rsif.2009.0228.focus](https://doi.org/10.1098/rsif.2009.0228.focus). URL: <https://doi.org/10.1098/rsif.2009.0228.focus>.
- Oran, Daniel P. and Eric J. Topol (Jan. 2021). "The Proportion of SARS-CoV-2 Infections That Are Asymptomatic". In: *Annals of Internal Medicine*. DOI: [10.7326/m20-6976](https://doi.org/10.7326/m20-6976). URL: <https://doi.org/10.7326/m20-6976>.
- Ortiz, Marco A., Marzieh Ghasemishkaftaki, and Philomena M. Bluysen (July 2021). "Testing of outward leakage of different types of masks with a breathing manikin head, ultraviolet light and coloured water mist". In: *Intelligent Buildings International*, pp. 1–19. DOI: [10.1080/17508975.2021.1951153](https://doi.org/10.1080/17508975.2021.1951153). URL: <https://doi.org/10.1080/17508975.2021.1951153>.
- Otter, J.A. et al. (Mar. 2016). "Transmission of SARS and MERS coronaviruses and influenza virus in healthcare settings: the possible role of dry surface contamination". In: *Journal of Hospital Infection* 92.3, pp. 235–250. DOI: [10.1016/j.jhin.2015.08.027](https://doi.org/10.1016/j.jhin.2015.08.027). URL: <https://doi.org/10.1016/j.jhin.2015.08.027>.
- Pifferi, Massimo et al. (Mar. 2009). "Exhaled air temperature in asthmatic children: a mathematical evaluation". In: *Pediatric Allergy and Immunology* 20.2, pp. 164–171. DOI: [10.1111/j.1399-3038.2008.00742.x](https://doi.org/10.1111/j.1399-3038.2008.00742.x). URL: <https://doi.org/10.1111/j.1399-3038.2008.00742.x>.
- Probs, Steve (2020). *UNDERSTANDING PARTICLE SIZE AEROSOL-BASED TRANSMISSION*.
- Raamsman, Martin J. B. et al. (Mar. 2000). "Characterization of the Coronavirus Mouse Hepatitis Virus Strain A59 Small Membrane Protein E". In: *Journal of Virology* 74.5, pp. 2333–2342. DOI: [10.1128/jvi.74.5.2333-2342.2000](https://doi.org/10.1128/jvi.74.5.2333-2342.2000). URL: <https://doi.org/10.1128/jvi.74.5.2333-2342.2000>.

- Raines, Kevin S., Sebastian Doniach, and Gyan Bhanot (July 2021). "The transmission of SARS-CoV-2 is likely comodulated by temperature and by relative humidity". In: *PLOS ONE* 16.7. Ed. by Siew Ann Cheong, e0255212. DOI: 10.1371/journal.pone.0255212. URL: <https://doi.org/10.1371/journal.pone.0255212>.
- Ram, Kirpa et al. (June 2021). "Why airborne transmission hasn't been conclusive in case of COVID-19? An atmospheric science perspective". In: *Science of The Total Environment* 773, p. 145525. DOI: 10.1016/j.scitotenv.2021.145525. URL: <https://doi.org/10.1016/j.scitotenv.2021.145525>.
- RIVM (2021). *Frisse Scholen: Rvo.nl: Rijksdienst*. URL: <https://www.rvo.nl/onderwerpen/duurzaam-ondernemen/gebouwen/technieken-beheer-en-innovatie/frisse-scholen>.
- RIVM (2020) (n.d.). <https://www.rivm.nl/sites/default/files/2020-10/1>. Accessed: May-28-2021.
- Sabino, Caetano P. et al. (Nov. 2020). "Light-based technologies for management of COVID-19 pandemic crisis". In: *Journal of Photochemistry and Photobiology B: Biology* 212, p. 111999. DOI: 10.1016/j.jphotobiol.2020.111999. URL: <https://doi.org/10.1016/j.jphotobiol.2020.111999>.
- Scharfman, B. E. et al. (Jan. 2016). "Visualization of sneeze ejecta: steps of fluid fragmentation leading to respiratory droplets". In: 57.2. DOI: 10.1007/s00348-015-2078-4. URL: <https://doi.org/10.1007/s00348-015-2078-4>.
- Schijven, Jack et al. (Apr. 2021). "Quantitative Microbial Risk Assessment for Airborne Transmission of SARS-CoV-2 via Breathing, Speaking, Singing, Coughing, and Sneezing". In: *Environmental Health Perspectives* 129.4. DOI: 10.1289/ehp7886. URL: <https://doi.org/10.1289/ehp7886>.
- Seinfeld, John (2016). *Atmospheric chemistry and physics : from air pollution to climate change*. Hoboken, New Jersey: John Wiley & Sons. ISBN: 978-1-118-94740-1.
- Somsen, G Aernout et al. (July 2020). "Small droplet aerosols in poorly ventilated spaces and SARS-CoV-2 transmission". In: *The Lancet Respiratory Medicine* 8.7, pp. 658–659. DOI: 10.1016/s2213-2600(20)30245-9. URL: [https://doi.org/10.1016/s2213-2600\(20\)30245-9](https://doi.org/10.1016/s2213-2600(20)30245-9).
- Tang, Julian W. et al. (June 2011a). "Qualitative Real-Time Schlieren and Shadowgraph Imaging of Human Exhaled Airflows: An Aid to Aerosol Infection Control". In: *PLoS ONE* 6.6. Ed. by Benjamin J. Cowling, e21392. DOI: 10.1371/journal.pone.0021392. URL: <https://doi.org/10.1371/journal.pone.0021392>.
- Tang, J.W. et al. (Mar. 2011b). "Observing and quantifying airflows in the infection control of aerosol- and airborne-transmitted diseases: an overview of approaches". In: 77.3, pp. 213–222. DOI: 10.1016/j.jhin.2010.09.037. URL: <https://doi.org/10.1016/j.jhin.2010.09.037>.
- Teichert-Filho, R. et al. (Aug. 2020). "Protective device to reduce aerosol dispersion in dental clinics during the COVID-19 pandemic". In: *International Endodontic Journal* 53.11, pp. 1588–1597. DOI: 10.1111/iej.13373. URL: <https://doi.org/10.1111/iej.13373>.
- TU Delft (2017). *The experience room*. URL: <https://www.tudelft.nl/bk/onderzoek/onderzoeksfaciliteiten/senselab/the-experience-room>. (accessed: 16.11.2021).
- Verma, Siddhartha, Manhar Dhanak, and John Frankenfield (June 2020). "Visualizing the effectiveness of face masks in obstructing respiratory jets". In: *Physics of Fluids* 32.6, p. 061708. DOI: 10.1063/5.0016018. URL: <https://doi.org/10.1063/5.0016018>.
- Wang, Dawei et al. (Mar. 2020). "Clinical Characteristics of 138 Hospitalized Patients With 2019 Novel Coronavirus-Infected Pneumonia in Wuhan, China". In: *JAMA* 323.11, p. 1061. DOI: 10.1001/jama.2020.1585. URL: <https://doi.org/10.1001/jama.2020.1585>.
- Wells, W. F. (Nov. 1934). "ON AIR-BORNE INFECTION*". In: *American Journal of Epidemiology* 20.3, pp. 611–618. DOI: 10.1093/oxfordjournals.aje.a118097. URL: <https://doi.org/10.1093/oxfordjournals.aje.a118097>.

- WHO (2021). *How long does it take to develop symptoms?* URL: <https://www.who.int/news-room/questions-and-answers/item/coronavirus-disease-covid-19>.
- Wong, Nicholas A. and Milton H. Saier (Jan. 2021). "The SARS-Coronavirus Infection Cycle: A Survey of Viral Membrane Proteins, Their Functional Interactions and Pathogenesis". In: *International Journal of Molecular Sciences* 22.3, p. 1308. DOI: [10.3390/ijms22031308](https://doi.org/10.3390/ijms22031308). URL: <https://doi.org/10.3390/ijms22031308>.
- Wrapp, Daniel et al. (Feb. 2020). "Cryo-EM structure of the 2019-nCoV spike in the prefusion conformation". In: *Science* 367.6483, pp. 1260–1263. DOI: [10.1126/science.abb2507](https://doi.org/10.1126/science.abb2507). URL: <https://doi.org/10.1126/science.abb2507>.
- Wu, Yu et al. (Aug. 2020). "Effects of temperature and humidity on the daily new cases and new deaths of COVID-19 in 166 countries". In: *Science of The Total Environment* 729, p. 139051. DOI: [10.1016/j.scitotenv.2020.139051](https://doi.org/10.1016/j.scitotenv.2020.139051). URL: <https://doi.org/10.1016/j.scitotenv.2020.139051>.
- Xie, X. et al. (June 2007). "How far droplets can move in indoor environments ? revisiting the Wells evaporation?falling curve". In: *Indoor Air* 17.3, pp. 211–225. DOI: [10.1111/j.1600-0668.2007.00469.x](https://doi.org/10.1111/j.1600-0668.2007.00469.x). URL: <https://doi.org/10.1111/j.1600-0668.2007.00469.x>.
- Xie, Xiaojian et al. (Oct. 2009). "Exhaled droplets due to talking and coughing". In: 6.suppl_6. DOI: [10.1098/rsif.2009.0388.focus](https://doi.org/10.1098/rsif.2009.0388.focus). URL: <https://doi.org/10.1098/rsif.2009.0388.focus>.
- Xu, C. et al. (June 2014). "Measuring the exhaled breath of a manikin and human subjects". In: *Indoor Air* 25.2, pp. 188–197. DOI: [10.1111/ina.12129](https://doi.org/10.1111/ina.12129). URL: <https://doi.org/10.1111/ina.12129>.
- Yang, Wan and Linsey C. Marr (June 2011). "Dynamics of Airborne Influenza A Viruses Indoors and Dependence on Humidity". In: *PLoS ONE* 6.6. Ed. by Ron A. M. Fouchier, e21481. DOI: [10.1371/journal.pone.0021481](https://doi.org/10.1371/journal.pone.0021481). URL: <https://doi.org/10.1371/journal.pone.0021481>.
- Zhu, Na et al. (Feb. 2020). "A Novel Coronavirus from Patients with Pneumonia in China, 2019". In: *New England Journal of Medicine* 382.8, pp. 727–733. DOI: [10.1056/nejmoa2001017](https://doi.org/10.1056/nejmoa2001017). URL: <https://doi.org/10.1056/nejmoa2001017>.